Characterization of isoform specific RET knockdown in cancer cell lines

By

Eric Lian

A thesis submitted to the Graduate Program in Pathology & Molecular Medicine

In conformity with the requirements for the

Degree of Master of Science

Queen's University

Kingston, Ontario, Canada

August 2013

Abstract

The REarranged in Transfection (RET) tyrosine kinase is an important signalling protein for the development of neural crest-derived tissues such as the enteric and sympathetic nervous systems. RET is constitutively activated in multiple human tumour types, such as thyroid carcinomas and some non-small cell lung cancers. RET has 3 distinct isoforms, RET9, RET43 and RET51, which are named after the lengths of their unique C-terminal tails. Here, we investigate the role of RET in the TT thyroid carcinoma cell line, where it is a driver of tumourigenesis, and in the MiaPaCa-2 pancreatic carcinoma cell line, where RET is not driving tumour initiation, but may nonetheless have a profound effect on tumour progression. We generated lentiviral constructs for shRNAs that target either RET9 or RET51 specifically, or a common region shared by all RET isoforms. TT and MiaPaCa-2 cells were transduced using these lentiviral particles to create stable cell lines containing knockdowns of total RET, RET9, or RET51. Using a variety of morphological and biochemical assays, we found that RET expression is critical for TT cell survival, and that both RET9 and RET51 play significant roles in driving cell proliferation in TT cells. Conversely, RET is not critical for MiaPaCa-2 cell survival, and RET knockdown had no effect on MiaPaCa-2 proliferation. MiaPaCa-2 cells instead underwent dramatic morphological changes, from their normal spindle-like mesenchymal appearance to an increasingly flattened and epithelioid character, in response to RET9, RET51 or total-RET knockdown. The observed morphological changes were coupled with significantly reduced invasiveness through matrigel towards a source of chemoattractant, suggesting a critical role for RET in mediating cell invasiveness. These results suggest that RET may not only drive tumourigenesis, but can also enhance disease progression when expressed in other tumour types. We predict that RET may play critical roles in perineural invasion in pancreatic cancers, a

process where cells invade along peripheral nerve fibers by following an increasing concentration of chemoattractants secreted by nerve and glial cells. Thus, RET may be a valuable target to slow, or stop this process, which would have significant clinical implications in a wide variety of cancers.

Contributions

Funding provided in part by the Terry Fox Training Program in Transdisciplinary Cancer Research in Partnership with CIHR. Fluorescent microscopy performed by Mathieu Crupi (Department of Pathology & Molecular Medicine, Queen's University).

Acknowledgements

Thank you to Lois for giving me this opportunity, and for your guidance and patience. Patience, especially, for reading this thesis repeatedly despite how badly I had written it. Thanks to everyone else at the Mulligan Lab as well, I could not have completed this project without your guidance and support.

Thanks to my committee members, Dr. Xiaolong Yang and Dr. Charles Graham, and graduate coordinator Dr. Peter Greer, for always making time for my questions and providing wonderful advice.

Thanks to my parents, friends and family for your support, and a special thanks to Serisha Moodley, for providing an endless supply of encouragement and more or less putting up with me. =:3

Table of Contents

List of Tables

List of Figures

Abbreviations

3'UTR	3' untranslated region
AKT	Protein kinase B
ARTN	Artemin
BCA	Bicinchoninic acid assay
CBL	Casitas B-lineage Lymphoma ubiquitin ligase
Cdc42	Cell division control protein 42 homolog
Ct	qRT-PCR crossing threshold
DMEM	Dulbecco's modified Eagle's medium
DOK	Docking protein
DUSP	Dual-specificity phosphatase
ECM	Extracellular matrix
EDTA	Ethylenediaminetetraacetic acid
EGF	Epidermal growth factor
EGFR	epidermal growth factor receptor
EMT	Epithelial to mesenchymal transition (Opposite of MET)
ERK	Extracellular-signal-regulated kinases
EV	Empty vector
FBS	Fetal bovine serum
FMTC	Familial medullary thyroid carcinoma
FRS2	Fibroblast growth factor receptor substrate 2
GDNF	Glial cell-line derived neurotrophic factor
GFL	GDNF-family of ligands
GFRα	GDNF-family ligand receptor alpha
GRB2	Growth factor receptor-bound protein 2
GTP	Guanosine triphosphate
GTPase	Guanosine triphosphatase
GUSB	Beta-glucuronidase gene
HCL	Hydrochloric acid
HER2	Human epidermal growth factor receptor 2
HGF	Hepatocyte growth factor
HRP	Horseradish peroxidase
IRS	Insulin receptor substrate
KD	Knockdown
MAPK	Mitogen-activated protein kinase
MEN 2	Multiple endocrine neoplasia type 2
MET	Mesenchymal epithelial transition (Opposite of EMT)
MMP9	Matrix metalloproteinase-9
Mowiol	Synonym: Polyvinyl alcohol
MTC	Medullary thyroid carcinoma
MTT	Methylthiazolyldiphenyl-tetrazolium bromide

NGF	Nerve growth factor
NRTN	Neuturin
PC	Pheochromocytoma
PCR	Polymerase chain reaction
PDAC	Pancreatic ductal adenocarcinoma
PDZ	Post synaptic density protein, Drosophila disc large tumor suppressor, and zonula occludens-1 protein shared domain
PI3K	Phosphatidylinositide-3 kinase
PIP3	Phosphatidylinositol (3,4,5) triphosphate
PKC	Protein kinase C
PLC	Phospholipase C
PNI	Perineural invasion
PSPN	Persephin
PTB	Phosphotyrosine binding domain
PTEN	Phosphate and tensin homolog
qRT-PCR	Quantitative real time reverse-transcription PCR
Rac1	Ras-related C3 botulinum toxin substrate 1
Ras	Rat sarcoma GTPases
RET	Rearranged during Transfection
RET51	Long isoform of RET
RET9	Short isoform of RET
RTK	Receptor tyrosine kinase
SDS	Sodium dodecyl sulphate
SH2	Src homology 2 domain
SH3	Src homology 3 domain
SHANK3	SH3 and multiple ankyrin repeat domains 3
SHC	Src homology 2 domain-containing
shRNA	Short hairpin RNA
Src	c-Src non-receptor tyrosine kinase
STAT3	Signal transducer and activator of transcription 3
TBST	Tris-buffered saline and tween 20
TP16 and TP53	Tumour suppressor proteins 16 and 53
Tris	Tris(hydroxymethyl)aminomethane
TrkA and TrkB	Neurotrophic tyrosine kinase receptor type 1 and type 2
VAV2/3	Guanine nucleotide exchange factor proteins VAV2 and VAV3
VEGFR	Vascular endothelial growth factor receptor
WT	Wild type
Y	Tyrosine
$\Delta\Delta$Ct	Delta-delta Ct method of gene expression quantification

Chapter 1. Introduction

1.1 RET

RET was discovered by Takahashi *et al*. in 1985 during a transformation assay where human lymphoma DNA was transfected into NIH-3T3 mouse cells [1]. The assay revealed the presence of a transforming gene which consisted of two normally unlinked segments of human DNA. This gene rearrangement was found in neither normal human DNA, nor the lymphoma DNA they had transfected. As a result, Takahashi *et al.* concluded that the gene rearrangement was caused by recombination and possible cointegration during transfection, and dubbed their newly discovered gene ***RE****arranged during* ***T****ransfection* (*RET*). We now know that *RET* codes for a receptor tyrosine kinase (RTK) glycoprotein expressed in cells derived from the neural crest as well as in tissues of the urogenital system [2]. RET is a transmembrane protein with three main regions (Figure 1.1A). The N-terminal extracellular domain of RET consists of four cadherin-like repeats and a cysteine rich region. This domain is linked to the C-terminal tyrosine kinase domain, responsible for downstream signalling, by a single-pass transmembrane domain.

As a result of alternative splicing after codon 1063, RET has three distinct isoforms named RET9, RET43 and RET51, after the number of amino acids in the C-terminal tail following the alternative splicing site (Figures 1.1B, C) [3, 4]. With the exception of RET43, the C-terminal amino acids of RET isoforms are highly conserved across species, and all isoforms are typically co-expressed during development in the kidneys, and in the tissues derived from the neural crest [5-8]. RET is critical during these developmental stages, and mice without functional RET display a range of kidney defects including kidney agenesis, hypodysplasia and multicystic kidneys [9, 10]. These defects stem from RET's role in directing the outgrowth of the ureteric bud during embryogenesis. In a process similar to how RET directs neuronal outgrowth and axon targeting, activation of RET expressed by the cells of the ureteric bud by neurotrophic factors secreted by surrounding tissues, directs outgrowth of the ureteric bud to form the structures of the kidney [11, 12]. Inactivating mutations of RET are additionally associated with developmental defects such as Hirschprung disease in humans, resulting from the failure of enteric neuroblasts to migrate to their target tissues and form sympathetic neurons [13-15]. Based on their highly conserved sequences and relatively high expression, it is thought that the RET9 and RET51 isoforms represent the majority of functional RET, and are the predominant functional isoforms.

1.2 RET Activation

The activation of RET requires the formation of a co-receptor complex which includes a ligand from the glial cell-line derived neurotrophic factor (GDNF) family, and a receptor of the GDNF-family ligand receptor alpha (GFRα) protein family [16]. The GDNF-family of ligands (GFLs) consists of four neurotrophic factors: GDNF, neurturin (NRTN), artemin (ARTN), and persephin (PSPN) [17]. Each of these neurotrophic factors bind strongly to one of four GFRα proteins, named GFRα1-4. These receptor proteins exhibit a preference for GDNF, NRTN, ARTN and PSPN, respectively [17]. Although GFRαs bind most strongly to their preferred ligand, crosstalk between GFRαs and non-preferred GFLs also occurs at a lower level [17]. GFRα proteins are linked to the cell surface through a glycosyl phosphatidylinositol (GPI)-anchor and contain either two or three cysteine-rich domains [18]. The binding of a GFL to the second cysteine-rich domain of a GFRα monomer or dimer recruits a pair of RET monomers

[19]. This leads to homodimerization of two RET molecules and autophosphorylation of a number of key tyrosine residues in the RET intracellular region, which allows binding of adaptor and signalling proteins (Figure 1.2).

1.2.1 The RET isoforms

The RET receptor tyrosine kinase is known to be involved in enteric nervous and urogenital system development [13, 14], but the functional differences between its isoforms in these processes is less clear. The molecular mechanisms that lead to isoform-specific functions of RET are poorly understood, and conflicting evidence has been presented in the past regarding the distinct roles of RET isoforms in cellular processes. *In vitro* studies have provided much of the knowledge regarding RET activity. Five key tyrosines (Y) within the kinase domain of RET (Y905, Y981, Y1015, Y1062 and Y1096) (Figure 1.1) have been particularly well characterized and are known to be required for signalling through the Rat sarcoma GTPases (Ras), Phosphoinositol-3 kinase/Protein kinase B (PI3K/AKT), and Mitogen-activated protein kinase (MAPK) pathways [2, 17]. Of particular interest are Y1062 and Y1096, which have been shown to bind different downstream proteins in RET9 and RET51 due to sequence divergence following the alternative splicing site at codon 1063 (Figures 1.1B, C). Y1062 binds adaptor molecules such as SHC, FRS2, IRS1, IRS2, Enigma and DOKs 2, 4, 5, 6, while Y1096, present only in RET51, binds GRB2 (Figure 1.2). The affinity of adaptor proteins for the binding site at Y1062 is influenced by its amino acid context, due to its position immediately before the splice junction at codon 1063 (Figure 1.1). For example, the amino acid sequence “YGRI” is found at codons 1062-1065 of RET9, while RET51 instead contains “YGMS” (Figure 1.1C). When phosphorylated at Y1062, the RET9 sequence corresponds to a pYXXI binding motif recognized by the SH2 domains of adaptor proteins such as SHC [20-22]. The binding of SHC to this site allows for interaction with additional proteins, such as GRB2, for downstream activation of PI3K/AKT to promote cell survival [23], Ras/MAPK to promote proliferation and differentiation [24], or CBL for ubiquitination and downregulation of RET [25]. In RET51, the sequence divergence at codon 1064 means this motif is eliminated, rendering RET51 unable to bind adaptor proteins through their SH2-domains at Y1062. Instead, adaptor proteins such as SHC can only bind through the IENKL phosphotyrosine-binding (PTB) consensus sequence directly upstream of Y1062 [26]. Further, differences at the carboxyl-termini of RET9 and RET51 may also influence the functions and interactions of the RET isoforms. The isoform specific tail of RET9 contains the amino acid sequence “FTRF” at codons 1069 to 1072, corresponding to a PDZ-binding motif XTXF, allowing RET9 to bind PDZ domain containing adaptor proteins such as SHANK3, and interact indirectly with GRB2 [27]. RET51 lacks a PDZ domain and cannot bind SHANK3, however the RET51 isoform can bind GRB2 directly through Y1096. Finally, RET51 is thought to bind the ubiquitin ligase c-CBL through interactions at both Y1062 and Y1096, granting it the ability to internalize rapidly following activation, and giving RET51 greater access to cytoplasmically localized proteins [25, 28]. These differences in the abilities of RET9 and RET51 to bind proteins by their SH2 or PTB domains, as well as their ability to bind different proteins may contribute to differences in RET isoform functionality.

Although the exact functional differences between the isoforms have not been defined, previous research has identified a number of differences between the isoforms: The intracellular tyrosines of RET9 and RET51 take on unique phosphorylation patterns after activation [29], and activation of RET9 and RET51 has been shown to induce distinct gene expression patterns [30]. Additionally, constitutively active mutants of RET9 and RET51 isoforms have different transforming abilities, with RET51 being significantly more effective at inducing anchorage-independent growth [31-34]. Clinically, the RET51 isoform has also been found upregulated in stage IIB pancreatic cancers, suggesting that it may affect tumour aggressiveness and play a role in disease progression [35].

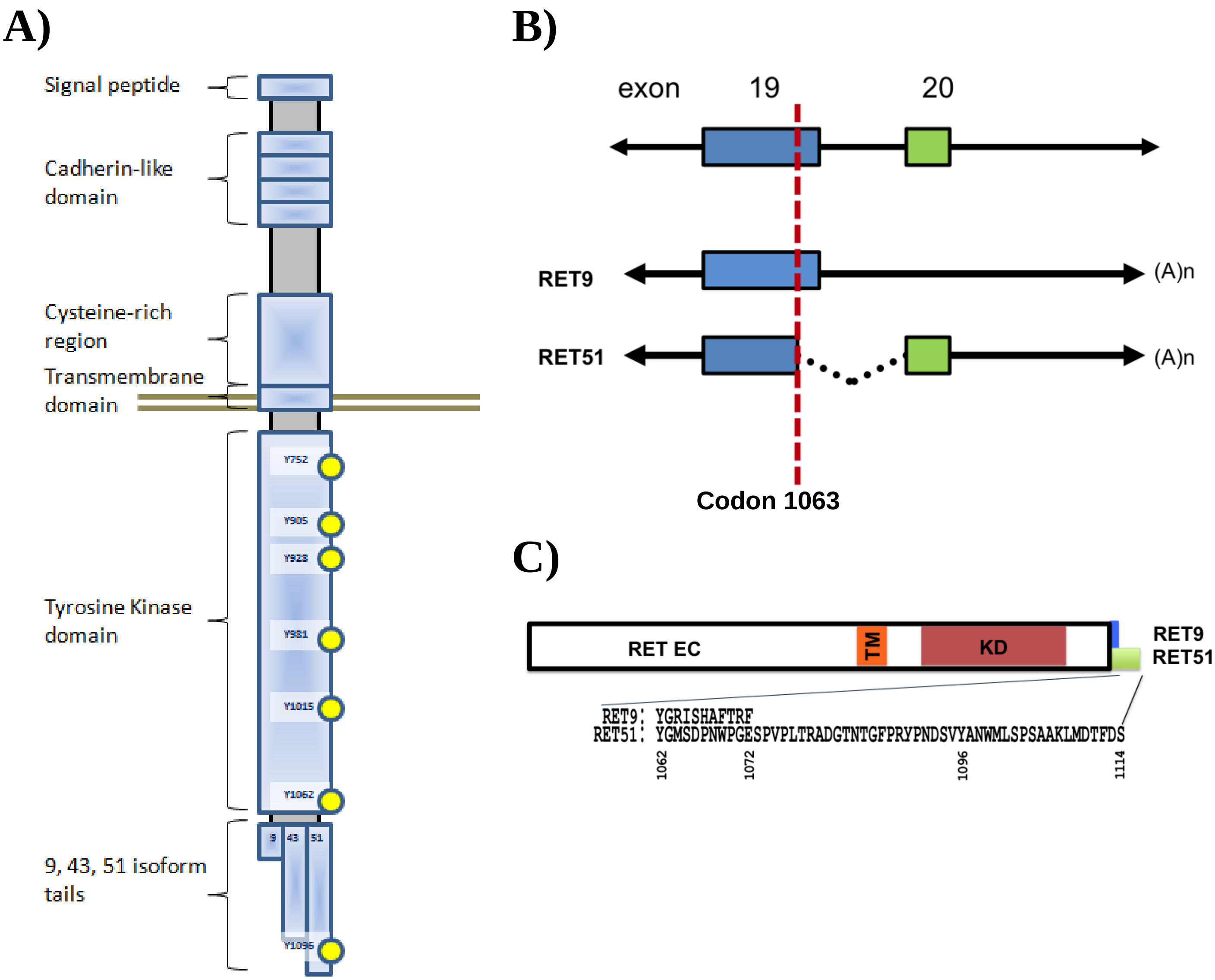

Figure 1.1 RET Structure, sequence and splice variants. A) Schematic representation of RET structural domains. Tyrosines phosphorylated during RET activation are indicated (yellow circles). The isoform specific splice site is located at codon 1063, directly after Y1062, before the isoform specific tails. Major domains are indicated including the signal peptide, 4 Cadherin-

like domains, the cysteine rich region, transmembrane domain, and the relative lengths of the RET9, 43 and 51 C-terminal tails. **B)** Splicing of the *RET* gene at codon 1063 generates two major mRNA transcripts which differ in their C-terminal tails. The RET43 transcript is not generated in significant quantities and is not shown here. **C)** Schematic representation of RET extracellular domain (RET EC), transmembrane (TM), tyrosine kinase domain (KD) and unique C-terminal tail sequences for RET9 and RET51.

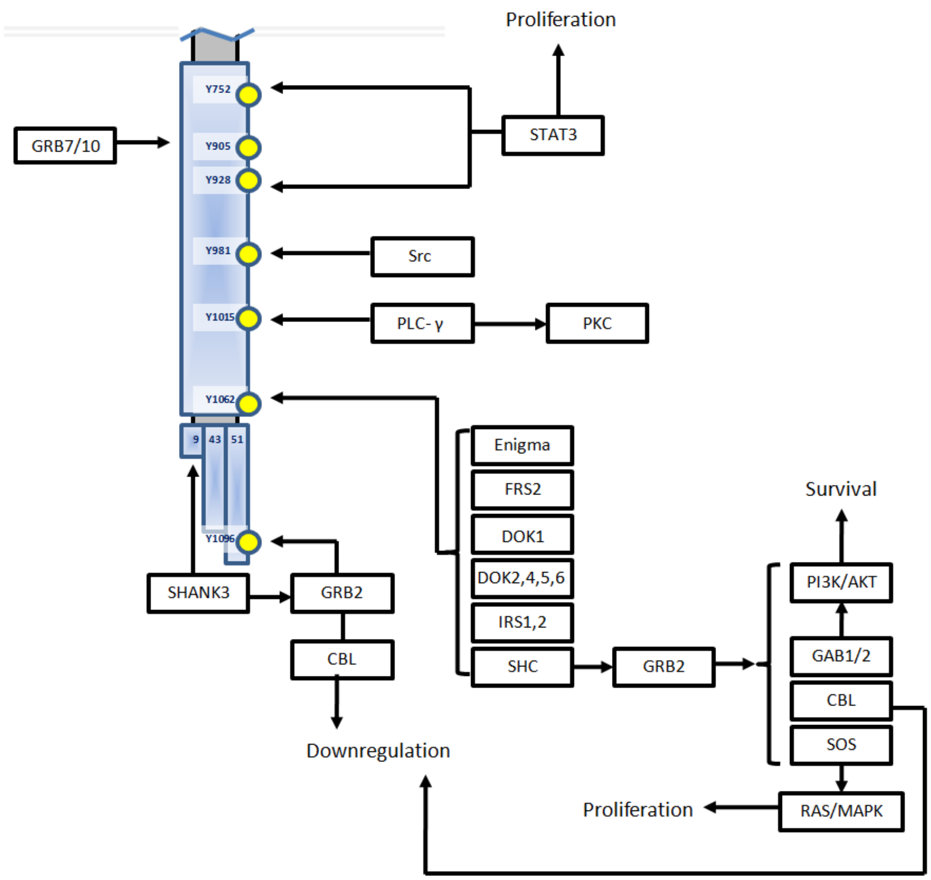

Figure 1.2 Schematic representation of pathways activated downstream of RET. Only the intracellular region of RET is shown. When RET is activated by GFL and co-receptor binding, a number of key tyrosines (yellow circles) are phosphorylated in the tyrosine kinase domain. Binding sites for adaptor proteins and signalling molecules on the RET intracellular region, and downstream protein interactions are indicated with arrows. The binding of adaptor and signaling proteins to this area mediate downstream signalling can affect cellular processes including proliferation and survival. Ubiquitination of RET by CBL also leads to internalization and downregulation of RET signalling.

1.2.2 Differential RET9 and RET51 functions

Several *in vivo* studies using animal models have added to the mounting body of evidence supporting distinct functional roles for the major RET isoforms. In humans, RET51 is expressed at very low levels relative to RET9 during early kidney development, but becomes highly expressed by 9 weeks of gestation. This regulation of RET isoform expression suggests that RET51 may contribute to differentiation related events later during development, while RET9 is involved in early development [36]. In rats, RET is expressed throughout the olfactory nervous system, but the distribution of RET9 and RET51 within tissues suggests unique functions for each isoform. One particular study showed that RET9 was expressed ubiquitously throughout the olfactory nervous system, while RET51 was expressed only in regions of the olfactory bulb innervated by sensory neurons extending from the olfactory epithelium [37]. Since RET activation by GFLs, such as ARTN secreted by target tissues during embryonic development, has been shown play important roles in the processes of sympathetic neuron migration and axon outgrowth [38], the restriction of RET51 expression to specific regions of the rat olfactory nervous system suggests that RET51 might play a specialized role in directing these processes. In addition, RET51 expressing cells were found to have a greater abundance RET localized on the cell membrane [28]. Greater cell membrane localization would grant RET51 more access to its coreceptor proteins and subsequently allow RET51 to become activated by GFLs in larger quantities relative to RET9, potentially allowing RET51 to modulate processes such as chemotaxis more effectively.

The quest to elucidate the isoform-specific functions of RET has not been without difficulty. Several studies have come to opposing conclusions regarding the functional differences between RET isoforms, and some have even concluded that there may be no functional differences. One pair of studies at the core of this controversy used mice engineered to express only one isoform of the RET protein in an attempt to elucidate the specific role of each isoform during embryogenesis. de Graaff *et al.*[13] generated transgenic mice by inserting cDNA coding for the human RET intracellular region into the mouse *Ret* exon 11 (Figure 1.3A, B) while Jain *et al.* [14] generated transgenic mice using a knock out-knock in approach to eliminate expression of mouse *Ret* and replace it with a complete human *RET* cDNA (Figure 1.3C, D). Using mice expressing combinations of wild type, chimeric isoform specific *RET* and *RET*-deletion (*null*) genes, de Graaff *et al.* [13] found that homozygous null mice were not viable, and died neonatally, while mice expressing at least a single functional copy of chimeric *RET9* (*RET9/RET9, RET9/RET51 or RET9/null* mice) developed normally. *RET51/null* and *RET51/RET51* expressing mice exhibited kidney hypodysplasia phenotypes, with mice expressing only a single copy of *RET51* exhibiting more severe defects, suggesting that although RET51 alone is incapable of supporting normal kidney development, greater RET51 expression resulted in kidneys with less severe malformations.

Contrary to these findings, Jain *et al.* [14] found that both *RET9* homozygous and *RET51* homozygous mice developed normally. A number of chimeric RET tail-swap constructs were also expressed in mice, resulting in the production of chimeric RET9 protein that contained the first 9 amino acid residues of the RET51 isoform-specific tail, and a chimeric RET51 protein, containing the first 9 amino acid residues of the RET9 isoform-specific tail (Figure 1.3E). The first of these tail-swaps truncates the RET51-specific tail sequence 9 amino acids after Y1062, thus maintaining the signalling hub at Y1062 in the amino acid context of RET51, but eliminating Y1096. The second tail-swap retains the signalling hub at Y1096, but places Y1062 into the amino acid context of RET9 by replacing the first 9 amino acids following Y1062 with those of the RET9-specific tail (Figure 1.3E), thus adding the SH2- and PDZ-binding motifs normally found only in the RET9 C-terminus. Mice homozygous for each tail-swap chimeric RET protein were also found to develop normally, and Jain *et al*. concluded that any alternative physiological roles of the RET isoforms were not due to differences in the isoform-specific C-termini [14]. Additionally, Jain *et al.* showed that the elimination of the signaling hub at Y1015 resulted in abnormal kidney development as a result of increased apoptosis and abnormal phospholipase C gamma (PLCγ) signalling in both RET9 and RET51 expressing mice, indicating that Y1015 mediated signalling is critical for normal kidney development. Conversely, the elimination of Y1062 had an effect only in RET9-expressing mice, suggesting that Y1096, which remained in RET51 expressing mice, facilitates signalling activity essential for normal kidney development and is redundant to Y1062.

Both de Graaff *et al.* and Jain *et al.* investigated the *in vivo* activity of RET, however neither model used in these studies was ideal. By splicing human *RET* into mouse *Ret*, de Graaff *et al.* generated a chimeric gene which is controlled by mouse regulatory elements while Jain *et al.* replaced the mouse *Ret* gene with whole human *RET* cDNA. Thus, any regulation based on intronic elements is preserved in the de Graaff *et al.* mice while it is deleted in the model of Jain *et al.* Loss of intronic regulation of *RET* is thought to play a major role in the genesis of Hirschsprung disease [39-44], and studies have shown that only 10-40% of cases are accounted for by mutations within *RET* exons [45]. Several deletions or SNPs within *RET* introns have been found to affect RET protein expression levels [39, 46]. Similarly, mice with renal agenesis or severe kidney defects, typically indicative of Ret dysfunction, have been shown to only rarely express mutant Ret [47], suggesting that the genomic alteration of Ret is not the major mechanism leading to kidney defects in mice. Instead, it is possible that aberrant regulation of Ret isoform expression caused by intronic alterations results in the observed defects.

Since de Graaff's study was conducted in 2001, it has also been shown that the expression of Ret9 and Ret51 in mice is differentially regulated both temporally and spatially. Ret9 is now known to be expressed highly in most Ret-expressing tissues during embryogenesis, while Ret51 expression is much lower in these tissues until later in development [48]. It is likely then, that there are numerous regulatory elements responsible for this regulation of Ret9 and Ret51 expression, and that differential regulation of Ret9 and Ret51 may contribute to observed differences between the isoforms. One possibility is that the results of de Graaff *et al.* reported were not a result of the inability of RET51 to sustain normal kidney development, but rather due to insufficient expression of the RET51 isoform. One possibility is that downregulation of RET51 during early development is mediated by suppressors or intronic miRNAs [49, 50], encoded in an intron in the mouse *Ret* gene. This would have been mitigated in the model by Jain *et al.* since their recombinant *RET* genes deleted all endogenous introns as well as all *Ret* exons beyond exon 1 (Figure 1.3C), thus eliminating all endogenous regulatory elements present in those regions, that may have suppressed RET51 expression. This may explain why the severity of kidney hypodysplasia reported by de Graaff *et al*. appeared to be dependent on the zygosity of the inserted *RET51* genomic construct. Although downregulated early during development by the presence of endogenous mouse regulatory elements, RET51 is still expressed at low levels in mouse kidneys [48], indicating that each copy of *RET51* retains some transcriptional activity. Since de Graaff's homozygous *RET51/RET51* mice develop kidneys with less severe hypodysplasia relative to *RET51/null* mice, it is possible that a single copy of the *RET51* allele simply does not produce enough RET51 protein to support normal kidney development.

Our lab has previously shown differences in RET9 and RET51 processing after activation [28, 51, 52], and it is possible that these differences in processing contribute to observed differences in function. RET51 has been shown to mature more efficiently than RET9. While RET9 mostly accumulates in the trans-golgi network as immature protein, RET51 matures and is transported in relatively greater quantities to the plasma membrane, despite lower overall expression of RET51 [28, 51]. Since RET requires cell surface localization in order to form an activation complex with GFRα, it is possible that RET51 has greater signaling activity relative to RET9. Additionally, activated RET interacts differentially with downstream proteins depending on its localization within the cell. Since membrane bound RET is recruited to lipid rafts following activation [53], it can readily interact with other membrane localized proteins, such as phospholipase C gamma (PLCγ) [54], or proteins recruited to lipid rafts, such as AKT [55]. However, signalling through other pathways, such as MAPK, requires access to cytoplasmic pools of MEK1/2 and ERK1/2 and thus the activated RET protein must be internalized [51]. Richardson *et al.* have shown that the RET51 isoform is internalized more rapidly than RET9 and is targeted back to the plasma membrane after internalization through a slow recycling process [51, 52]. The RET9 isoform is not appreciably recycled, and is instead targeted to lysosomes for rapid degradation. This means that RET51 may spend a relatively greater proportion of time localized within the cytoplasm following activation, and thus has greater access to molecules such as MEK1/2 and ERK1/2 compared to RET9, which remains localized near the cell membrane relatively longer to signal through PI3K/AKT. These differences in processing and localization appear to be supported by other studies that have shown constitutively active RET51 to have greater transforming ability relative to constitutively active RET9 [31-34], suggesting that RET51 may have greater signalling activity down pathways responsible for cellular processes critical during transformation, such as migration, growth or adhesion [56].

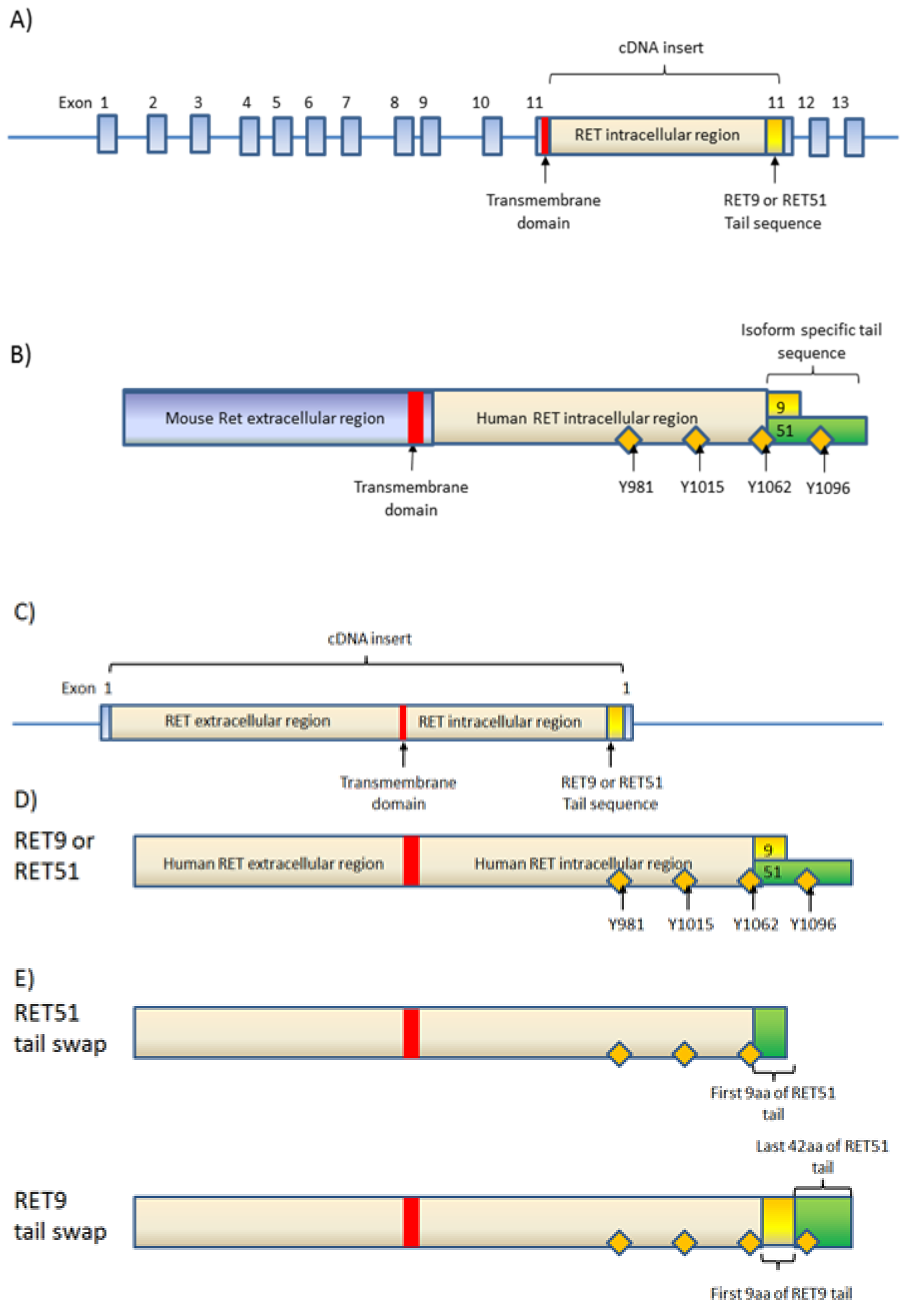

Figure 1.3 Schematic representation of RET transgenes used in previous monoisoformic mouse studies. A) Transgene generated by de Graaff *et al [13]*. RET introns 1-10 are preserved, and human RET cDNA is inserted into mouse Ret exon 11, under regulation of the endogenous mouse Ret elements. **B)** Chimeric protein generated by construct in A) showing mouse and human regions with either a RET9 or RET51 specific tail. **C)** Transgene generated by Jain *et al.*

[14] showing whole human RET cDNA inserted into mouse exon 1, and deletion of remaining mouse Ret introns and exons. **D)** Protein generated by the construct in C). **E)** Tail swap proteins generated by Jain *et al*. [14] showing the positions of RET9 and RET51 tail sequences in a RET51 or RET9 size protein.

1.4 RET and Cancer

In humans, RET activation by GDNF during embryogenesis plays a critical role in the development of the enteric nervous system and is required for enteric neuroblast proliferation, migration and survival [Reviewed in 57, 58]. These same cellular processes are critical not only during development, but also in cell transformation and tumour progression [56]. Thyroid cancer is one of the predominant diseases associated with RET activity, and RET mutations have been found in nearly one third of all thyroid cancers, rendering genetic alteration of the *RET* gene the most common driver of thyroid cancer tumourigenesis [59]. Constitutively active mutants of RET have been linked to both inherited thyroid cancer syndromes, such as multiple endocrine neoplasia type 2 (MEN 2), as well as sporadic thyroid carcinomas [60]. As described above, RET is a potent modulator of several signalling pathways, and, in addition to driving the initiation and development of thyroid cancers, has also been found to be a passenger protein overexpressed in certain aggressive pancreatic, lung, kidney and breast cancers [35, 61-63].

1.4.1 RET & Thyroid Cancer

Constitutively active RET mutants, resulting from missense point mutations [60, 64], are known to be the driver of MEN 2, an autosomal dominant heritable cancer syndrome associated with the development of medullary thyroid carcinoma (MTC) [65]. In order of increasing severity, the three subtypes of MEN 2 are: Familial MTC (FMTC), MEN 2 type A (MEN 2A) and MEN 2 type B (MEN 2B) [66-68]. All three subtypes of MEN 2 involve the development of MTC, which arises from neural crest-derived parafollicular cells of the thyroid [65]. Whereas FMTC involves only the development of relatively indolent MTC tumours, MEN 2A is additionally associated with the adrenal tumour, pheochromocytoma (PC), and with hyperparathyroidism [69]. The most severe form of the disease, MEN 2B, includes MTC, PC and additionally a range of developmental abnormalities such as mucosal neuromas and marfanoid habitus, but excludes the development of hyperparathyroidism [69].

Several key mutations within RET have been correlated with specific MEN 2 phenotypes. More than 85% of MEN 2A cases result from substitutions of one of five cysteine residues in the extracellular RET cysteine-rich region [67]. Normally, these cysteine residues form intramolecular disulphide bonds, but these MEN 2A mutations leave one or more cysteines free to form intermolecular bonds with other RET molecules [67]. As a result, RET proteins become constitutively dimerized and active in the absence of ligand/co-receptor binding [64, 70]. A single amino acid substitution (M918T) in the RET kinase domain is responsible for more than 95% of MEN 2B cases [68]. This mutation changes the conformation of the RET kinase domain, and allows RET to bind ATP more stably, thus allowing autophosphorylation through transient interaction with another RET molecule [71]. Additionally, this mutation introduces conformational changes in the kinase domain that permit some kinase activity even in the absence of ligand activation [71]. Overall, the results of this mutation are high levels of continuous downstream signalling by M918T RET. Several theories have been proposed to explain the severity of MEN 2B. One theory states that M918T might cause a conformational change in the RET active site to alter substrate specificity [72], but to date no alternative substrates have been confirmed. Another possibility is that MEN 2B is caused simply by the increased kinase activity of M918T RET, which would allow it to signal more than normal [71]. A third theory suggests that in addition to M918T RET signaling more efficiently, it also begins signalling much earlier during protein maturation resulting in a cumulative effect [73].

In addition to activating point mutations, somatic chromosomal rearrangements are also known to result in constitutively active RET signalling. This group of gene rearrangements, known as RET/PTC, is the most common cause of RET-mediated tumourigenesis [70]. These rearrangements are the result of the fusion of the RET kinase domain with N-terminal sequences of another protein, which is ubiquitously expressed and contains a homodimerization domain capable of mediating dimerization and activation of the resulting chimeric papilliary thyroid carcinoma (PTC) RET forms [74, 75]. Several chimeric RET oncogenes have been described in PTCs, which arise from thyroid follicular cells [74]. Although follicular cells typically express low levels of RET [76], the fusion of *RET* with the 5' half of other genes places RET under the control of the fusion partner's promoters, resulting in a relatively highly expressed RET fusion protein [77]. Recently, constitutively active RET fusion proteins have additionally been identified as drivers of some non-small cell lung cancers [78]. RET's ability to drive tumourigenesis in multiple tissue types positions it as a potentially valuable therapeutic target in the treatment of RET expressing tumours.

1.4.2 RET & Pancreatic Cancer

In addition to driving transformation, RTKs can play secondary roles by enhancing tumourigenesis and affecting the behaviour of cancers driven by other proteins. A classic example of this behaviour is the overexpression of human epidermal growth factor receptor 2 (HER2) in a subset of breast cancers. Although these cancers are typically driven by mutations of tumour suppressor protein 53 (TP53) or PI3K [79], HER2 overexpression is known to have severe clinical implications. Clinical inhibition of this receptor has been shown to improve patient outcome [80], indicating that an increase in signalling through this receptor promotes oncogenesis and more aggressive tumour behaviour.

Activating mutations of RET are well documented as drivers of initiation and progression in thyroid tumourigenesis, but the overexpression of wild type RET may additionally play a clinically relevant role in other cancers. RET overexpression has been documented in some 50-65% of pancreatic tumours [35, 81] and, although this is not one of the defining features of pancreatic cancer oncogenesis, its expression in some particularly aggressive tumours suggests that RET expression may have significant effects on disease progression [81].

Pancreatic ductal adenocarcinoma (PDAC) is the most common form of pancreatic neoplasm, and is thought to result from the effects of accumulated mutations within the ductal epithelium of the pancreas [82, 83]. The vast majority of PDACs arise sporadically, with only 5 to 10% of patients having a family history of the disease [84]. As a result of this sporadic nature, the genetic basis of PDAC is extremely heterogeneous, and a tumour will often contain several subpopulations of cells which are resistant to conventional treatment [83]. This, in combination with an ability to rapidly disseminate to distant organs with few identifiable symptoms, results in an extremely low 5-year survival rate (< 5%) [82]. The progression of normal pancreatic ductal cells to invasive carcinoma is marked by several driving mutations, including constitutive activation of the Kirsten rat sarcoma viral oncogene homolog (K-Ras) GTPase, and inactivation of TP16 and TP53 tumour suppressor genes [83]. Nearly 90% of pancreatic cancers have been found to contain one or more of these gene defects [83, 85-87]. In addition to these driving mutations, several clinical markers for poor prognosis have been identified [88], including enhanced angiogenesis and perineural invasion (PNI).

1.4.3 RET-mediated perineural invasion

PNI is of particular interest, since the ability of certain cancer cells to migrate along and invade nerve fibers is now known to be common among several diseases, including pancreatic, head & neck, prostate, breast and gastrointestinal cancers [89, 90]. The presence of PNI is a marker of poor clinical outcome, and limits treatment options such as curative tumour resection [90, 91]. The molecular mechanisms that drive PNI have not been fully explored, however, it is thought that the secretion of GFL neurotrophic factors by supportive glial cells surrounding nerve fibers plays a critical role in initiating and driving PNI in pancreatic cancers. RET and GFRα receptor proteins are expressed in both pancreatic cancer cell lines, and in clinical samples of PDAC [92, 93]. In addition, pancreatic cancer cells have been found to increase matrix metalloproteinase-9 (MMP9) expression in response to RET activation by GDNF [93], suggesting a role for RET in the degradation of the extracellular matrix (ECM), and subsequent PNI.

In normal nerve bundles, the glial cells surrounding nerve axons secrete various GFLs to promote neural cell survival, increase neuronal density, and induce neurite outgrowth through RET/GFRα activation [38, 94, 95]. Additionally, secretion of GFLs by other cell types, such as the smooth muscle lining of blood vessels, serves to direct cell migration and guide neurite outgrowth to their target tissues [38] through a RET-mediated chemotactic pathway [96]. In this pathway, the phosphatase and tensin homolog (PTEN) protein antagonises the activity of PI3K by dephosphorylating the phosphatidylinositol triphosphates (PIP3) produced by PI3K. The presence of a GFL concentration gradient across the length of a cell results in asymmetrical RET activation, and subsequently, asymmetrical PI3K activation by RET [96], producing a concentration gradient of PIP3 within the cell. PTEN is able to block PI3K-mediated signalling through dephosphorylation of PIP3 in intracellular areas where RET activation is low, but becomes saturated in areas of high RET activity. This results in polarization of the cell through localization of PIP3 along the cell leading edge, to mediate directional cell migration, or neurite outgrowth [96]. This same mechanism may provide a model for RET mediated PNI in pancreatic cancer. Nerve bundles have been found to secrete ARTN in response to damage [97], and the location of the pancreas, neighbouring several abdominal nerve plexuses, means that the growth of a pancreatic tumour can damage these nerves [98]. In response, the supportive glial cells secrete ARTN to mediate repair [97], simultaneously generating a chemotactic gradient that facilitates RET-mediated cell migration and invasion of the nerve fibers.

1.4.4 RET as a therapeutic target

As a driver of thyroid cancer tumourigenesis, and a protein expressed in some aggressive pancreatic, lung, kidney and breast cancers [35, 61-63], RET is an attractive target for cancer therapy. Several small-molecule RET inhibitors developed in the last decade are being evaluated clinically for efficacy against thyroid neoplasms and some, such as vandetanib, have been approved for clinical use against late-stage MTC [99-101].

One of the difficulties encountered with small-molecule inhibitors targeting RET, is the structural and sequence similarities shared between RET and other RTKs such as the vascular endothelial growth factor receptor (VEGFR) family [100]. Currently available kinase inhibitors are not RET-specific, and act on several RTKs. Vandetanib, for example, inhibits VEGFR2 and epidermal growth factor receptor (EGFR) in addition to RET, and numerous side effects have been reported, including cardiomyopathy, hypertension, skin rashes, and elevated thyroid stimulating hormone levels [100]. Although found to reduce or stabilize thyroid tumour size in some patients, tumours quickly build resistance to these inhibitors and resume growth, relegating these targeted treatments to extending patient life duration, or improving quality of life, rather than curative treatment [100].

Despite these drawbacks of RET-targeted treatments in thyroid cancers, the potential for these therapies to improve patient well-being and extend life makes them invaluable. RET's ability to mediate chemotactic response during development [96], and upregulate expression of proteinases critical for tissue remodelling [93, 102] positions it as a promising target to limit PNI in pancreatic cancer and in other cancers where PNI holds clinical significance. Although the importance of perineural invasion for PDAC metastasis is becoming increasingly recognized, to date, there has been little progress in understanding the specific mechanisms behind PNI, and no targeted treatments are currently available. To fully evaluate RET's potential as a therapeutic target will require more in-depth study of RET and the mechanisms through which it affects cancer cell behaviour.

1.5 Rationale & Hypothesis:

RET activation by GDNF is known to be critical during embryogenesis, but the specific functional differences between its isoforms are poorly understood. Previous attempts to clarify the mechanisms through which RET and its individual isoforms contribute to these processes have presented conflicting evidence as a result of the methodology employed. Since RET is an attractive target for cancer therapy, plays a critical role in driving thyroid tumourigenesis, and potentially mediates clinically relevant processes such as metastasis and perineural invasion, it is vital that we gain a better understanding of the unique functions of the two major RET isoforms. The goal of this work is to unravel the specific functions of each RET isoform using an isoform-specific shRNA knockdown of RET in endogenously-expressing cells in order to avoid the shortcomings of previous *in vivo* mouse models. Based upon our previous knowledge of signalling pathways induced by RET, and the differential subcellular localization and trafficking of the RET isoforms, I propose that the RET9 and RET51 isoforms have distinct functions within the cell, and that the RET51 isoform has relatively greater influence over cell proliferation, migration and invasion.

The following aims are outlined to address this hypothesis:

1. Develop an *in vitro* cell based model of individual RET isoform activity by generating isoform-specific knockdown cell lines using shRNA.
2. Assess phenotypic and biochemical changes induced by RET isoform specific knockdown by:
    a. Assaying for changes in cell proliferation, migration, invasiveness, and cell protrusion formation in response to isoform specific knockdown.
    b. Assessing differences in phosphorylation of downstream proteins following RET isoform specific knockdown.

Chapter 2. Materials & Methods

2.1 Cell line selection & cell culture:

MiaPaCa2 & PanC-1 pancreatic carcinoma, SK-N-SH & SH-SY5Y neuroblastoma, and TT thyroid carcinoma human cell lines were obtained from ATCC (Manassas, Virginia). TPC-1 cells were a gift from Dr. Silvia Asa (University Health Network, Toronto). These cell lines were selected due to their endogenous RET expression, and represent a variety of cell types in which RET activity has been shown to be important [103]. RET expression in each cell line was quantified using qRT-PCR, and MiaPaCa-2 and TT cells were used throughout our studies to determine the result of RET isoform knockdown. HEK293T packaging cells were gifted by Dr. Xiaolong Yang (Queen's University) and used during the production of lentiviral particles.

Cells were grown in 100mm polystyrene cell culture dishes (BD Biosciences, Mississauga, Ontario) with 10mL of Dulbecco's Modified Eagle's Medium (DMEM, Sigma-Aldrich, Oakville, Ontario) supplemented with 10% fetal bovine serum (FBS, Sigma-Aldrich). Growth medium was additionally supplemented with 1% Ciprofloxacin (GenHunter, Nashville, Tennessee) and 1% Penicillin-Streptomycin (Sigma-Aldrich) as per manufacturer instructions to prevent contamination during the first week of culture. Unless otherwise noted, cells were incubated in a 37°C humidified incubator with 5% CO_2. Cell confluence was monitored daily, and not allowed to exceed 80%. Cells were sub-cultured as necessary using TrypLE (Life Technologies, Burlington, Ontario) as a dissociation agent.

2.2 PCR Primer design:

RET9, RET43 and RET51 isoform specific PCR primer pairs were designed using the Primer3 software (frodo.wi.mit.edu/primer3) and checked for primer-dimer formation using Amplify 3 (http://engels.genetics.wisc.edu/amplify/). The primers were designed in such a way that the forward and reverse primers flanked the splice site at RET codon 1062 (Figure 2.1) in order to avoid amplification of any DNA contaminants. All three primer pairs shared the forward primer sequence 5’-CGTCCACTCCATCTGACTCC-3’, which binds upstream of codon 1062. The reverse primer for each RET isoform are as follow: RET9 5’-GATAGTGCAGAGGGGACAGC-3’, RET43 5’- AGCTGCTGAGACTTCCCAAA-3’ and RET51 5’-CCAGTGTTAGTGCCATCAGC-3’. Primer specificity was validated using RET isoform specific constructs previously generated in our lab (Figure 2.2) [51, 71, 104].

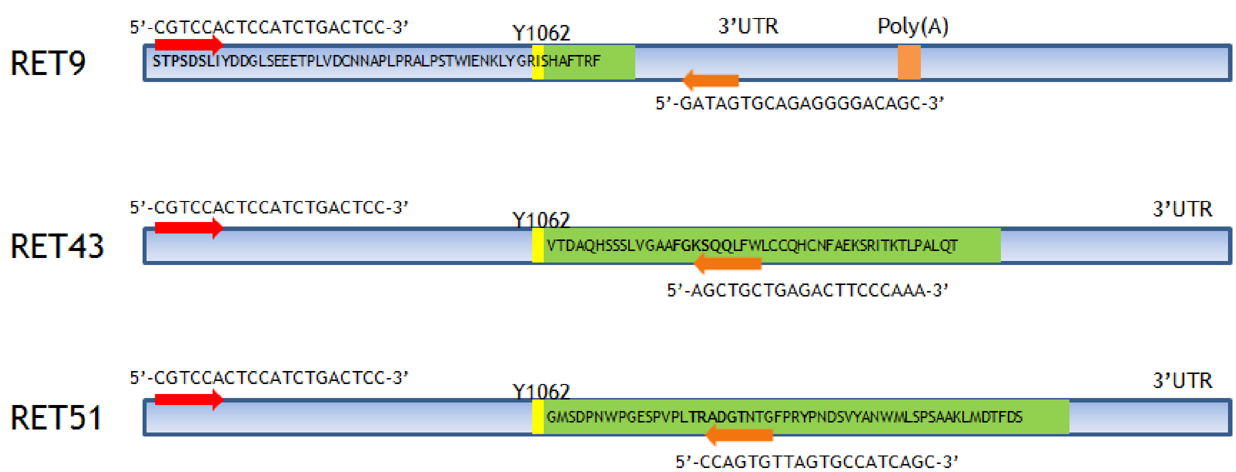

Figure 2.1 Schematic representation of RET isoforms showing isoform specific PCR strategy. Arrows indicate forward and reverse primers we have designed to be specific to each isoform. The isoform specific splice site is located directly after Y1062. All 3 primer pairs share the same forward primer and yield a PCR product approximately 200 base pairs in length.

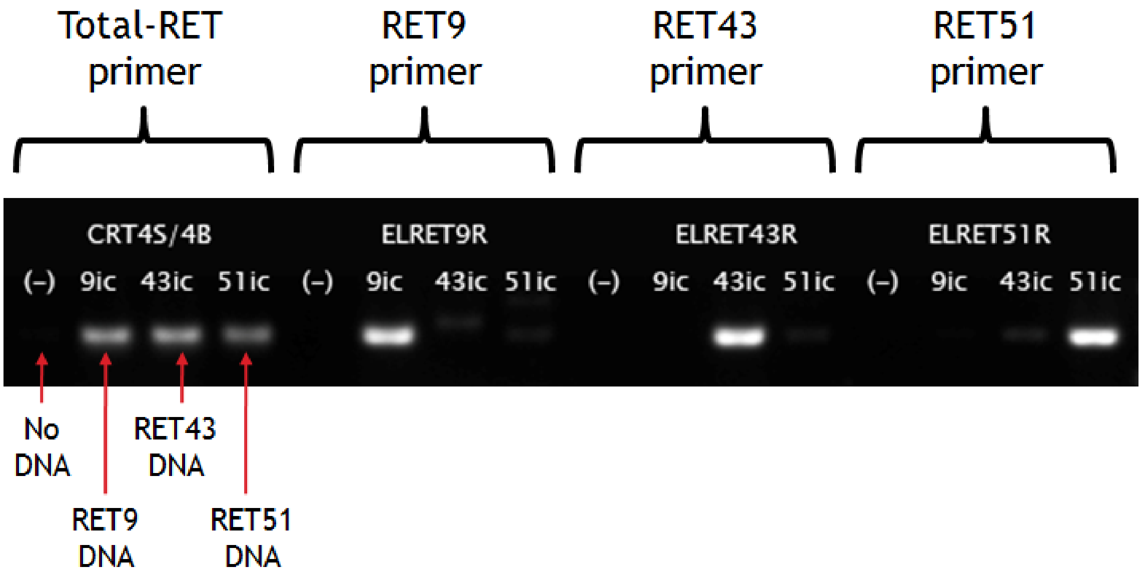

Figure 2.2 RET isoform specific primer validation. DNA expression constructs for the RET9, RET43 and RET51 intracellular regions previously generated by our lab [51, 71, 104]. were amplified with total-RET primers and our isoform specific primers. PCR products for each construct were separated on 2% agarose gels and visualized using ethidium bromide. The total-RET primer pair amplifies RET9, RET43, and RET51 constructs DNAs, while each of the isoform-specific primers amplifies only its respective RET DNA.

2.3 Quantitative real time reverse-transcription PCR (qRT-PCR) and standard PCR:

qRT-PCR: Cells were cultured to 70% confluence before total RNA was harvested using Trizol reagent (Life Technologies), according to manufacturer's instructions. Isolated total RNA was diluted to a standard concentration of 200ng/µL and 25µL reactions containing 400ng of total RNA were prepared using the one step QuantiTect SYBR Green Real-time PCR kit (Qiagen, Mississauga, Ontario) as per manufacturer's instructions. qRT-PCR reactions were performed using a SmartCycler II automated real-time PCR system (Cepheid, Sunnyvale, California), and crossing threshold (Ct) values for each RNA sample were determined in triplicate using SmartCycler II software (Cepheid). The Ct values were normalized to expression of the housekeeping gene *GUSB*, and RET transcript copy-number for each RNA sample was then calculated using a standard curve generated with linearized RET plasmid construct DNA as described below (Figure 2.3).

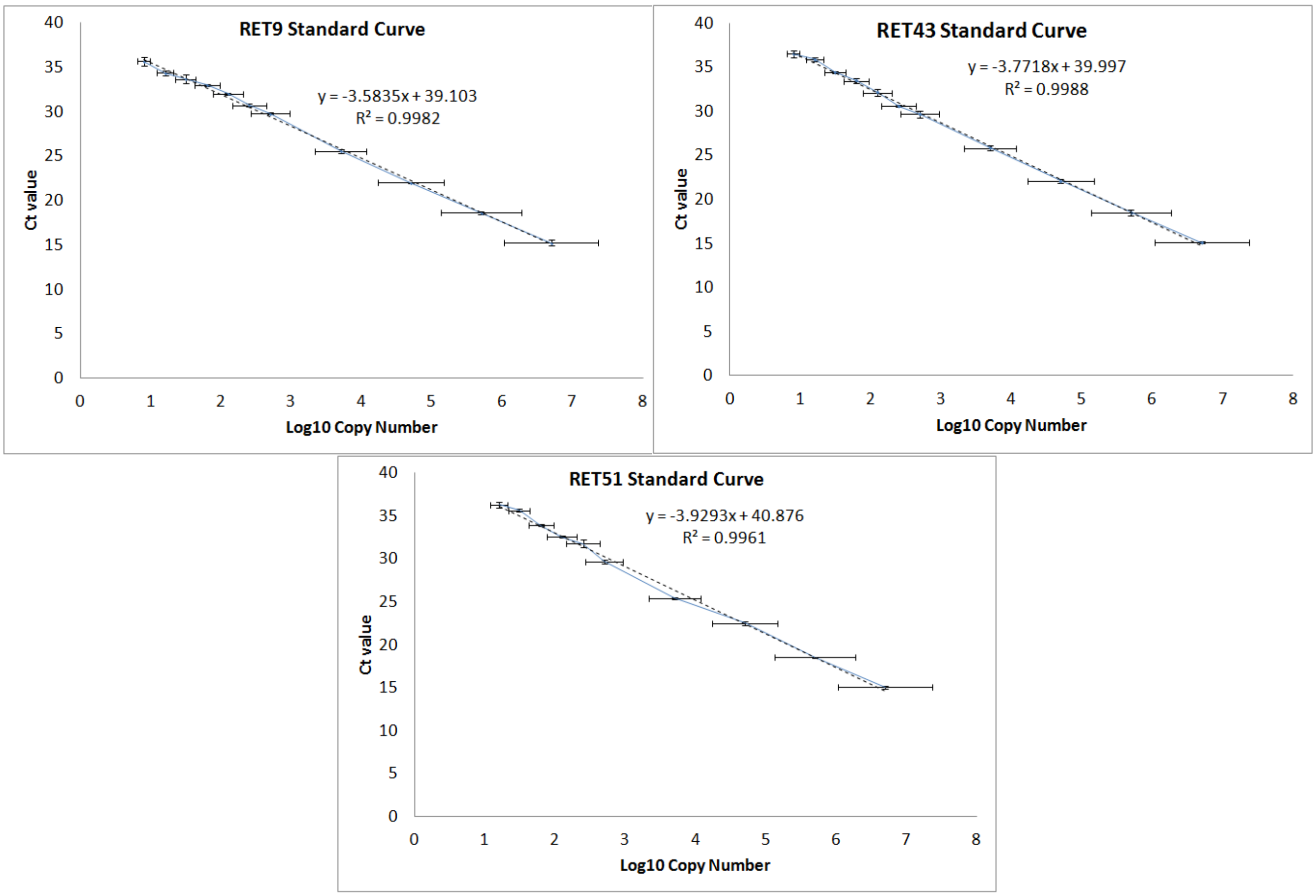

Figure 2.3 RET isoform specific standard curves for qPCR based quantification. Representative standard curves generated by amplifying linearized RET9, RET43 or RET51 intracellular RET plasmid DNA (FKBP-L2-9ic, FKBP-L2-43ic and FKBP-L2-51ic respectively). The equation displayed beside each curve (y = Slope*x + Intercept) is used to calculate the transcript number for any given Ct value, where y = Ct value, and x = Log_{10}(Copy number). Given any Ct value, the transcript copy number is derived using the equation Copy Number = $10^{[(\text{Ct} - \text{Intercept})/\text{Slope}]}$. Error bars represent standard deviation across three independent PCR reactions each containing three technical replicates.

Standard PCR: Cells were cultured and total-RNA harvested as described for qRT-PCR above. Isolated total RNA was diluted to 200ng/µL and PCR reactions were prepared using GoTaq Green master mix (Promega, Madison, Wisconsin) according to manufacturer's instructions. Reactions were performed for 10 cycles in an Omnigene thermal cycler (Thermo Hybaid, Middlesex, England) and products were separated and visualized by gel electrophoresis, on 2% agarose gels.

2.4 Standard Curve:

Standard curves for copy number for each of RET9, RET43 and RET51 were generated using previously described RET constructs FKBP-L2-9ic, FKBP-L2-43ic and FKBP-L2-51ic, respectively [28]. The plasmid DNA was linearized using SpeI and XhoI restriction enzymes (New England BioLabs, Ipswitch, Massachusetts) and diluted to a concentration of 10ng/µL. The mass of each construct was derived as follows: length of each construct (base pairs, bp) was multiplied by the average mass of a double stranded DNA base pair (660g/mol), and then divided by Avogadro's number (6.022×10^{23}) to yield an approximate mass per individual construct (Table 2.1A). A stock solution was made for each construct containing 2.5×10^{6} copies/uL, and a series of 13 standards was made via serial dilution (Table 2.1B). qRT-PCR was performed on these samples, as described above, to yield a Ct value corresponding to each dilution. The qRT-PCR data were plotted on a graph with construct copies/uL represented on the X-axis and Ct value represented on the Y-axis. An equation describing the relationship between construct copy number and Ct value was generated using the qRT-PCR data and used to determine RET9, RET43 or RET51 copy number in subsequent qRT-PCR reactions.

Table 2.1 Constructs used to generate standard curves. A) The mass of FKBP-L2-9ic (RET9), FKBP-L2-43ic (RET43) and FKBP-L2-51ic (RET51) constructs were calculated and displayed below. These values were used to create 13 standards containing the number of DNA copies shown in B).

A)

	Length (bp)	Mass (g/mol)	Mass (g/copy)	Copies/ng
RET9	6306	4161960	6.9111E-18	144694843.3
RET43	5545	3659700	6.07707E-18	164552873.2
RET51	5678	3747480	6.22284E-18	160698429.3

B)

Standard	Copy #/ul	Copy #/rxn
1	2500000	5000000
2	250000	500000
3	25000	50000
4	2500	5000
5	250	500
6	125	250
7	62.5	125
8	31.25	62.5
9	15.625	31.25
10	7.8125	15.625
11	3.90625	7.8125
12	1.953125	3.90625
13	0.9765625	1.953125

2.5 shRNAs and constructs:

The lentiviral packaging and envelope vectors psPAX2 and pMD2.G, generated by Dr. Didier Trono (Ecole Ploytechnique Fédérale de Lausanne, Switzerland), were obtained from Addgene (Cambridge, Massachusetts). In addition, previously characterized sets of shRNAs, including the RHS4533 and RHS4430 RET shRNA sets (Open Biosystems, Huntsville, Alabama) and SHCLNG-NM_020630 shRNA set (Sigma-Aldrich) were obtained. These shRNA sets were selected because they contained a wide selection of RET-specific shRNAs in pLKO.1 or pGIPz vectors, which could potentially target RET9, RET51 or total-RET for knockdown. The shRNA hairpin sequences were validated using BLAST (http://blast.ncbi.nlm.nih.gov/) to check for potential nonspecific knockdowns. Purified plasmid DNA for each shRNA was isolated using the Qiagen Midiplasmid Prep kit according to manufacturer's instructions, and the utility of individual shRNAs was further validated by transient transfection into TPC-1 cells, as described below. RET knockdown was quantified by qRT-PCR using total RNA from the cells, or by harvesting whole cell lysates and detecting RET protein by immunobloting (see below). Individual shRNAs targeting RET9 or total-RET were found to yield knockdowns between 25 and 40% at the mRNA level, while shRNAs targeting RET51 were found to yield knockdowns between 40 and 60%. A panel of nine shRNA-containing vectors that yielded the greatest knockdown for each of RET9, RET51 and total-RET (3 vectors each) were selected for further characterization (Table 2.2, Figure 2.4). Knockdown was further optimized by co-transfection of multiple selected shRNAs for each target to generate the greatest knockdown. A pLKO.1 vector containing no shRNA was used as an empty vector (EV) control in all transfection and transduction experiments (described below).

Table 2.2 List of selected shRNA clones used for generation of lentiviral particles and for subsequent knockdown experiments. Target sequence identity and specificity was verified using BLAST (http://blast.ncbi.nlm.nih.gov/). Clones 1-3 and 7-9 are available from Open Biosystems (Huntsville, Alabama). Clones 4-6 are available from Sigma-Aldrich (Oakville, Ontario).

#	Clone ID	Target sequence 5'-3'	Target location
1	TRCN0000000405	GCTGCATGAGAACAACTGGAT	RET exon 2
2	TRCN0000040027	CCTGTTTGTGAATGACACCAA	RET exon 7
3	TRCN0000000404	CCGCTGGTGGACTGTAATA	RET exon 17
4	TRCN0000194736	CCATGCATTTACTAGATTCTA	RET9 C-terminus
5	TRCN0000195643	CCAGCAACTTAGGATGGTAGA	RET9 3'UTR
6	TRCN0000194948	CCAGTTTACATTTAGGCATTA	RET9 3'UTR
7	RHS4430-101102412	TAACTATCAAACGTGTCCA	RET51 C-terminus
8	TRCN0000000402	TGGCTCTAATTTGGGCTGTTT	RET51 3'UTR
9	TRCN0000009864	TTGTAATCAAGGTGACTAAGA	RET51 3'UTR

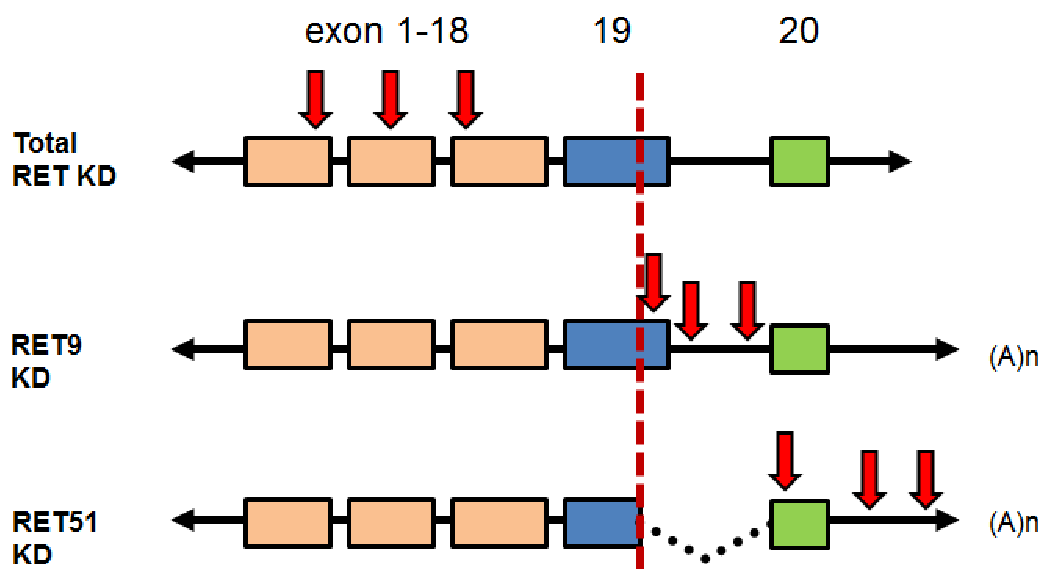

Figure 2.4. Schematic representation of RET locus showing shRNA target sites. Red arrows indicate shRNA target sites for total RET KD, RET9 KD and RET51 KD shRNA sets, as indicated. Note that if RET9 mRNA transcription does not terminate at sites in intron 19 following exon 19 [4], it is possible for RET9 UTR and RET51 coding mRNA sequences to overlap in exon 20, resulting in some cross reactivity between RET51-specific shRNAs and some RET9 transcripts.

2.6 Transfection and selection:

TPC-1 cells cultured to 70% confluence were transiently transfected with either pLKO.1 empty vector, or shRNA constructs targeting RET9, RET51, or total-RET. Transfections were performed in serum-free OptiMEM medium using Lipofectamine 2000 (both Life Technologies) according to manufacturer's instructions. After a 24 hour incubation, the transfection medium was replaced with selection medium (DMEM supplemented with 10% FBS) containing 1µg/mL puromycin (Sigma-Aldrich), and the cells were incubated for an additional 48 hours. The selected cells were then gently washed with warm (37°C) serum free DMEM to remove dead or floating cells prior to harvesting total RNA, as previously described.

2.7 Lentivirus production:

Lentiviral particles were produced using a modified transient transfection protocol. HEK293T packaging cells were grown to 60-70% confluence in 60 mm cell culture dishes (BD Biosciences) containing DMEM supplemented with 10% FBS (Sigma-Aldrich). Prior to transfection, the growth medium was replaced with serum-free OptiMEM (Life Technologies), and the cells were incubated while plasmids were prepared for transfection. An empty pLKO.1 vector, or pLKO.1 containing shRNA for RET9, RET51, or total-RET was prepared for transfection in combination with psPAX2 and pMD2.G packaging and envelope vectors using Lipofectamine 2000 (Life Technologies) according to manufacturer's instructions. Following transfection, the packaging cells were allowed to recover overnight, then the transfection medium was supplemented with FBS to a final concentration of 10%. The medium was harvested every 12 hours for 48 hours, and replaced with DMEM supplemented with 30% FBS after each harvest. The harvested medium was centrifuged at 1000rpm for 10 minutes to remove suspended cells and debris, and passed through a 0.45µm filter (EMD Millipore, Billerica, Massachusetts) to yield lentivirus stock. The purified supernatants were stored at 4°C and pooled following the final harvest. The titre of the pooled lentivirus stock was determined by transducing TPC-1 cells with various volumes of each lentivirus stock and selecting the dilution required for 80-90% cell survival when treated with 2µg/mL puromycin for 48 hours in DMEM supplemented with 10% FBS. Finally, the pooled lentivirus stock was aliquoted and stored at -80°C.

2.8 Transduction and colony selection:

MiaPaCa-2 and TT cell lines were cultured to 50-70% confluence in DMEM supplemented with 10% FBS. Prior to transduction, growth medium was replaced with serum free DMEM supplemented with 8µg/mL polybrene (Sigma-Aldrich). The cells were then transduced with 750µL of virus stock for an empty vector or a set of three shRNA-containing lentiviral particles targeting one of RET9, RET51 or total-RET (Table 2.2). The cells were incubated for 24 hours and then the transduction medium was replaced with selective medium, as described above. TT cells underwent a 14 day selection in DMEM supplemented with 20% FBS, 1% ciprofloxacin, 1% penicillin-streptomycin and 1µg/mL puromycin, and were then maintained in DMEM supplemented with 10% FBS and 1µg/mL puromycin as polyclonal RET-knockdown cell lines. MiaPaCa-2 cells were selected in DMEM supplemented with 10% FBS and 2µg/mL puromycin for a short 48 hour selection in preparation for colony picking. Following this selection, the cells were dissociated from the plate using TrypLE (Life Technologies) and sub-cultured at a dilution of 1:10 in DMEM supplemented with 10% FBS, 1% ciprofloxacin, 1% penicillin-streptomycin and 2µg/mL puromycin to allow for the formation of small clonal colonies. A minimum of 12 colonies of various sizes were dissociated from the plate with TrypLE and cultured individually in DMEM supplemented with 10% FBS and 1µg/mL puromycin to yield clonal RET knockdown cell lines.

2.9 Knockdown quantification:

RET knockdown was quantified whenever possible using qRT-PCR with total-RNA harvested from cells at 70% confluence, as described above. The Delta-Delta Ct (ΔΔCt) method [56] was used to determine the relative fold change in RET expression in response to shRNA mediated knockdown. When shRNA target sites lay outside of the PCR primer amplified gene segment, immunoblotting of RET proteins and densitometric quantification were used as an additional validation step to quantify RET protein levels (below). This is due to a tendency for qRT-PCR to detect cut fragments of RNA in the sample that have not yet been degraded [105], particularly when PCR primers do not flank at least one cut site, and thus return artificially higher Ct values that do not accurately represent the actual quantity of viable mRNA in the sample.

2.10 Immunoblotting and densitometry:

Prior to harvesting, cells were serum starved for 24 hours and either stimulated with 50ng/mL GDNF or ARTN (Peprotech, Rocky Hill, New Jersey) for 30 minutes, or left in serum-free DMEM medium. Whole cell lysates were harvested using lysis buffer (20 mM Tris-HCl pH 7.8, 150 mM NaCl, 1 mM sodium orthovanadate, 1% Igepal, 2 mM EDTA, 1 mM phenylmethylsulfonyl fluoride, 10 µg/mL aprotonin, and 10 µg/mL leupeptin), and protein concentrations were determined using the BCA Protein Assay (Pierce Protein Research, Rockford, Illinois), according to the manufacturer's instructions. Whole cell lysates were mixed with Laemmli buffer (250 mM Tris pH 6.8, 4% SDS, 10% glycerol, 0.006% bromophenol blue, 2% 2-mercaptoethanol), denatured for 5 minutes at 95°C, and separated by electrophoresis on 7% SDS-polyacrylamide gels. Proteins were transferred to nitrocellulose membranes (Bio-Rad Laboratories, Mississauga, ON), and membranes were blocked in 5% milk in Tris-buffered saline with 0.1% Tween-20 (TBST). The blocked membranes were incubated with primary antibody, diluted 1:1500, overnight at 4°C. Primary antibodies used included SC-167-G #H0911 C19 RET9, SC-1290 #J0312 C20 RET51, SC-94 #I2512 ERK, SC-7383 #C2409 phospho-ERK (Santa Cruz Biotechnology, Santa Cruz, California), AKT #9272S, phospho-AKT #4058S, STAT3 #9132L, and phospho-STAT3 #9131L (Cell Signaling Technologies, Danvers, Massachusetts). Tubulin was probed using T6557 #128K4806 Tubulin antibody (Sigma-Aldrich) to serve as a loading control.

After incubation, membranes were washed in TBST to remove unbound primary antibody, and incubated with the appropriate species-specific horse radish peroxidise (HRP)-conjugated secondary antibody at a 1:3000 dilution (Santa Cruz Biotechnology). Bound antibody was detected using Western Lightning Chemiluminescence Reagent Plus (PerkinElmer, Waltham, Massachusetts), and exposed on CURIX Ultra UV-G Plus film (AFGA Healthcare, Toronto, Ontario). Digital images were generated by scanning the films at 600 dpi using an Epson Perfection 4990 photo scanner (Epson, Long Beach, California).

The digital images were used for the quantification of RET knockdown. ImageJ (http://rsbweb.nih.gov/ij/) was used to measure mean pixel intensity of the 175kDa and 155kDa bands representing mature and immature RET protein, respectively, in empty vector transduced control cells. These pixel density values, representing the amount of RET protein in each protein sample, in the absence of RET knockdown, were normalized to tubulin pixel intensity, and then compared to pixel density values from RET shRNA transduced cells to calculate the relative quantity of RET9, RET51 or total-RET remaining following knockdown. Similarly, to quantify the relative change in the quantity of phosphorylated ERK, AKT, or STAT3 in the presence or absence of RET knockdown, the mean pixel intensity of the total and phosphorylated proteins in empty vector control cells were measured and compared to the respective mean pixel intensity of the total and phosphorylated proteins in digitally scanned western blots for each RET knockdown cell line, following normalization to tubulin pixel intensity.

2.11 Cell proliferation assay:

Cell proliferation was evaluated by methylthiazolyldiphenyl-tetrazolium bromide (MTT, Life Technologies) reduction assay using a protocol previously optimized in our lab [52, 104]. Empty vector control, RET9 knockdown, RET51 knockdown or total-RET knockdown cells and parental TT or MiaPaCa-2 cell lines were cultured to 70% confluence, and then dissociated using TrypLE (Life Technologies), as previously desccribed. The dissociated cells were seeded into a 96-well plate at a concentration 1 x 10^4 cells per well in 100µL of DMEM supplemented with 0.1% FBS either with or without 50ng/mL GDNF (Peprotech). The cells were allowed to proliferate for 72 hours prior to the addition of MTT in phosphate-buffered saline (PBS) to a final concentration of 45µg/mL MTT per well. Following an additional 24 hour incubation to allow the cells to metabolize the MTT into insoluble purple formazan, 100µL of 20% SDS acidified with 0.04M HCl was added to each well, and the plate was incubated in complete darkness for 4 hours (room temperature with shaking) in order to lyse the cells and dissolve the formazan solids. The amount of formazan produced by the cells was quantified by measuring the absorbance at 570nm of the resulting solution (ELx 800UV plate reader, Bio-Tex Instruments, Houston, Texas), normalized to empty wells containing only MTT, DMEM and acidified SDS. The absorbance of wells containing empty vector control cell lines was used as a baseline to determine the relative difference in cell proliferation in RET knockdown cell lines.

2.12 Migration and invasion assays:

Motility in MiaPaCa-2 was evaluated preliminarily using a scratch assay with protocols and conditions previously established in our lab [106]. Briefly, cells were cultured to 90-100% confluence, serum starved for 3 hours, and the monolayer of cells was then scratched with a p200 pipette tip. The wounded cell layer was gently washed with warm serum-free DMEM to remove floating cells and debris, and the growth medium was replaced with DMEM supplemented with 0.1% FBS, either with or without 50ng/ml GDNF. Wounds were photographed at several fixed locations every 8 hours for 32 hours. ImageJ software was used to measure the average width of the wound at each time point, and cell migration was expressed as a percentage wound closure relative to empty vector cell migration at 32 hours.

A Boyden Chamber assay was used to evaluate chemotactic response. MiaPaCa-2 and TT cells were cultured to 70% confluence and serum starved for 24 hours prior to the assay. Cells were dissociated using TrypLE, and 5 x 10^4 cells suspended in 100µL of serum free DMEM were seeded into cell culture inserts (PET membrane, 8µm pores, BD Biosciences) fitted in 24-well plates. The cells were then stimulated by adding 750µL of DMEM containing 100ng/mL GDNF or ARTN (both Peprotech) to the lower chamber. Cells seeded into cell culture inserts with 0.1% FBS DMEM added to the lower chamber were used as a negative control, while cells stimulated by the addition of DMEM supplemented with 10 % FBS to the lower chamber were used as a positive control. MiaPaCa-2 cells were incubated for 18 hours, while TT cells were incubated for 72 hours. At the end of the incubation period, the cells adhering to the upper surface of the cell culture insert membrane were removed, and the cells that had migrated through the membrane were fixed with 4% paraformaldehyde (pH 7-8) and stained with 0.25% crystal violet in 20% methanol. The PET membrane was excised from the cell culture insert and mounted on a microscope slide with MOWIOL (EMD Millipore). The chemotactic response of each cell line was determined by counting the total number of cells that had migrated through the pores of the tissue culture insert membrane, and was expressed as a ratio between the experimental condition and the positive control.

Cell invasiveness was evaluated using a modified Boyden chamber assay based on previously established protocol [103, 107]. In this assay, matrigel (BD Biosciences) was used to provide ECM proteins and serve as a barrier to cell invasion. Prior to use, cell culture inserts were chilled at -80°C for 30 minutes and then coated with 40μL of 0.125μg/μL growth factor reduced matrigel diluted in cold (4°C) sterile water (Life Technologies), and allowed to dry overnight at room temperature. These coated cell culture inserts were rehydrated for 1 hour at 37°C prior to cell seeding using 40μL serum-free DMEM. Cell seeding and quantification of invasiveness then proceeded as described above.

2.13 Cell protrusion assay:

Wild type, empty vector, RET9 knockdown, RET51 knockdown, or total-RET knockdown MiaPaCa-2 cells were cultured as previously described and then seeded into 6-well plates at a density of 5 x 10^4 cells per well, and allowed to adhere for 24 hours at 37°C. Cells were starved for 3 hours in serum-free DMEM, and the medium was then supplemented with 0.1% FBS. Experimental cells were additionally stimulated with 50ng/mL GDNF, while cells receiving only 0.1% FBS served as negative controls. The cells were then incubated for 24 hours, and 30 random microscope fields were photographed at 200x magnification. The captured images were analyzed using ImageJ software to calculate average cell protrusion frequency and length as follows: The total number of observed cell protrusions, defined as a thin projection extending from the body of a cell a distance exceeding one cell body in length, was recorded and divided by the total number of cells visible to determine the cell protrusion frequency (average number of cell protrusions per cell) for each cell line in the presence or absence of GDNF. Changes in cell protrusion frequency in response to RET knockdown were expressed as a ratio of knockdown cell protrusion frequency relative to the cell protrusion frequencies of empty vector control or wild type cell lines.

Cell protrusion length was measured by tracing the length of an protrusion from the center of a cell body to its point of termination, as described in existing cell protrusion tracing and quantification software [108]. This length, represented in pixels, was determined for every cell containing protrusions and averaged across 30 microscope fields for each experimental condition to yield an average cell protrusion length for each cell line in the presence or absence of GDNF. Changes in cell protrusion length were determined by a ratio between average protrusion length of RET knockdown cell lines and control empty vector or wild type cell lines.

2.14 Significance analyses:

Results are expressed as mean ± standard error of the mean. A two-tailed unpaired student's t-test was used to determine statistical significance. Significance was set at $p < 0.05$. Unless otherwise noted, a minimum of three experimental replicates with three technical replicates each were performed for each assay.

Chapter 3. Results

3.1 Endogenous RET expression in human cell lines

As described above, total RNA was harvested from PanC-1, MiaPaCa-2, SK-N-SH, SH-SY-5Y, TT and TPC-1 human cell lines for use in qRT-PCR quantification of endogenous RET isoform expression. These cell lines represent several cell types in which RET activation may have clinical relevance. For example, GDNF/RET activity has been shown to have strong influence on the invasion and adhesion of pancreatic carcinoma cell lines [103]. SK-N-SH, and its subclone SH-SY5Y, are neural cell lines, and represent a cell type in which RET activity has been shown to be critical for survival, migration and differentiation [76, 109, 110]. TPC-1 and TT cells are representative of thyroid carcinomas where constitutively active RET has been linked to disease phenotype and progression [66, 74].

We first quantified the expression level of individual RET isoforms in wild-type cell lines. All cell lines were found to co-express the transcripts for the three isoforms of RET, with RET9, and RET51 comprising the majority of RET expression, and RET43 expressed only at low levels (Figure 3.1). With the exception of TPC-1, all cell lines expressed RET9 at approximately twice the level of RET51, while the TPC-1 thyroid carcinoma cell line was found to express RET9 and RET51 at similar levels (Figure 3.1). The RET43 transcript was found to comprise fewer than 10% of total RET transcripts in all cell lines.

We did not detect any relationship between cell growth rate and RET expression in the cell lines selected for this project. TPC-1 thyroid and MiaPaCa-2 PDAC cell lines were found to grow extremely quickly, but expressed very high, and very low quantities of RET, respectively.

Similarly, both TT and PanC-1 expressed high levels of RET, but while PanC-1 cells typically reached confluence within days of subculturing, TT cells grew at an extremely slow pace, despite possessing the highest overall RET expression among all cell lines examined (Figure 3.1). Following quantification of RET isoform transcript expression across a range of cell types, we proceeded with isoform specific knockdown using shRNA carrying lentiviral particles in only MiaPaCa-2 and TT cells due to slow growth of neuroblastoma cells, and the lack of wild type RET expression in the RET/PTC cell line TPC-1.

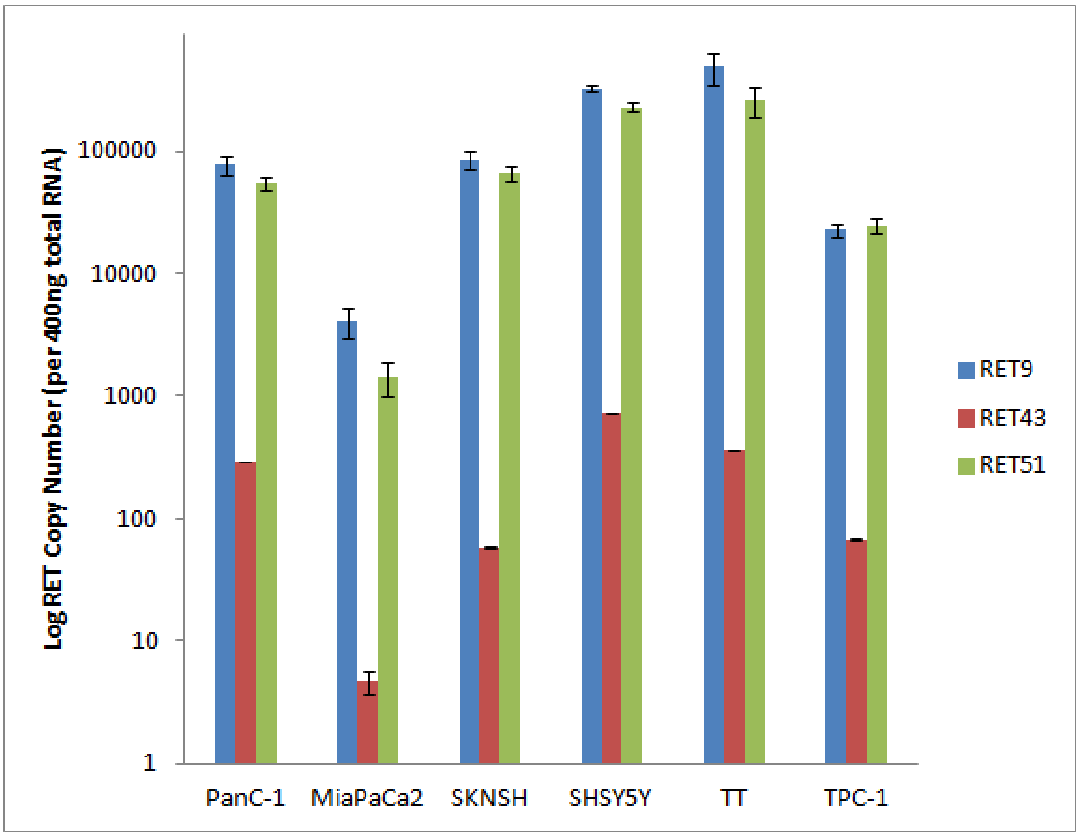

Figure 3.1 RET isoform expression in human carcinoma cell lines. Relative expression levels of RET9, RET43 and RET51 transcripts in MiaPaCa2 & PanC-1 pancreatic carcinoma, SK-N-SH & SH-SY5Y neuroblastoma, and TPC-1 and TT thyroid carcinoma human cell lines. Error bars represent standard error across a minimum of three PCR reactions.

3.2 Quantification of isoform specific RET knockdown in Pancreatic & Thyroid carcinoma cell lines

We used lentiviral particles to generate stable isoform specific knockdowns in extremely slow-growing and difficult to transduce cell lines such as the TT thyroid carcinoma line. To take full advantage of this tool, we chose TT cells and MiaPaCa-2 PDAC cells to explore the functions of RET and its isoforms two distinct cell models. One where RET is a driver of tumourigenesis, and the other where is sporadically expressed, but may still contribute to tumour aggressiveness.

Thyroid carcinoma (TT cells): To determine the effect of isoform specific RET knockdown in the MEN 2A thyroid carcinoma TT cell line, lentiviral particles containing shRNA constructs specific for RET9, RET51 or total-RET were stably transduced into TT cells and transduced cells were selected for using puromycin as previously described. RNA was harvested from the resulting polyclonal knockdown (KD) cell lines and relative RET KD compared to control (EV) cells was quantified by densitometry, as previously described, with standard PCR (10 cycles). RET9 and RET51 specific knockdowns appeared to reduce each RET isoform mRNA expression by approximately 60% relative to control empty vector (Figure 3.2A, B). Isoform specific KD was confirmed in whole cells by Mathieu Crupi using immunofluorescence and confocal microscopy for RET9 and RET51 (Personal communication; Figure 3.2C). We were unable to quantify the extent of total-RET knockdown in TT cells as these conditions led to cell death in this cell line (Figure 3.3A). Following quantification of RET knockdown cell lines, all TT RET knockdown cell lines were examined for morphological changes. Under normal culture conditions, wild type (WT) TT cells appeared to form two distinct populations of cells: an adherent population, and a free-floating population capable of reattaching to the tissue culture dish to form new colonies. RET9 KD, RET51 KD cells and empty vector (EV) transduced control cells were morphologically similar to WT cells and displayed a clumping growth habit, where cells were observed clustered together and in direct contact with adjacent cells (Figure 3.3 A, B). When TT cells were subjected to total-RET KD, we observed a dramatic morphological change. The cells appeared smaller and no longer exhibited clumping. Instead, the total-RET knockdown cells were more evenly distributed over the surface of the tissue culture plate, with very few cells in direct contact with other cells. These cells did not appear to proliferate, and the cell density in the plate declined over a period of approximately 2 weeks, at which point very few living cells could be found.

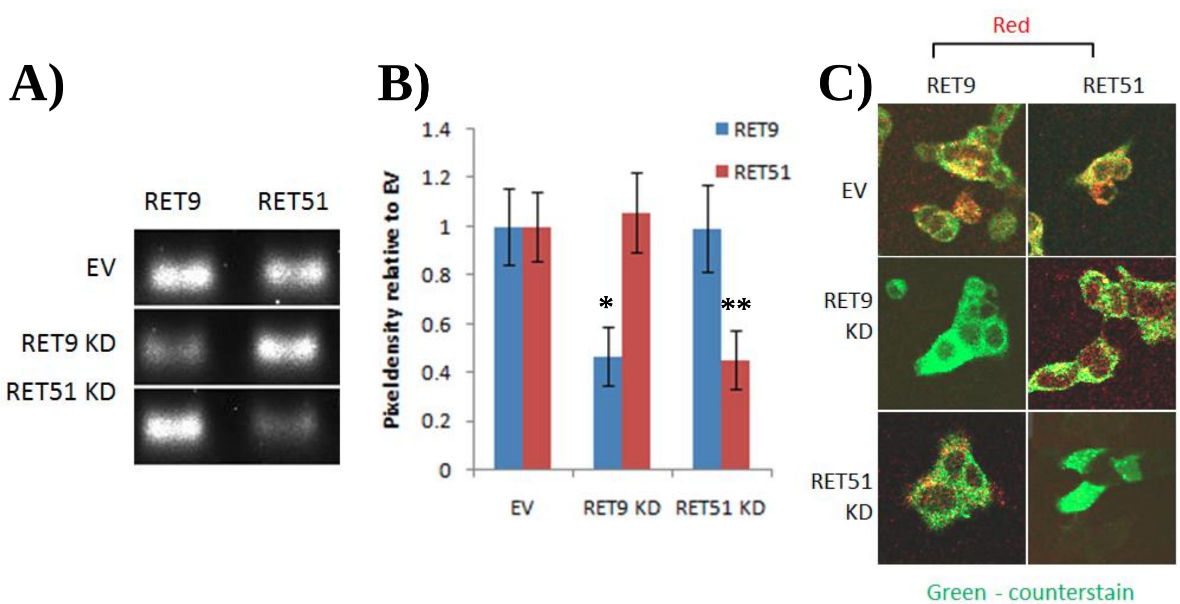

Figure 3.2 Quantification of RET knockdown in TT cells. A) PCR amplification products generated using RET9 or RET51-specific primers and total RNA from empty vector (EV), RET9 knockdown (RET9 KD) and RET51 knockdown (RET51 KD). **B)** Densitometric quantification of pixel intensities of the bands in A) and additional experimental replicates relative to EV. The pixel densities of RET9 KD and RET51 KD PCR products when amplified with RET9 or RET51 PCR primer were significantly lower relative to their respective EV levels (* $p = 0.02$ and ** $p = 0.01$). Error bars represent standard error across a minimum of three experimental replicates. **C)** Confocal immunofluorescence detection of RET9 (C19 antibody) and RET51 (C20 antibody), visualized using Alexa Fluor fluorescent secondary antibodies (Life Technologies, Burlington, Ontario), shown in red. Counterstained using TGN38 trans-Golgi network protein 2 antibody (Santa Cruz Biotechnologies), shown in green. Fluorescent microscopy performed by MathieuCrupi (Mulligan Lab).

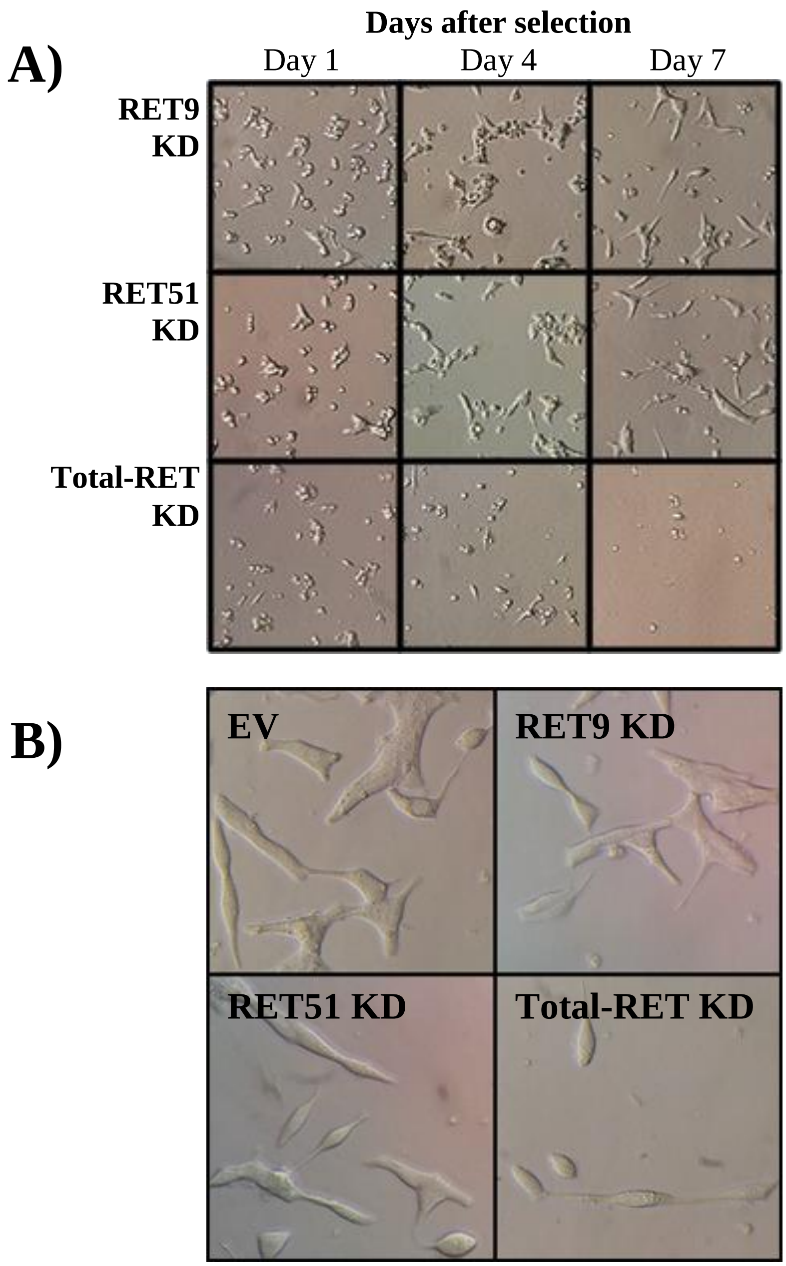

Figure 3.3 Morphological changes in TT cells in response to RET knockdown. A) TT cells with the indicated RET knockdown (KD) following selection with 1µg/mL puromycin, are shown at 100x magnification. Healthy cells appear either flat or spindle-like. RET9 and RET51 KD cells eventually recover from KD and selection, shown as an increasing number of healthy cells, while total-RET KD cells do not. RET 9 KD and RET51 KD cells exhibit a clumping growth habit which is lost in total-RET KD. **B)** TT cells with indicated RET KD shown at 400x magnification. Photos taken 4 days following selection with 1µg/mL puromycin for 2 weeks. Empty vector (EV) transduced cells, RET9 and RET51 KD cells are morphologically similar and display characteristic cell protrusions visible as thin projections extending outward from the cell body. Total-RET KD cells appear smaller than EV, RET9 KD or RET51 KD cells, but continue to form cell protrusions.

Pancreatic adenocarcinoma (MiaPaCa-2): MiaPaCa-2 cells were transduced with RET9, RET51, total-RET or empty vector shRNA constructs as previously described, and colony selection was performed to generate multiple clonal cell lines containing isoform specific knockdowns. The effectiveness of RET isoform knockdown was quantified by both qRT-PCR and western blot (Figure 3.4). Transduction of empty vector (EV) did not alter RET9 or RET51 expression relative to parental wild type (WT) MiaPaCa-2 ($p = 0.15$ and 0.09 respectively). Simultaneous transduction of three shRNAs for RET9 or RET51, targeting the isoform-specific C-termini and 3' UTRs, was found to significantly reduce expression of the targeted isoform ($p = 0.005$ and 0.001 for RET9 and RET51 respectively) to approximately 40% of WT expression at the mRNA level (Figure 3.4A), and 20% of WT expression at the protein level (Figure 3.4B). Due to overlapping sequences in RET9 and RET51 mRNA transcripts, some cross reactivity was noted for shRNAs targeting RET51 (Figure 2.4). These shRNAs were found to reduce RET9 mRNA by approximately 20% (Figure 3.4A), and RET9 protein by 50% (Figure 3.4B, C). Total-RET knockdown was also achieved using a combination of three shRNAs targeting exons 2, 7 and 17 of RET (Table 2.2, Figure 2.4). These shRNAs were found to reduce the levels of RET9 and RET51 mRNAs by 60% and 80% respectively, and protein levels by 90% and 95% respectively ($p = 0.005$ for RET9 and 0.001 for RET51).

Upon knockdown of either a single RET isoform or total RET, striking morphological changes were observed in MiaPaCa-2 cells (Figure 3.5). Wild type (WT) and empty vector transduced control cells (EV) typically maintained a spindle-like morphology and appeared to have dark outline which runs the perimeter of the cell when observed via bright field microscopy, indicative of a rounded, thick cell profile. WT and EV cells also prominently displayed the formation of long hair-like cell protrusions visible as dark coloured filaments extending from the cell body. When MiaPaCa-2 was subjected to RET9, RET51, or total-RET KD, the cells took on an increasingly flattened morphology and appeared to form shorter and fewer cell protrusions. Cells appeared to respond differently to each isoform specific knockdown. RET9 KD cells appeared morphologically similar to WT/EV cells, while RET51 KD cells began to lose their spindle-like shape and took on a more noticeably flattened morphology. The most severe change in cell morphology were observed in total-RET KD cells. These cells appeared completely flat and scale-like, and appeared to form very few cell protrusions (Figure 3.5).

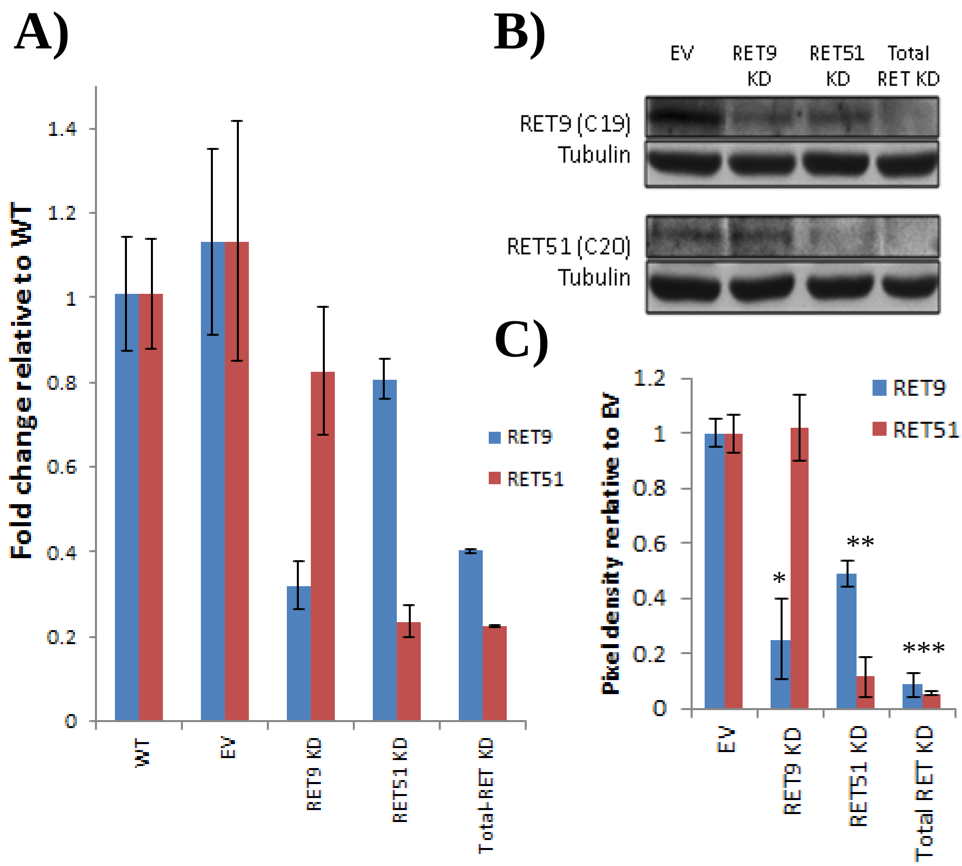

Figure 3.4 Quantification of RET knockdown in MiaPaCa-2. A) RET9, RET51 and total-RET knockdown (KD) in selected MiaPaCa-2 cell lines, quantified using qRT-PCR as previously described. Fold change in RET isoform expression was determined using ΔΔCt relative to parental wild type (WT) cells with *GUSB* as a reference gene. Error bars represent minimum and maximum range of fold change as determined via ΔΔCt across a minimum of three experimental replicates. **B)** Representative immunoblot for RET9 and RET51 protein in the indicated RET KD MiaPaCa-2 cell lines using total cell lysates probed for RET9 (C19 antibody) or RET51 (C20 antibody). Tubulin serves as a loading control. **C)** RET protein levels, normalized to tubulin expression and expressed relative to empty vector (EV). RET9 KD using 3 shRNA containing lentiviral vectors resulted in a significant reduction in RET9 protein relative to EV (*$p = 1.3 \times 10^{-4}$). RET51 KD using a different set of 3 shRNAs significantly reduced both RET9 and RET51 protein levels relative to EV (**$p = 3.6 \times 10^{-4}$, and 1.0×10^{-4} respectively). Both RET9 and RET51 protein levels were also significantly reduced by total RET KD (***$p = 2.7 \times 10^{-5}$ and 7.8×10^{-5} respectively). No significant change in RET9 or RET51 protein levels were found between WT and EV cells ($p = 0.15$ and 0.09 respectively, not shown). Error bars represent standard error across a minimum of three replicates.

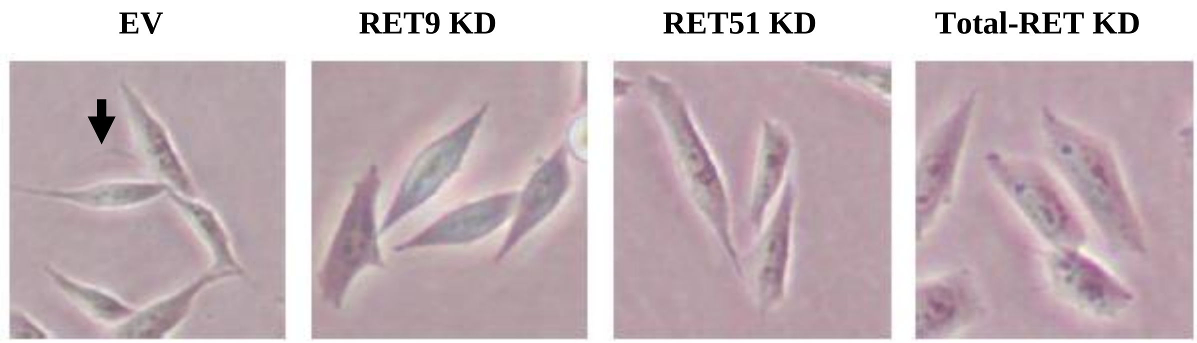

Figure 3.6 Morphological changes in MiaPaCa-2 in response to RET knockdown. Typical morphologies of MiaPaCa2 with the indicated RET KD or EV are shown at 400x magnification using bright field microscopy. Empty vector control (EV) cells appeared spindly and formed cell protrusions visible as thin hair-like projections (typical protrusion indicated with arrow). Cells became flatter and cell protrusions appeared shorter with RET9 KD, RET51 KD and total-RET KD. Total-RET KD cells were no longer thin and spindle-like, and more closely resemble scale-like epithelial cells.

Total-RET knockdown in MiaPaCa-2 increases expression of E-cadherin:

The morphological changes observed in total-RET KD cells were similar to changes noted for cells undergoing processes such as mesenchymal to epithelial transition (MET) [111]. In order to determine whether changes observed were due to MET, we evaluated the expression of E-cadherin by qRT-PCR and determined fold change in E-cadherin mRNA expression relative to EV cells by the $\Delta\Delta$Ct method. E-cadherin expression appeared to decrease with RET9 or RET51 KD, although the observed decreases were not statistically significant ($p = 0.15$ and 0.08 respectively) (Figure 3.6). However, E-cadherin expression increased significantly relative to EV (up to 1.7 fold) when total-RET was knocked down ($p = 0.02$)

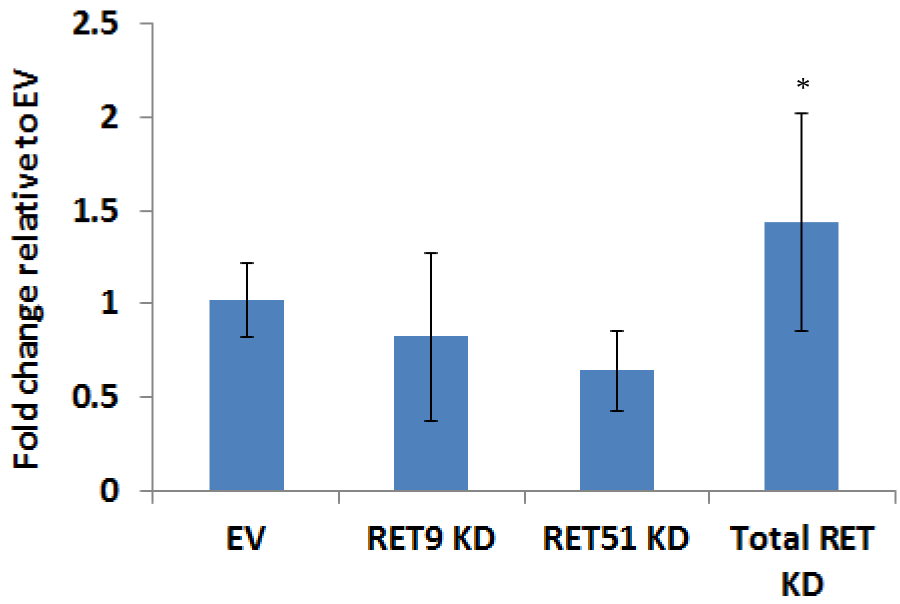

Figure 3.6 Quantification of E-Cadherin expression in MiaPaCa-2 knockdown (KD) cell lines. E-cadherin expression levels are shown as fold change relative to empty vector (EV) control cells. Fold change was determined using ΔΔCt with *GUSB* as a reference gene. Error bars represent minimum and maximum range of fold change as determined by ΔΔCt. No significant difference in E-cadherin expression relative to EV was found for either RET9 KD or RET51 KD cells ($p = 0.15$ and 0.08 respectively). Total RET KD cells expressed significantly greater amounts of E-cadherin relative to EV ($p = 0.02$). Values averaged across a minimum of three experimental replicates.

3.3 Effect of RET knockdown on cell proliferation

Single isoform RET knockdown reduces TT cell proliferation: The effect of single isoform RET knockdown was assessed in TT cells using an MTT assay with polyclonal stably transduced RET9 or RET51 KD cell lines and compared to an EV transduced control cell line. EV cells displayed significantly reduced cell proliferation in response to stimulation by 50ng/mL GDNF relative to unstimulated cells (Figure 3.7, $p = 0.04$). This reduction in cell proliferation in response to GDNF was also observed in RET9 and RET51 KD cells, however, the response was not as pronounced as was observed in EV cells, suggesting it was RET dependent. GDNF-treated RET9 or RET51 KD cell lines did not proliferate significantly less than untreated RET9 or RET51 KD ($p = 0.07$ for both). Overall, both RET9 and RET51 KD were found to significantly reduce cell proliferation in all conditions relative to EV cells ($p = 0.04$, $p = 0.02$ and $p = 0.03$ for cells treated with 10% FBS, 50ng/mL GDNF and 0.1% FBS respectively). No statistically significant difference was observed between RET9 KD and RET51 KD cell lines, however RET51 KD cells appeared to proliferate slightly less than RET9 KD cells across all conditions.

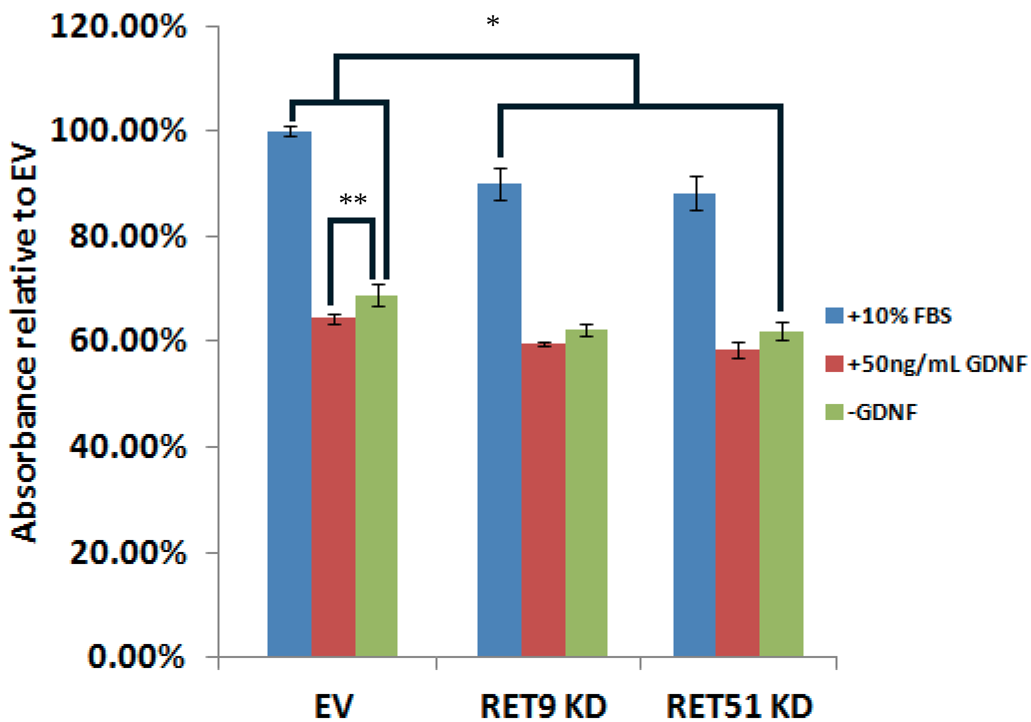

Figure 3.7 MTT assay of RET9 or RET51 knockdown (KD) polyclonal TT cell lines. Proliferation is represented relative to empty vector (EV) transduced control cells cultured with 10% FBS. RET9 KD and RET51 KD cell lines exhibited significantly reduced proliferation with respect to EV in all culture conditions (* +10% FBS $p = 0.04$; +50ng/mL GDNF $p = 0.02$; -GDNF $p = 0.03$). In EV cells, proliferation was slightly reduced by stimulation with 50ng/mL GDNF in comparison to the –GDNF control (** $p = 0.04$). This change in proliferation was also observed in RET9 KD and RET51 KD cells, but was not found to be statistically significant ($p = 0.07$). Similarly, RET51 KD cell proliferation was slightly reduced from RET9 KD across all conditions, but no statistical significance was found. Error bars represent standard error across

three experimental replicates. Statistical significance determined using a two-tailed student's t-test.

Single isoform or total-RET knockdown has no effect on MiaPaCa-2 cell proliferation: An MTT assay was performed on selected MiaPaCa-2 clonal cell lines as previously described. Unstimulated EV transduced cells were used as a baseline for cell proliferation. No significant changes in cell proliferation were found in response to RET9, RET51 or total-RET KD in the presence or absence of stimulation by 50ng/mL GDNF (Figure 3.8).

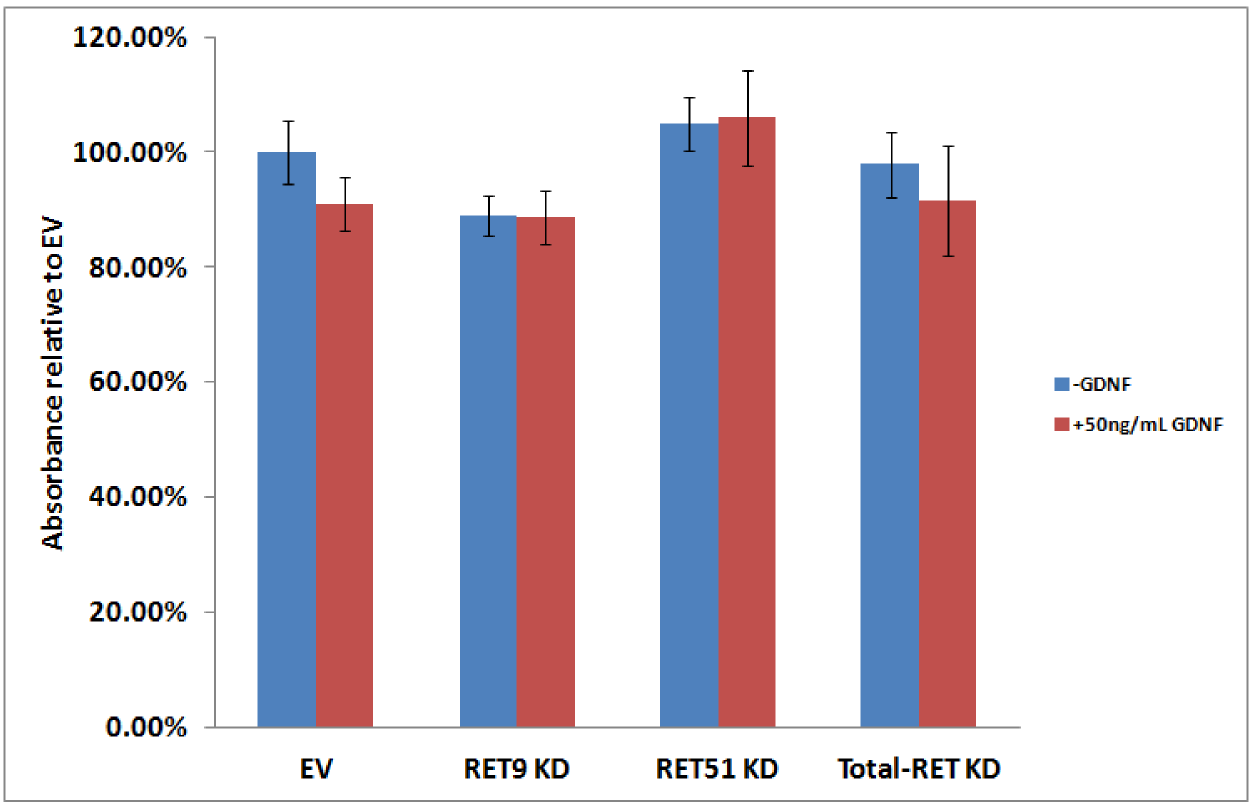

Figure 3.8 MTT assay of clonal RET9 KD, RET51 KD or total-RET KD MiaPaCa2 cells. Cell proliferation for the indicated cell lines is shown relative to that of unstimulated (-GDNF) empty vector (EV) control cells and is expressed as relative absorbance at 570nm. No significant differences in cell proliferation were found under any condition. Error bars represent standard error over a minimum of three replicates.

3.4 Effect of RET knockdown on cell migration & invasion

Single isoform RET knockdown reduces chemotactic response in TT cells: TT cell migration was evaluated using a Boyden chamber assay as previously described. A baseline for cell motility was established by quantifying cell migration through the cell culture insert membrane using unstimulated EV control cells cultured in DMEM supplemented with 0.5% FBS (-GDNF condition, Figure 3.9). Using this baseline, represented as 100%, cell motility in both RET9 KD and RET51 KD cells cultured in similar conditions was slightly reduced (87% and 81% the baseline migration of EV cells respectively), but the reduction in cell migration was not statistically significant ($p = 0.08$) (Figure 3.9). When the cells were stimulated by addition of medium supplemented with 100ng/mL GDNF to the lower chamber, a 51% reduction in cell migration was observed in EV cells ($p = 0.004$). No reduction in cell migration was observed in either RET9 KD or RET51 KD cells, which migrated at 92% and 79% of the established baseline, respectively. Initially, we expected that the addition of GDNF to the lower chamber would increase cell migration through the cell culture insert, so DMEM supplemented with 10% FBS added to the lower chamber was selected as a positive control. Under these conditions however, EV cells displayed a 69% decrease in cell migration which was significantly reduced from both the baseline and 100ng/mL GDNF conditions ($p = 0.001$ & 0.005, respectively). Both RET9 KD and RET51 KD also displayed significantly reduced cell migration when stimulated with 10% FBS. RET9 KD cell migration was reduced from the baseline by 90%, and RET51 by 83% both being significantly different from EV cell migration in 10% FBS ($p = 0.02$ and 0.04, respectively). Except when stimulated with 10% FBS, RET9 KD cell migration was not different from RET51 KD cell migration in all conditions. When DMEM supplemented with 10% FBS was added to the lower chamber, RET9 KD cells displayed significantly lower levels of cell migration than RET51 KD cells (10% and 17% migration respectively, p = 0.02).

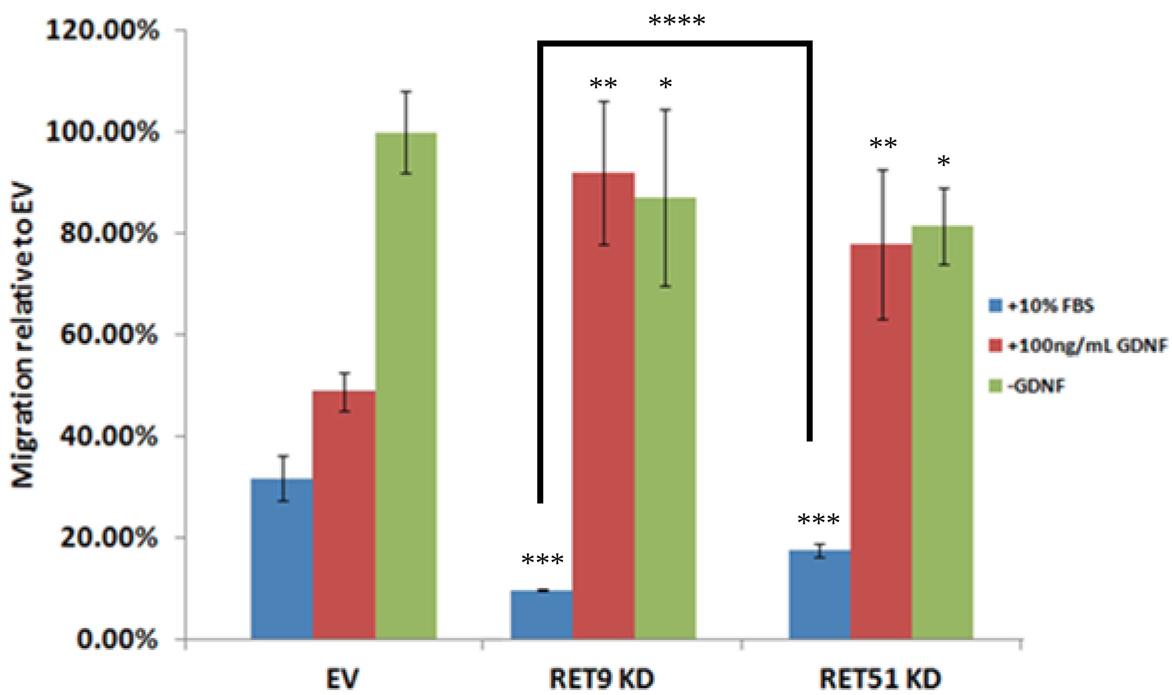

Figure 3.9 Migration assay of RET KD TT cells. Migration of indicated TT polyclonal lines relative to EV lines. All values are represented as a percentage of EV cell migration through an uncoated cell culture insert (8µm pores) in 0.5% FBS (–GDNF) conditions. RET9 and RET51 KD cell migration was not significantly different relative to EV cells (* p = 0.08). EV cells displayed significantly reduced migration when stimulated with 100ng/mL GDNF or 10% FBS, with cell migration reduced by 51% or 69% respectively (** p = 0.005, *** p = 0.001). RET9 KD and RET51 KD cells did not display reduced cell migration when stimulated with GDNF, but did show significantly reduced migration when stimulated with 10% FBS (***p =0.004 and p = 0.005 respectively). RET9 KD and RET51 KD cell migration was significantly different only when stimulated with 10% FBS, with RET9 KD cells displaying a significantly greater reduction in cell migration than RET51 KD cells (****p = 0.01). Significance was determined using a two-tailed student's t-test. Error bars represent standard error over a minimum of three replicates.

Single isoform RET knockdown reduces invasiveness in TT cells: A modified Boyden chamber assay was designed to evaluate TT cell invasiveness in response to single isoform RET KD. Cell culture inserts with 8µm pores were coated with 5µg matrigel. RET9 KD, RET51 KD, or EV control cells were seeded into the cell culture insert and 100ng/mL GDNF in 0.5% FBS DMEM was added to the lower chamber to induce invasion through the matrigel. DMEM supplemented with either 0.5% or 10% FBS was added to the lower chamber of negative or positive controls, respectively. A baseline for cell invasion established using EV cells stimulated by DMEM with 100ng/mL GDNF added to the lower chamber was used to represent 100% cell invasiveness (Figure 3.10). Neither EV or RET KD cells were found to invade through the matrigel and membrane pores under either 10% FBS or 0.5% FBS control conditions. When stimulated with GDNF, both RET9 KD and RET51 KD cells were significantly less invasive than GDNF stimulated EV cells (20% and 17% of EV cell invasiveness, respectively, p = 0.01 and 0.003, respectively). Although RET51 KD cell invasion appeared to be slightly less than that of RET9 KD cells, invasiveness was not found to be significantly different between RET9 KD and RET51 KD under similar conditions (p = 0.29).

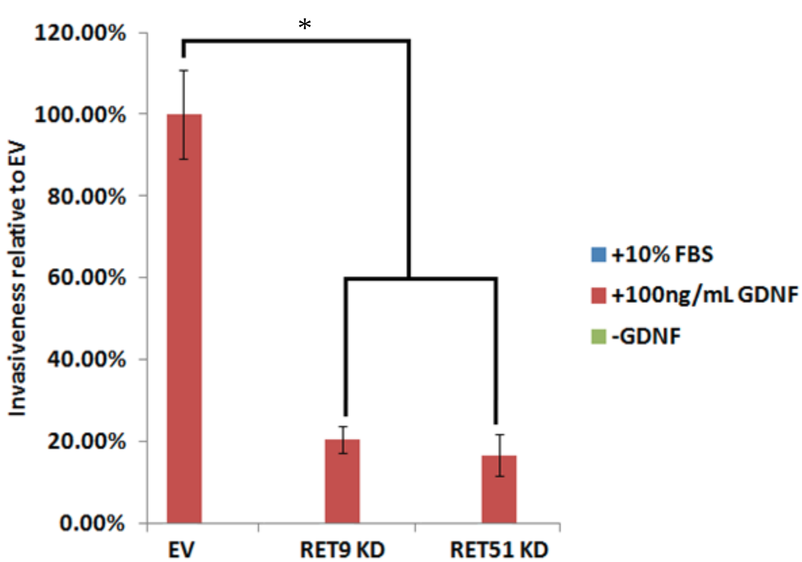

Figure 3.10 TT cell invasion through matrigel determined using a modified Boyden chamber assay. No cells were found to invade in unstimulated 0.5% FBS (-GDNF) or +10% FBS controls. EV control cells stimulated with 100ng/mL GDNF were used as a baseline for invasion (100% invasiveness). A significant decrease in invasiveness was found for RET9 KD and RET51 KD cell lines (*p = 0.01 and 0.03, respectively). Error bars represent standard error over a minimum of three experimental replicates.

MiaPaCa-2 cells show decreased migration following total-RET knockdown: A scratch assay was used to determine the effects of RET knockdown on cell migration. MiaPaCa-2 cells were grown to confluence and the monolayer of cells was wounded and monitored as previously described. Total-RET knockdown cells displayed the flattened morphology described previously (Figure 3.5), and did not appear to form as many cell protrusions into the wounded region (Figure 3.11A). Detailed wound closure measurements made with ImageJ software showed no significant differences in wound closure for any of WT, EV and RET9 KD cell lines following 32 hours of incubation (Figure 3.11B). RET51 KD cell line, however, was able to migrate significantly more than either WT or EV controls both when stimulated with 50ng/mL GDNF in DMEM ($p = 0.03$) and when left unstimulated in serum-free DMEM ($p = 0.04$), resulting in greater wound closure after 32 hours (Figure 3.11.B). A similar trend was observed in RET9 KD cells, but the increased migration did not result in statistically significant difference in wound closure relative to EV (-GDNF $p = 0.35$ and +GDNF $p = 0.26$) or WT (-GDNF $p = 0.47$ and +GDNF $p = 0.25$) cells following 32 hours of incubation. The total-RET knockdown cell line was the only cell line to display reduced wound closure relative to EV, both when unstimulated, and when stimulated with 50ng/mL GDNF ($p = 0.01$ and 0.008, respectively).

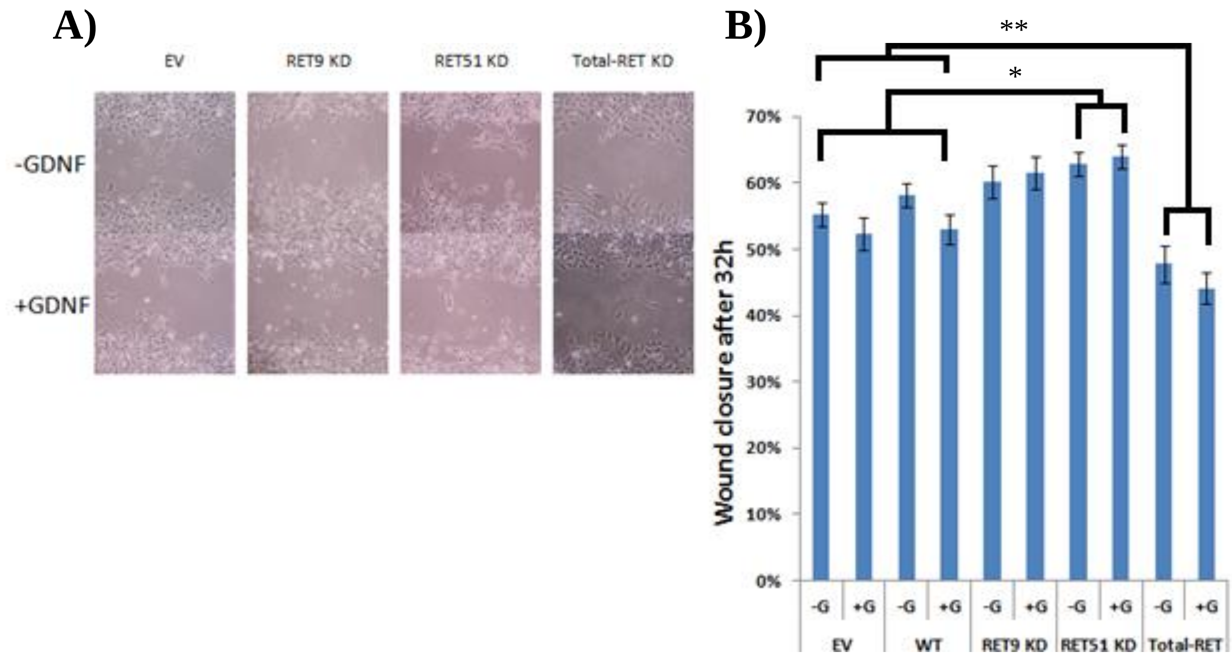

Figure 3.11 MiaPaCa-2 migration in 2D. A) Representative scratch assays showing wound diameter 32 hours following initial wounding for empty vector (EV) control and knockdown MiaPaCa2 cell monolayers. Cells were grown to confluence and serum starved 3 hours before wounding in the presence of 50ng/mL GDNF (+GDNF) or were left unstimulated (-GDNF). Cells shown at 100x magnification. **B)** Percentage wound closure determined using ImageJ software as previously described. No significant difference in wound closure was found between the wild type (WT), EV and RET9 KD cell lines either with or without GDNF stimulation (+G and -G, respectively). RET51 KD cell lines migrated into the scratch wound significantly more than either WT or EV controls, both when stimulated with GDNF or left unstimulated (* p = 0.04 and 0.03, respectively). A significant reduction in wound closure with respect to EV cells was observed in total RET knockdown cells in both GDNF stimulated and unstimulated conditions (**p = 0.008 and 0.01 respectively). Error bars represent standard error over a minimum of three experimental replicates.

RET knockdown decreases cell protrusion frequency and cell protrusion length in MiaPaCa-2 cells: In order to further characterize the decrease in cell protrusion formation observed during the scratch assay, a cell protrusion assay was performed, as previously described. Stimulation of empty vector (EV) control cell lines with 50ng/mL GDNF was found to both increase cell protrusion frequency, and increase the length of cell protrusions relative to unstimulated EV cells (Figure 3.12A, B). GDNF stimulated RET9 KD and RET51 KD cell lines produced significantly fewer cell protrusions compared to stimulated EV cells ($p = 0.01$ and 7×10^{-4}, respectively). Additionally, the protrusions were significantly shorter in both isoform-specific KD cell lines ($p = 0.003$ and 2.8×10^{-7}, respectively). No significant difference in cell protrusion frequency was found between RET9 KD and RET51 KD cell lines, however, the cell protrusions produced by RET51 KD cells were significantly shorter than those produced by RET9 KD cells ($p = 0.01$). The total-RET KD cell line was found to form the fewest cell protrusions ($p = 1.8 \times 10^{-12}$), as well as the shortest overall cell protrusions ($p = 3.7 \times 10^{-20}$). The same morphological changes observed previously upon RET knockdown (Figure 3.5) were again seen during the cell protrusion assay under both unstimulated and GDNF stimulated conditions. EV cells appeared spindly when unstimulated, and formed long dark cell protrusions upon stimulation with GDNF (Figure 3.12C). These cell protrusions typically extended from the ends of the spindle-like cell, emerging from cone shaped structures on the cell body. RET9 KD cells appeared morphologically similar to EV cells, but RET51 KD cells were noticeably more flattened and formed shorter cell protrusions. Total-RET knockdown cells were completely flattened in the absence of GDNF, but recovered a slightly more spindle-like morphology when stimulated. Under both conditions, however, total-RET KD cells formed virtually no cell protrusions, and instead formed short cone-like protrusions on the cell body (Figure 3.12D).

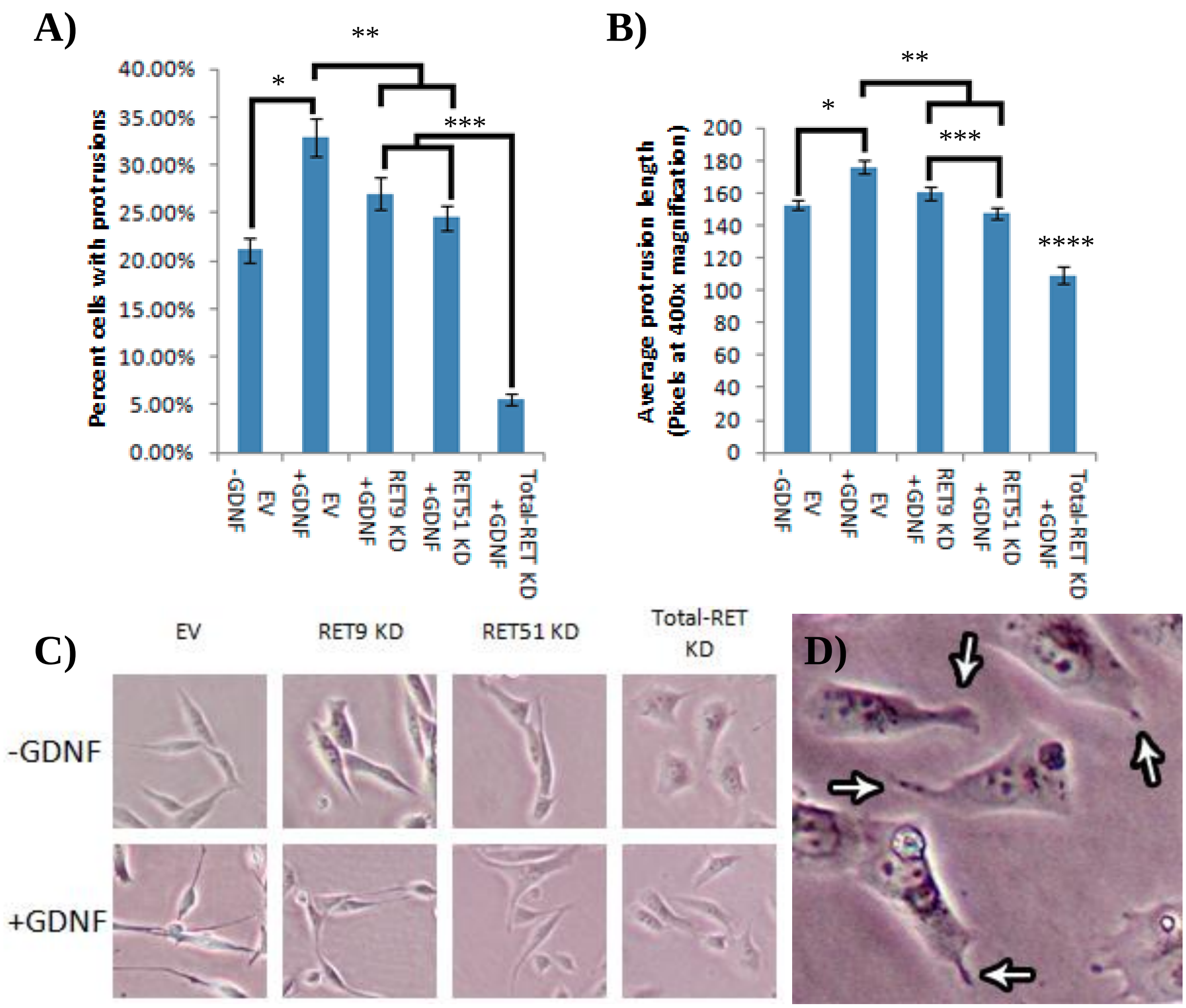

Figure 3.12 MiaPaCa-2 cell protrusion formation. A) Cell protrusion assay using control and knockdown MiaPaCa-2 cells. Cells were serum starved 3h prior to 24h incubation in the presence of GDNF (+GDNF) or left unstimulated (-GDNF). Empty vector cells (EV) stimulated with GDNF were found to form significantly more cell protrusions relative to unstimulated EV cells (*p = 6.9 x 10^{-6}). Both RET9 and RET51 KD cell lines formed fewer cell protrusions than stimulated EV cells (**p = 0.01 and 7 x 10^{-4}, respectively), but no significant difference in cell protrusion frequency was observed between RET9 KD and RET51 KD (p = 0.18). Total-RET KD cells were found to form the fewest cell protrusions (***p = 1.8 x 10^{-12}). **B)** Treatment with 50ng/mL GDNF was found to significantly increase cell protrusion length in EV cells versus an unstimulated EV control (*p = 7.8 x 10^{-6}). GDNF stimulated RET9 KD and RET51 KD cell lines were found to form significantly shorter protrusions compared to GDNF stimulated EV (**p = 0.003 and 2.8 x 10^{-7}, respectively). Cell protrusion length was also found to be significantly different between RET9 KD and RET51 KD, with RET51 KD cells forming shorter protrusions (***p = 0.01). Total-RET KD cells were found to form the shortest cell protrusions (****p = 3.7 x 10^{-20}). **C)** Typical cell morphology after 24 hours of incubation under indicated conditions. Shown at 400x magnification. **D)** Cone-like protrusions formed by total-RET knockdown cells shown at 400x magnification (indicated by arrows).

Total-RET knockdown in MiaPaCa-2 cells decreases cell invasion through matrigel matrix: An invasion assay was performed to further investigate the effects of RET knockdown on MiaPaCa-2 cells, using a modified Boyden Chamber protocol as previously described. Unstimulated empty vector (EV) transduced MiaPaCa-2 cells in serum-free DMEM were used to determine a baseline (100% cell invasion) for relative cell invasion through matrigel coated cell culture inserts (Figure 3.13A). EV cells stimulated by the addition of 100ng/mL GDNF to the lower chamber of the cell culture dish significantly increased in invasiveness to 171% of the baseline ($p = 0.005$). Relative to unstimulated EV cells, RET9 KD cells displayed significantly decreased cell invasiveness both when unstimulated, and when stimulated (39% and 63% of baseline, $p = 0.001$ and 7.4×10^{-4}, respectively). Similarly, RET51 KD cells showed decreased invasiveness in both unstimulated and stimulated conditions (36% and 57% of baseline, $p = 0.001$ for both). With the exception of total-RET KD cells, which did not show a measurable response, all other cell lines showed significant increases in cell invasion in response to stimulation by 100ng/mL GDNF ($p = 0.02$ and 0.01 for RET9 KD and RET51 KD, respectively). Total-RET knockdown cells invaded significantly less than EV, RET9 KD and RET51 KD both when unstimulated (*** -GDNF $p = 1.5 \times 10^{-3}$, 9.2×10^{-5} and 1.0×10^{-3}, respectively) and when stimulated (*** +GDNF $p = 1.5 \times 10^{-3}$, 2.1×10^{-6} and 3.7×10^{-3}, respectively). When left unstimulated, total-RET KD cells were found to invade very little (11% of baseline), and there did not appear to be a significant increase in cell invasion upon stimulation with GDNF (12% of baseline, $p = 0.37$). No statistically significant difference in invasiveness was observed between RET9 KD and RET51 KD cells in either unstimulated or GDNF stimulated conditions (-GDNF $p = 0.07$ and +GDNF $p = 0.08$), however RET51 KD cell invasiveness when stimulated with GDNF was consistently slightly lower than that for RET9 KD cells.

Significantly greater levels of cell invasion through matrigel were observed when the invasion assay was repeated using the GFL artemin (ARTN) in place of GDNF. Unstimulated EV cells were used as the baseline for cell invasiveness in both GDNF and ARTN invasion assays. Unstimulated cell lines during the ARTN invasion assay showed no significant differences in baseline cell invasion relative to the previous baselines established during the GDNF invasion assay ($p = 0.48$, 0.17, 0.08 and 0.19 for EV, RET9 KD, RET51 KD and total-RET KD, respectively), so the relative increases in cell invasiveness should be directly comparable (Figure 3.13B). EV cells stimulated with ARTN increased in invasiveness to 349% of the baseline, compared with 171% when stimulated with GDNF. The same trend was observed in RET9 KD and RET51 KD cell lines, where invasiveness increased to 3 or 4 times the levels observed when stimulated with GDNF. Although stimulation of total-RET KD cells with GDNF did not significantly increase their invasiveness (15% of EV), treatment with 100ng/mL ARTN resulted in a significant increase in invasiveness from 15% of EV when unstimulated, to 58% of EV. This increase in invasiveness was statistically significant relative to unstimulated total-RET KD cells ($p = 0.02$), but remained significantly lower than the relative invasiveness of ARTN stimulated EV, RET9 KD and RET51 KD cells ($p = 0.02$, 2.4×10^{-3}, and 0.02, respectively).

When stimulated with ARTN, differences between RET9 KD and RET51 KD cell lines also became more apparent: Although there was still no significant difference in invasiveness when unstimulated, ARTN stimulated RET9 KD cells invaded at 222% of the baseline, while RET51 KD cells invaded significantly less, at only 141% of baseline ($p = 0.02$). The increase in cell invasiveness when stimulated with ARTN, relative to GDNF might have been due to the relative abundance of ARTN’s receptor, GFRα3, compared to GDNF’s receptor, GFRα1 (Figure 3.13C).

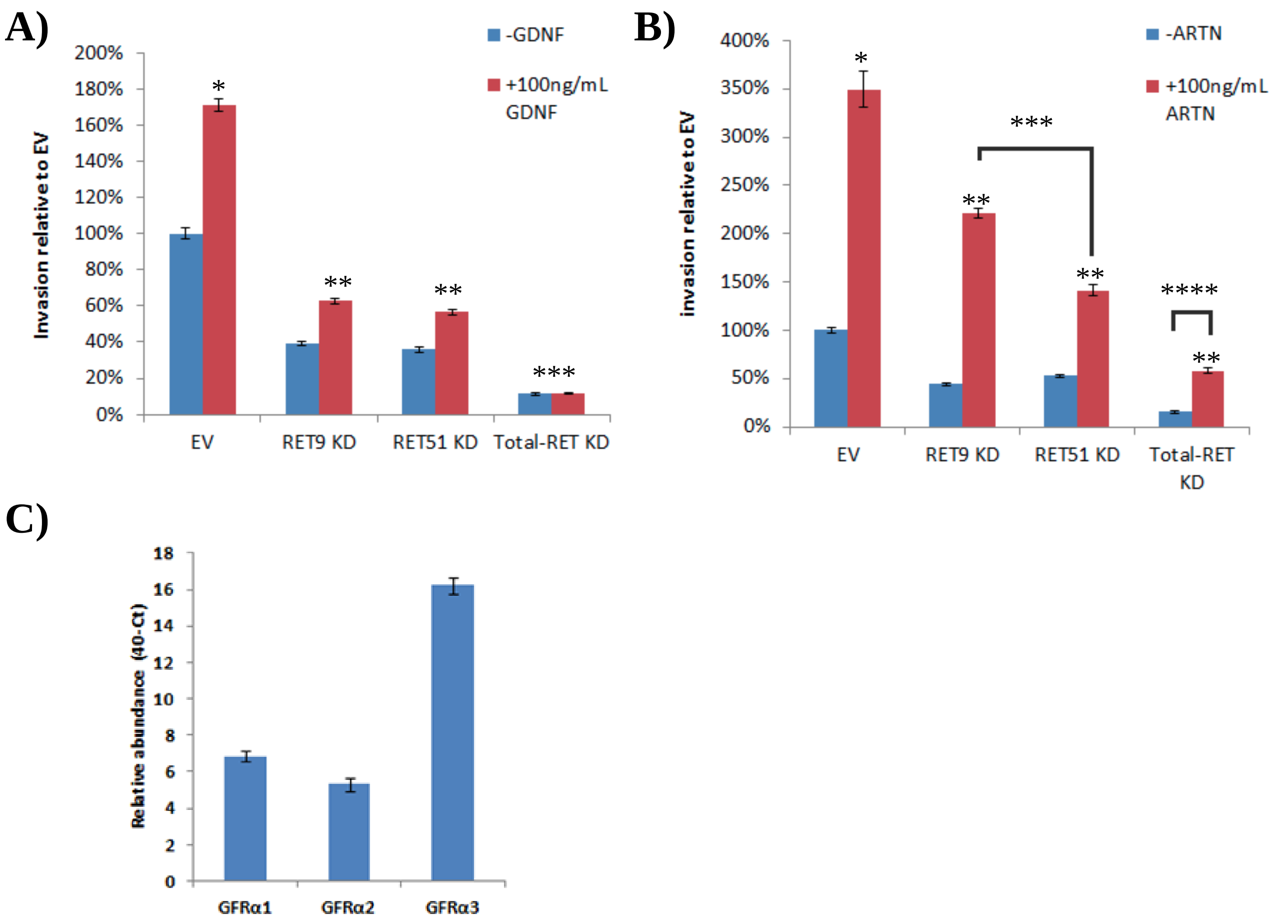

Figure 3.13 MiaPaCa-2 invasion through matrigel determined using a modified Boyden chamber assay. A) Modified Boyden chamber assay results for EV, single isoform KD and total-RET KD MiaPaCa-2 cell lines. Invasion is shown relative to unstimulated (-GDNF) EV cells. EV cells stimulated with GDNF show a significant increase in invasiveness over the baseline (*p = 0.005). RET9 and RET51 KD cell lines are significantly less invasive than EV when unstimulated (** -GDNF p = 0.006 and 0.003, respectively), and do not increase in invasiveness to as great an extent when stimulated with GDNF (** +GDNF p = 1.6 x 10^{-3} and 7.4 x 10^{-4}, respectively). No significant difference between RET9 KD and RET51 KD cell lines was observed (-GDNF p = 0.08, +GDNF p = 0.07). The total-RET KD cell line was significantly less invasive than EV, RET9 KD and RET51KD both when unstimulated (*** -GDNF p = 1.5 x 10^{-3}, 9.2 x 10^{-5} and 1.0 x 10^{-3}, respectively) and when stimulated (*** +GDNF p = 1.5 x 10^{-3}, 2.1 x 10^{-6} and 3.7 x 10^{-3}, respectively). Stimulation of total-RET KD cell line with GDNF did not increase invasiveness significantly relative to unstimulated levels (p = 0.37). **B)** Modified Boyden chamber assay results for cells stimulated with 100ng/mL ARTN in place of GDNF. Invasion is shown relative to unstimulated EV cells. The

invaseness of unstimulated cell lines the set of experiments shown in **B** was not significantly different relative to their unstimulated counterparts shown in **A** ($p = 0.48$, 0.17, 0.08 and 0.19 for EV, RET9 KD, RET51 KD and total-RET KD, respectively). However, EV, RET9 KD, RET51 KD and total-RET KD cell lines all show significantly greater increases in invasiveness when stimulated with ARTN (relative to +GDNF cells in **A**, $^{**}p = 0.002$, 2.6×10^{-6}, 2.5×10^{-4} and 2.5×10^{-5}, respectively). RET51 KD cell line stimulated with ARTN had significantly lower invasiveness than RET9 KD ($^{***}p = 0.02$). ARTN stimulated total-RET KD cells continued to invade significantly less than EV, RET9 KD, and RET51 KD cells (**Total-RET KD +ARTN $p = 0.02$, 2.4×10^{-3}, and 0.02, respectively), but displayed a significant increase in invasiveness relative to unstimulated total RET KD cells which was not observed with GDNF stimulation ($^{****}p = 0.02$). **C)** Relative abundance of RET coreceptor GFRα1, 2 and 3 in MiaPaCa-2 cells, determined using qRT-PCR.

3.5 MiaPaCa-2 ERK, STAT3, AKT phosphorylation status following RET knockdown

EV transduced, single isoform KD and total-RET KD cell lines were serum starved for 24h before being stimulated with 50ng/mL GDNF. Whole cell lysates were harvested and probed for ERK, pERK, STAT3, pSTAT3, AKT and pAKT, using tubulin as a loading control (Figure 3.14). Expression and phosphorylation were compared by densitometry as described previously, using tubulin to normalize the pixel density of each band. When unstimulated, total ERK expression level was consistent for all cell lines relative to EV (Figure 3.14A, $p = 0.48$, 0. 16 and 0.21 for RET9 KD, RET51 KD and total-RET KD, respectively). Similarly, unstimulated RET9 KD, RET51 KD, and total-RET KD pERK levels were not significantly different relative to EV ($p = 0.62$, 0.76 and 0.74, respectively). Only GDNF stimulated total-RET KD cells were found to have a significantly reduced level of phosphorylated ERK relative to other GDNF stimulated cell lines ($p = 0.02$, 0.02 and 0.03 relative to +GDNF EV, RET9 KD and RET51 KD, respectively). Total STAT3 levels of RET9 KD, RET51 KD or total-RET KD cells were not significantly different relative to EV in either unstimulated (Figure 3.14B, $p = 0.34$, 0.21, and 0.14, respectively) or GDNF stimulated conditions ($p = 0.73$, 0.15, and 0.43, respectively). EV cells were found to have significant increases in pSTAT3 levels upon treatment with GDNF ($p = 0.003$). This behaviour was also observed in RET9 KD cells ($p = 0.02$), but was not present in RET51 KD cells ($p = 0.25$). Conversely, total-RET KD cells were found to have significantly lower pSTAT3 levels following stimulation with GDNF ($p = 1.8 \times 10^{-5}$). All knockdown cell lines were found to have significantly lower levels of pSTAT3 relative to EV both when unstimulated ($p = 2.9 \times 10^{-5}$, 0.001 and 7.4×10^{-4} for RET9 KD, RET51 KD and total-RET KD, respectively) and when treated with GDNF ($p = 0.001$, 0.001 and 4.7×10^{-4} for RET9 KD, RET51 KD and total-RET KD, respectively). Both total AKT and pAKT levels were found to decease significantly in RET9 KD, RET51 KD and total-RET KD cell lines relative to EV both in the presence (Figure 3.14C, total AKT $p = 0.004$, 0.015 and 0.008, respectively. pAKT $p = 0.008$, 0.02 and 0.002, respectively) and absence of GDNF (total AKT $p = 0.02$, 0.02, and 0.04, respectively. pAKT $p = 0.022$, 0.007 and 7.2×10^{-4}, respectively). No significant changes were found between total AKT and pAKT levels in response to GDNF treatment, or RET knockdown. Additionally, no significant differences in either total AKT or pAKT levels were found between any RET KD cell lines in the presence or absence of GDNF.

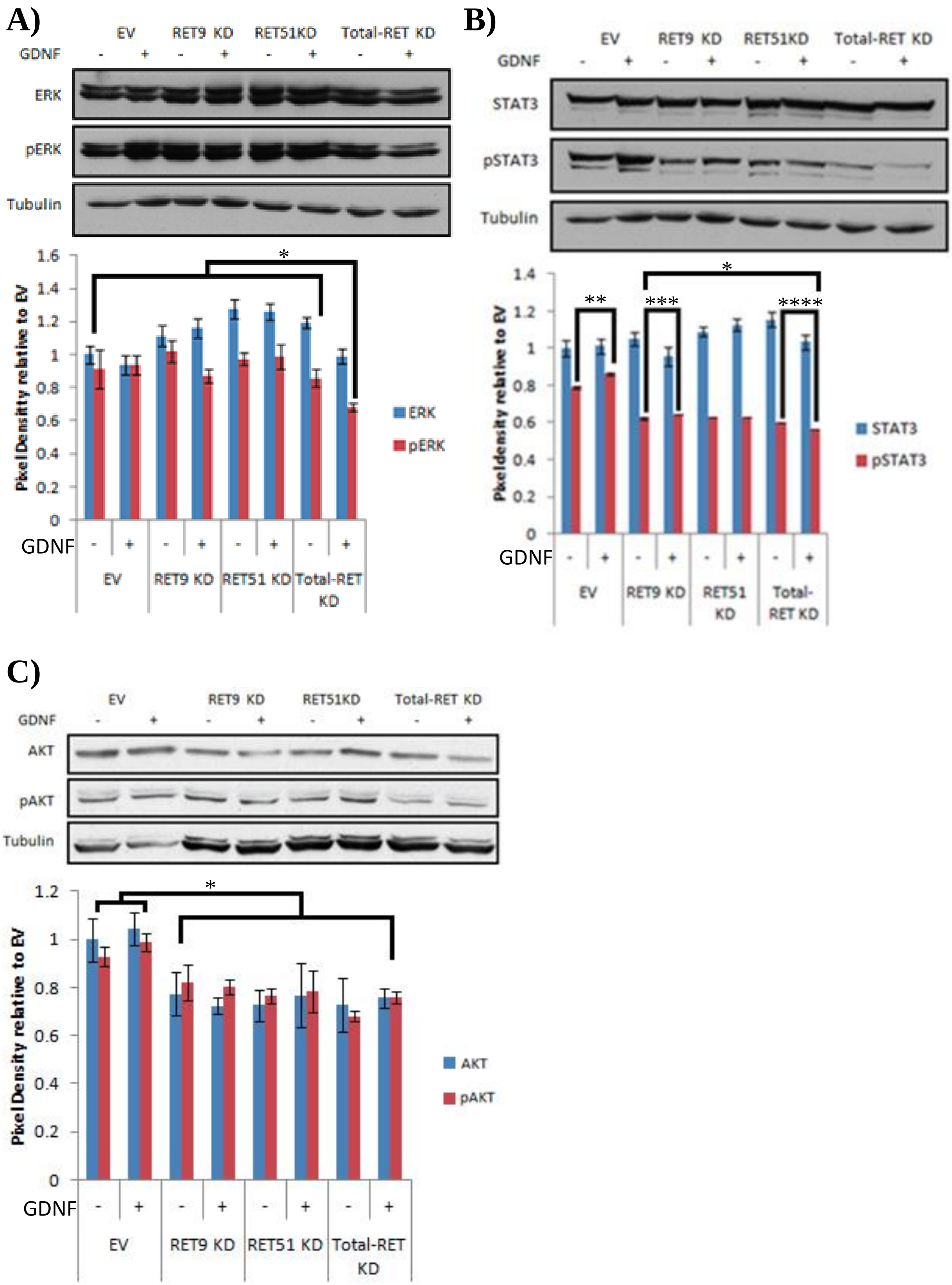
A)
EV
RET9 KD
RET51KD
Total-RET KD
GDNF
ERK
pERK
Tubulin
Pixel Density relative to EV
ERK
pERK
*
RET51 KD
Total-RET KD
B)
STAT3
pSTAT3
Pixel density relative to EV
**
***
****
RET51 KD
Total-RET KD
C)
AKT
pAKT
Pixel Density relative to EV

Figure 3.14 ERK, STAT3 and AKT status in response to RET knockdown. Whole cell lysate from indicated clonal MiaPaCa-2 cell lines were immunoblotted for the indicated proteins and densitometrically normalized relative to tubulin. Representative immunoblots shown. Error bars represent standard error over a minimum of three experimental replicates. **A)** Representative ERK phosphorylation status with densitometry for total ERK and pERK. In all cell lines total ERK expression level was not significantly different from EV when unstimulated (*p = 0.48, 0. 16 and 0.21 for RET9 KD, RET51 KD and total-RET KD, respectively). Similarly, unstimulated RET9 KD, RET51 KD and total-RET KD cells did not have significantly different levels of pERK relative to EV (*p = 0.62, 0.76 and 0.74, respectively). Only GDNF stimulated total-RET KD cells had significantly reduced level of phosphorylated ERK relative to other GDNF stimulated cell lines (p = 0.02, 0.02 and 0.03 relative to +GDNF EV, RET9 KD and RET51 KD, respectively). **B)** Representative STAT3 phosphorylation status with densitometry for total STAT3 and pSTAT3. Total STAT3 levels of RET9 KD, RET51 KD and total-RET KD cells did not change relative to EV either when unstimulated (* -GDNF p = 0.34, 0.21, and 0.14, respectively) or when stimulated with GDNF (* +GDNF p = 0.73, 0.15, and 0.43, respectively). When treated with GDNF, both EV and RET9 KD cells had significantly increased pSTAT3 levels relative to untreated control (** p = 0.003, *** p = 0.02, respectively), but no such increase in pSTAT3 was observed in RET51 KD cells (p = 0.25). Only total-RET KD cells showed a decrease in pSTAT3 in response to GDNF (**** p = 1.8×10^{-5}). **C)** Representative AKT phosphorylation status and densitometry for total AKT and pAKT. Total AKT and pAKT levels decreased significantly in RET9 KD, RET51 KD and total-RET KD cell lines relative to EV in both unstimulated and GDNF stimulated cells (*total AKT +GDNF p = 0.004, 0.015 and 0.008, respectively. pAKT +GDNF p = 0.008, 0.02 and 0.002, respectively. Total AKT –GDNF p = 0.02, 0.02, and 0.04, respectively. pAKT –GDNF p = 0.022, 0.007 and 7.2×10^{-4}, respectively).

Chapter 4. Discussion

Activating mutations of RET play an important role in thyroid cancers including both PTC and MTC and have recently been identified in lung adenocarcinoma [65, 74, 112]. More broadly, recent studies have also shown that RET may be active in other tumour types such as pancreatic and breast cancers, and that the overexpression and activation of RET may be linked to more aggressive disease [35, 61-63]. We have examined the contribution of RET and its isoforms to cell proliferation, migration and invasion in neoplastic models of MTC (TT cells) and PDAC (MiaPaCa-2). We have observed what appear to be striking differences in the behaviours of TT cells and MiaPaCa-2 both in response to normal RET activation and to total and isoform-specific RET knockdowns.

4.1 Immediate morphological changes in response to RET knockdown

One of the most dramatic events observed in these studies was the immediate morphological change seen in both TT and MiaPaCa-2 cells in response to total-RET knockdown. We have previously observed that wild type (WT), empty vector (EV) transduced, and RET9 or RET51 KD TT cells grow in a clumping manner (Figure 4.1), and that TT cells stimulated with either GDNF or FBS exhibited significantly reduced cell migration relative to serum-starved cells (Figure 3.9). It is possible that the clumping behaviour of TT cells may be a result of this immobility: When cells from the free-floating population adhered to the plate, they began to proliferate and form clumps of cells which did not migrate large distances away from their sister cells.

A) B)

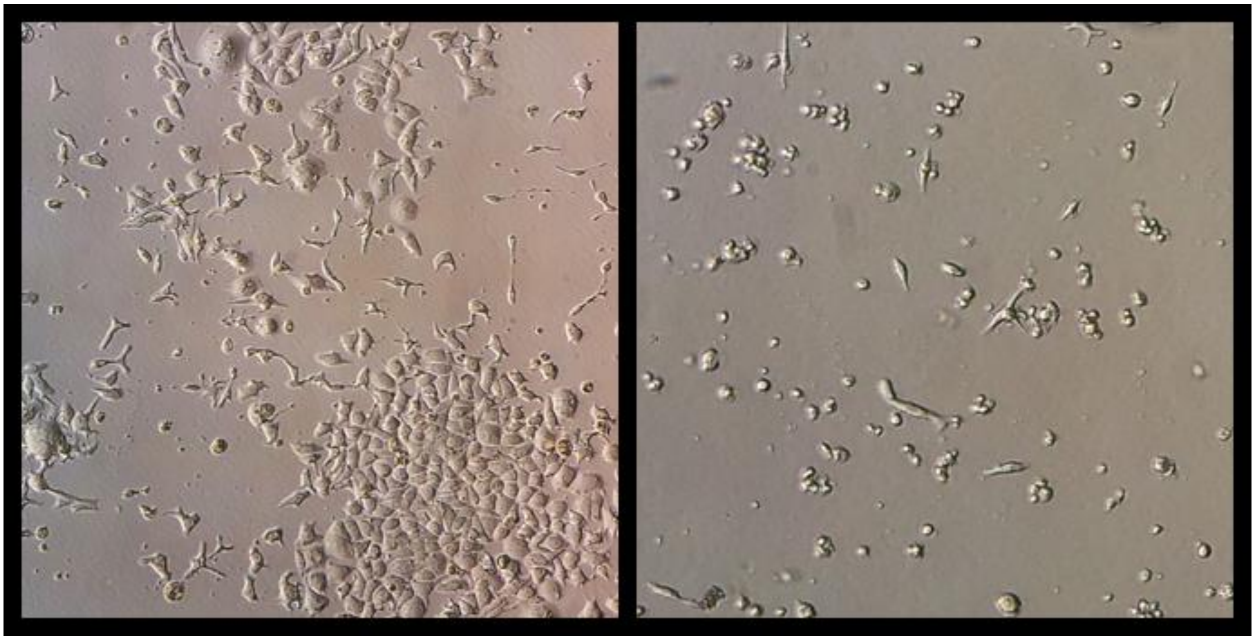

Figure 4.1 TT cell growth pattern before and after RET knockdown. Cells shown at 100x magnification. **A)** Typical clumping growth pattern of TT cells (RET51 KD polyclonal TT cells pictured). Different cell morphologies observed at low and high cell densities. Clumped cells appear flattened, while cells growing at lower density around the periphery of each clump are somewhat more spindle-like. **B)** Scattered growing pattern seen in total-RET KD polyclonal TT cells. Live cells are adherent to the culture plate and are morphologically more similar to typical low density TT cells.

When TT cells were subjected to total-RET KD the cells were dramatically smaller and no longer exhibited clumping. Instead, the total-RET knockdown cells formed a sparsely populated layer over the surface of the tissue culture plate (Figure 4.1), and appeared to die off over a period of approximately 2 weeks. Although the specific mechanisms behind the lack of clumping in total-RET KD cells is not yet known, there are several factors which may come into play. First, it is possible that by knocking down total-RET, we have caused the cells to migrate rather than remain stationary and clump together. We were unable to test the effects of GDNF with respect to the motility of total-RET knockdown cells in our Boyden chamber assays due to the lethality of total-RET knockdown in TT cells. However, we have shown here that TT cells only migrate appreciably under serum starved conditions, and that the activation of RET through the addition of GDNF significantly reduced migration in EV controls. Contrary to this finding, single isoform RET KD TT cells did not have reduced migration in response to GDNF (Figure 3.9). It is possible, that by eliminating RET signalling using total-RET knockdown, the cells became more mobile in culture conditions, and no longer formed clumping colonies. Another possibility is that by knocking down total-RET, we abolished the protein responsible for driving cell proliferation and survival in MTC. As a result, the cells which adhered to the tissue culture plate were incapable of proliferation and therefore did not give rise to clumps of cells. Finally, it is possible that by knocking down total-RET, we induced apoptosis. However, if this is the case, then we would have expected to see typical morphological changes associated with apoptosis, such as rounding of the cells, and blebbing of the cell membrane [Reviewed in 113]. Although we did observe more rounded cells in total-RET KD cell cultures relative to WT, EV or single isoform RET KD, the majority of total-RET knockdown cells still appeared morphologically normal. This suggests that rather than inducing apoptosis, total-RET knockdown may simply stop cell proliferation in TT cells, causing the cells to undergo senescence.

While MiaPaCa-2 cells did not exhibit changes as dramatic as the cell death observed in TT cells, they did undergo some very obvious morphological changes in response to RET knockdown. We saw that our MiaPaCa-2 RET KD cells took on distinct cell morphologies that can be arranged on a scale from most spindle-like, to most flattened and scale-like (Figure 3.5). We observed that MiaPaCa-2 cells subjected to EV transduction appeared morphologically identical to mesenchymal-like, spindle shaped WT cells, while RET9 KD, and RET51 KD, became increasingly flattened. Total-RET KD cells no longer resembled WT or EV MiaPaCa-2 cells, and were instead scale-like, flattened, and morphologically epithelial-like. This dramatic morphological change in total-RET knockdown cells might be attributed to mesenchymal-epithelial transition (MET), as is suggested by the increased expression of E-cadherin, a protein known to be upregulated in epithelial cells (Figure. 3.2.4) [111]. Another feature of these knockdown cell lines, is that the behaviour of RET9 KD cells was consistently more similar to WT and EV cells, while RET51 KD cells differed more significantly from either WT or EV, and more closely resembled total-RET knockdown cells. This trend was consistently observed across several experiments.

4.2 RET expression and cell proliferation

TT cells contain a heterozygous activating mutation of RET consisting of a cysteine to threonine substitution at codon 634 (C634T) [114]. This MEN 2A-type mutation induces ligand independent dimerization and constitutive activation of RET [70]. However, due to the heterozygous nature of this mutation, TT cells subsequently express a combination of both wild type (WT) RET and constitutively active C634T RET. As a result, TT cells experience continuous RET signalling through C634T RET, but wild type RET remains at the cell surface and can be activated by GFL binding and recruited to lipid rafts by GFRα [53, 115], either to increase overall RET activity, or to alter RET signalling by interacting with pools of lipid raft enriched signalling molecules which might be relatively inaccessible to C634T RET. This simultaneous expression of both normal and mutant RET may explain the results of the proliferation assay. As predicted, both RET9 and RET51 KD cell lines show significantly decreased proliferation relative to the EV control across all experimental conditions, independent of stimulation by GDNF, suggesting that constitutively active C634T RET in TT cells plays a significant role in cell proliferation (Figure 3.7). What was unexpected, however, is the significant decrease in cell proliferation when TT cells were treated with GDNF. This decrease was only found to be statistically significant in EV cells, but was also observed in RET9 KD and RET51 KD cell lines to a lesser extent. A possible explanation for this reduction in cell proliferation induced by GDNF lies in the differential activation and processing of C634T RET molecules relative to wild type RET molecules. The C634T mutation results in a RET molecule that is capable of dimerization, autophosphorylation and signalling not only while localized at the cell membrane, but also when localized in cytosolic compartments [73, 116]. Contrary to this, the addition of a GFL to TT cells activates only wild type RET protein localized at the cell surface through a GFRα coreceptor, which then mediates RET recruitment to lipid rafts [53, 115]. This difference in the localization and activation of C634T RET and wild type RET molecules might allow them differential access to downstream proteins which are localized to either the cytosol or enriched in lipid rafts, and result in differential signalling activity by WT RET to reduce cell proliferation.

Due to the intracellular localization of the majority of RET proteins [28], it is likely that the majority of C634T RET signals intracellularly through the PI3K/AKT pathway to signal for cell proliferation and survival in a similar manner to other cytoplasmically localized RET mutants such as RET/PTC fusion proteins [117]. C634T RET proteins which are localized at the cell membrane signal independently of GFRα, and therefore are not recruited to lipid rafts [53, 115] (Figure 4.2). The regulation of GDNF-stimulated RET downstream signalling by proteins such as AKT is thought to involve lipid rafts on the cell surface, where certain molecules and proteins are enriched, suggesting that membrane localization of RET and recruitment of RET to lipid rafts by GFRαs is a critical step in the regulation of normal RET signalling [53, 115, 118]. This behaviour has previously been documented by Freche *et al*. [118], who showed differences in downstream activation of PI3K/AKT depending on the method of RET activation (either ligand-dependent or ligand-independent). In their report, artificially dimerized RET, mimicking a constitutively active MEN 2A mutant, was found to induce sustained AKT phosphorylation, while wild type RET induced rapid phosphorylation and dephosphorylation of AKT. The sustained phosphorylation of AKT by ligand-independent RET activation was found to result in a significant increase in resistance to apoptosis, and an overall increase in cell proliferation [118]. Deregulation of downstream signalling caused by ligand-independent RET activation may be attributed to the displacement of RET signalling from lipid rafts to other regions of the cell membrane and cytoplasm, where RET has less access to proteins that regulate AKT activity [119]. For example, the activation of lipid raft localized PLCγ by RET, is known to activate PKC [54, 120], a protein kinase shown to negatively regulate AKT [121, 122]. As a result, we would expect the activation of membrane localized wild type RET by GDNF to increase PKC activity and subsequently reduce the levels of phosphorylated AKT present within the cell and reduce proliferation (Figure 4.2).

Overall in TT cells, it appears that C634T RET is responsible for the majority of proliferative and survival signalling, as demonstrated by the decrease in cell proliferation relative to EV we observed in our RET9 KD or RET51 KD TT cells in the absence of GDNF. Since C634T RET is the only active RET molecule in the absence of GDNF, and we showed that the activation of WT RET did not increase proliferation (Figure 3.7), any changes in cell proliferation in the absence of GDNF was mostly likely a direct result of reduced C634T RET protein levels caused by RET knockdown.

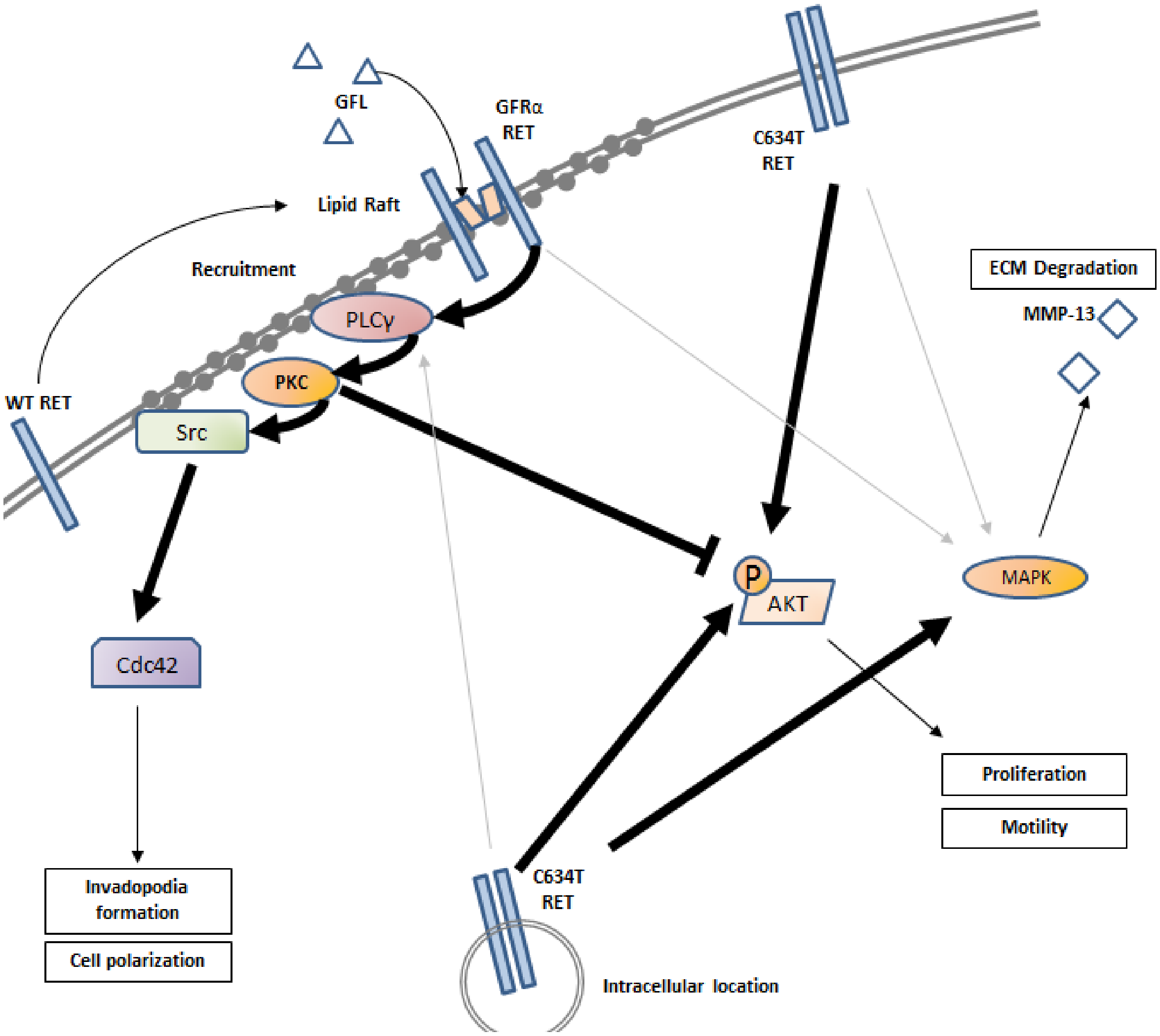

Figure 4.2. Putative pathways activated by ligand-dependent RET (GFRα RET) and constitutively active C634T RET. Greater activation of downstream molecules represented as thick arrows, weaker activation represented as thin, grey arrows. In this model WT RET and C634T RET are expressed simultaneously, as they are in TT cells, in the presence of a GFL. Due to differences in the localization of active WT RET and active C634T RET, the two proteins have differential access to downstream signalling proteins. Activated C634T is localized throughout the cell, both intracellularly, and at the cell membrane, and can phosphorylate large quantities of AKT, in addition to greater relative access to MAPK [51]. WT RET, is recruited to lipid rafts by GFRα and activated by GDNF [53, 115], and has greater access to other lipid raft enriched proteins, such as PLCγ [54], which can activate PKC to dephosphorylate AKT. In

addition, ligand-activated WT RET might play a role in modulating cell polarization by activating lipid raft localized Src downstream of PKC, resulting in the activation of Cdc42, a protein involved in cell polarization and chemotaxis.

In contrast to what we observed in TT cells, the proliferative activity of the MiaPaCa-2 PDAC cell line appeared to be unaffected by either RET activation by GDNF or RET knockdown (Figure 3.8). It may be that the K-Ras protein expressed by MiaPaCa-2, which contains an activating mutation in codon 12, activates pathways such as ERK and AKT [123-125] to such an extent that any additional activation or downregulation initiated by RET signalling is not detectable in our assays. This appears to be the case when we examine the phosphorylation status of ERK and AKT (Figure 3.14) where ERK and AKT are highly phosphorylated even in the absence of RET activation.

These results highlight one of the main differences between TT cells and MiaPaCa-2: In TT cells, as well as many thyroid carcinomas [60, 114], a constitutively active mutant of RET acts as a driver of disease by signalling for cell proliferation and survival through pathways such as AKT. The RET protein expressed by MiaPaCa-2 cells, and expressed in 50-65% of PDACs, is activated by GFL binding [126], and is not critical to cell survival. In spite of this, RET expression has been linked to particularly aggressive clinical PDACs [35], strongly suggesting that RET activation in these cells might contribute to disease progression by enhancing cellular processes such as invasion and migration.

4.3 RET, cell migration and invasiveness

The differential processing of C634T RET and WT RET in TT cells may also explain some of the observed differences between single RET isoform knockdowns and EV cells when we assayed them for chemotactic response. Under serum starved conditions, only C634T RET actively signals, so the migration of TT cells through the tissue culture insert membrane is representative of the ability of C634T RET to induce cell migration (Figure 3.9). When wild type RET is activated by the addition of GDNF, we see a significant reduction in cell migration in EV cells, but both RET9 and RET51 KD cells continue to migrate as they did under serum starved conditions (Figure 3.9). Given the aforementioned differences in processing and signalling potentials of C634T RET and WT RET, this reduction in cell migration could be attributed to dephosphorylation of AKT downstream of WT RET activation. In this assay, the cell culture insert was not treated with basement membrane extract, so there was no physical barrier to migration, and any cells which moved to the underside of the cell culture insert were counted as migratory cells. Therefore, this initial assay, using an untreated cell culture insert, was a measure of gross cell migration, and did not assess the activation of any pathways that might facilitate greater cell invasiveness. The AKT pathway is well documented to signal downstream through numerous pathways to promote both epithelial mesenchymal transition (EMT) and cytoskeletal remodelling to facilitate increased cell motility [Reviewed in 127]. In the absence of GDNF, sustained AKT phosphorylation resulting from C634T RET signalling could activate these EMT and cytoskeletal remodelling pathways, and contribute a motile, mesenchymal morphology.

Notably, we did not observe reduced cell migration in either RET9 KD or RET51 KD TT cells in response to GDNF (Figure 3.9). This was likely a result of differences in the localization and activation of C634T RET and WT RET. Dr. Doug Richardson previously showed that only

27% of RET9 and 39% of RET51 is localized to the cell membrane, while the majority of these molecules were found intracellularly [28]. Only WT RET which is transported to the cell membrane can become activated by GFRα and a GFL. On the other hand, C634T RET is constitutively active, and can signal regardless of its localization within the cell. Following knockdown, it is possible that enough C634T RET remains active at the cell membrane or within the cell to activate AKT at near normal levels. Meanwhile, the relatively reduced pool of membrane localized WT RET in single isoform KD TT cells may become depleted following GDNF treatment before it can mediate sufficient AKT dephosphorylation for us to detect as a reduction in cell migration relative to EV cells.

The modified Boyden chamber assay used to quantify invasiveness towards a source of GFL revealed an important distinction between cell migration and invasion. The cell culture insert used in this assay was coated with basement membrane extract (matrigel) to provide a physical barrier to migrating cells, and to allow GFLs added to the lower chamber to diffuse slowly into the upper chamber, creating a GFL concentration gradient. In order for cells to invade through the matrigel and pass through the pores of the cell culture insert, multiple signalling pathways that modulate degradation of the ECM and cell migration must be activated. As previously discussed, AKT signalling in TT cells likely promotes ECM remodelling and motility, but in order for the cells to invade through matrigel and migrate towards a source of GFLs, additional pathways, such as those that mediate cell polarization and invadopodia formation, might be required [127, 128]. Our lab has previously shown that internalized RET has greater access to molecules such as MAPK [51], and Lu et al. [102] previously reported that the activation of the MAPK pathway by RET results in cell migration and expression of MMP-13, resulting in increased invasiveness in glioma cells. It is possible that C634T RET contributes to numerous pathways, including those for cell migration, cytoskeletal remodelling and matrigel degradation, through sustained AKT phosphorylation and its relatively greater ability to signal through MAPK. Despite these contributions to invasiveness by C634T RET, TT cells were found to invade only when stimulated with GDNF, suggesting that the activation of WT RET is a critical step in cell invasion (Figure 3.10). In addition, neither WT RET9 nor WT RET51 appeared to play a relatively greater role in mediating invasiveness, and we observed no significant differences in the invasiveness of RET9 KD and RET51 KD cells (Figure 3.10), suggesting that activation of either wild type RET isoform is sufficient to promote invasion in TT cells.

While our previous findings suggest that membrane bound, ligand-activated WT RET and constitutively active C634T RET have differential functions in terms of proliferative signalling (Figure 3.7), it appears that the signalling of these two proteins can also function synergistically to promote cell invasion. Earlier, we proposed that the observed differences between these two proteins, within the context of cell proliferation, was due to the recruitment of WT RET to lipid rafts, and its relatively greater access to pools of lipid raft enriched molecules which dephosphorylate AKT [53, 115]. In the same manner, it is possible that ligand-activated RET has relatively greater access to molecules which modulate pathways critical for cell invasion, such as those required to polarize the cell and mediate chemotaxis. One such pathway involves Protein Kinase C (PKC), a molecule activated by lipid raft localized PLCγ [54] is known to be involved in invadopodia formation through a signalling cascade involving Src, another lipid raft enriched protein [129], and Cdc42 [130] (Figure 4.2). Most notably, Cdc42 is additionally known to play a critical role in both cell polarization and chemotaxis [128] A putative pathway illustrating the interaction of RET, C634T RET and the aforementioned pathways is shown in Figure 4.2. In this figure, C634T signalling strongly activates AKT and MAPK to promote EMT, cell motility, and

ECM degradation, as we have previously described [127]. However, due to its activation independently from GFRα, C634T RET is not recruited to lipid rafts, and has relatively little access to lipid raft localized proteins such as PLCγ [54] or Src [129]. As a result, C634T RET does not activate these proteins as effectively as WT RET, and cannot effectively modulate cell polarization, invadopodia formation and chemotaxis [130].

RET is known to mediate both motogenic and chemotactic responses in cells following activation by GDNF [131]. These responses play a critical role during embryogenesis where cells originating from the neural crest require migratory stimulus and guidance to reach their destination sites. The ability of RET to promote cell polarization and directional cell migration, was also observed during a scratch assay using the MiaPaCa-2 PDAC cell line (Figure 3.11). Both WT and EV cells migrated less in the presence of GDNF (Figure 3.11A), although the difference in cell migration was not statistically significant. A possible source for this statistical insignificance might be the low expression of GFRα1 in MiaPaCa-2 relative to the more highly expressed GFRα3 receptor, which binds ARTN (Figure 3.13C), and if we were to repeat the assay using ARTN to activate RET at higher levels, we might be able to resolve significant differences in cell migration. Consistent with this, RET activation in MiaPaCa-2 using ARTN during the matrigel invasion assays revealed significant differences in RET9 KD and RET51 KD cell invasiveness which were undetectable when the cells were treated with GDNF (Figure 3.13A, B). Additionally, during the scratch assay, both RET9 KD and RET51 KD cell lines migrated more than the WT or EV cell lines in the presence of GDNF, but only RET51 KD cells showed a significant increase relative to WT or EV. This suggests that RET activation resulted in reduced cell migration in MiaPaCa-2 cells. This effect of RET activation might be attributed to the diffusion of GDNF throughout the growth media during our scratch assay. The absence of a

GDNF concentration gradient would not differentially activate RET across the cell body, and would not induce cell polarization, which is required for directional migration [96, 132]. This may mimic the environment found at a destination tissue during embryogenesis, when a RET expressing cell migrating along a GFL concentration gradient reaches the source. At this location, the concentration of GFLs is sufficient to activate RET throughout the cell surface, abolishing cell polarization, and halting directional cell migration [96]. This ability of RET to first mediate chemotaxis towards a source of GFL, and then stop migration upon reaching its destination might be critical during embryogenesis to ensure that migrating cells remain at their target tissues. Additionally, this response resulting from uniform activation of RET throughout the cell membrane could play a role in the establishment of distant metastases or PNI in cancer, by inducing migration towards a source of GFLs, and then allowing migrating tumour cells to become stationary and establish a population close to that source.

It is possible that a RET-mediated chemotactic pathway involving Src and Cdc42 is responsible for cell polarization and migration towards a source of GFLs. Normally, the activation of RET results in its recruitment to lipid rafts by GFRα [115], and activation of PI3K [133], which is antagonised by PTEN [96]. In regions of the cell where RET activation is low, PTEN is able to block PI3K mediated signalling by dephosphorylation of PIP3(PI(3,4,5) triphosphate) [96]. Regions of cell membrane with greater RET activation, resulting from higher concentrations of GFLs, accumulate enough activated PI3K to saturate PTEN, resulting in the subsequent accumulation PIP3 in areas of the cell with higher RET activation. The guanine nucleotide exchange factors VAV2 and VAV3 (VAV2/3) are recruited by PIP3, and become localized in areas of high PIP3 concentration [134]. Activated RET additionally activates lipid raft localized Src, which mediates actvation of VAV2/3 to activate Cdc42, and may additionally activate Cdc42 through other pathways [130, 134-136]. The net result of these processes is that activated Cdc42 becomes enriched in areas of the cell where RET is highly activated, thus contributing to cell polarization towards a source of GFLs (Figure 4.3) [128]. When RET is uniformly activated across the cell membrane, Cdc42 is not activated within specific region of the cell, but is instead active uniformly throughout the cell. In this scenario, Cdc42 activation has been shown to prevent the cell from becoming polarized, abolishing directional cell migration [61, 65].

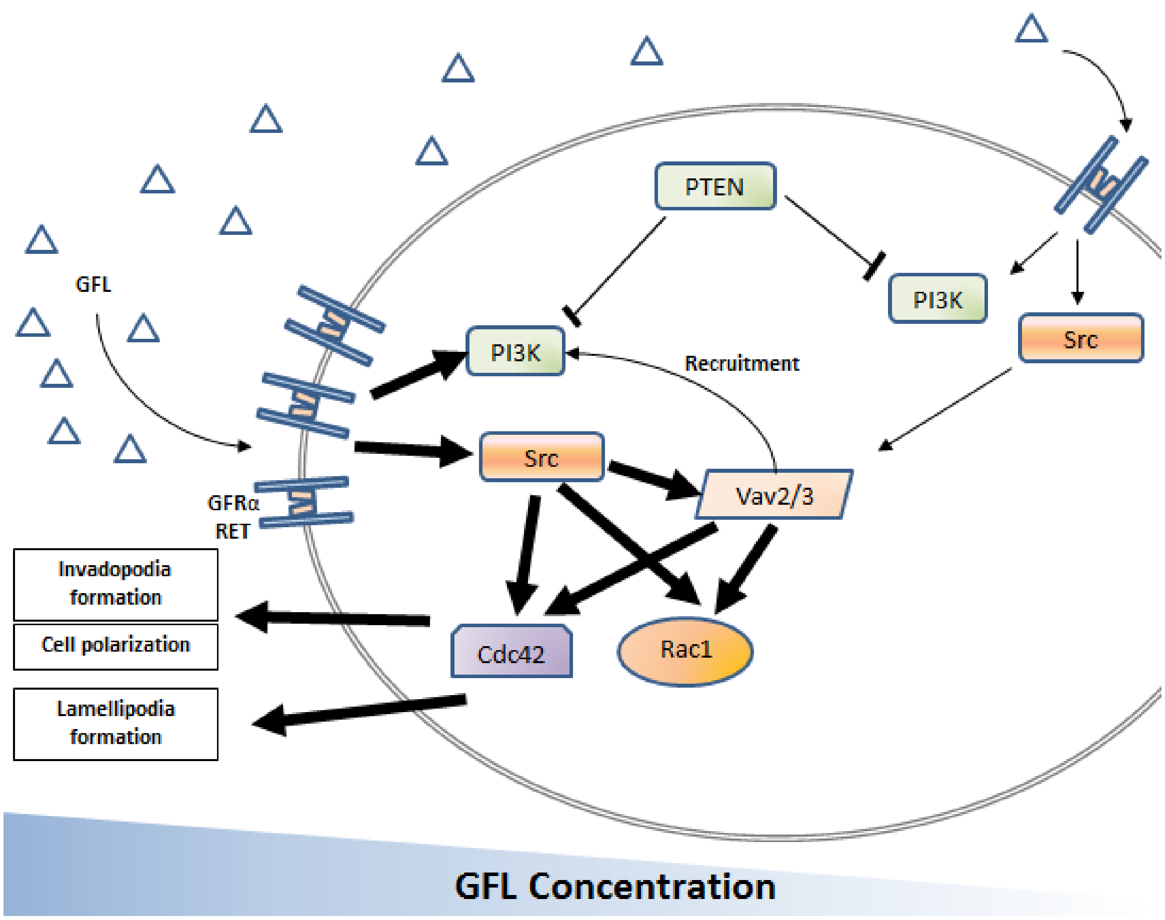

Figure 4.3. Putative model showing pathways through which RET can mediate cell polarization and migration towards a source of GFLs. Thick arrows represent greater activation. RET activation at the cell membrane activates PI3K which is normally antagonized by PTEN. In regions of the cell where RET is highly activated by a higher concentration of GFLs, enough PI3K becomes activated to saturate PTEN, resulting in the accumulation of active

PI3K in areas of the cell where RET is most active. In areas of the cell where extracellular GFL concentration is lower, RET is not as highly activated and PTEN is able to dephosphorylate PI3K. RET also activates lipid raft localized Src, which can mediate Cdc42 and Rac1 activation either through VAV2 and VAV3, which are recruited by PI3K, or through other pathways [130, 134-137]. The net result of these processes is that Cdc42 and Rac1 become activated in areas of the cell where RET highly activated by an external concentration of GFLs to mediate cell polarization and subsequent processes critical to cell invasion and migration, such as the formation of lamellipodia and invadopodia.

Another possible explanation for the ability of RET activation to reduce cell migration in WT and EV MiaPaCa-2 cells, is that the 2D migration assay used simply did not provide an environment conducive to cell migration. Previous studies have shown that migrating cells can exhibit a variety of properties that lie on a spectrum between mesenchymal and amoeboid modes of cell migration [138]. The mesenchymal mode of cell migration relies on integrins for adhesion to the ECM substrate and proteases to drive ECM remodelling [138]. This mode of cell migration is directional and requires a concentration gradient of an extracellular ligand, such as GDNF, to bind cell surface receptors and mediate chemotactic migration. In the absence of such a gradient, cells do not polarize and thus migrate randomly in an amoeboid fashion, with no net directional movement [139]. Mesenchymal migration takes place in spindle shaped fibroblast-like cells and requires several interdependent events that occur cyclically to drive movement. To initiate mesenchymal cell migration, a cell must first become polarized, for example, through uneven RET activation across the cell membrane [96]. The polarized cell then undergoes cytoskeletal remodelling, and extends a pseudopod, which must come into contact with ECM. Integrins then localize to the pseudopod and initiate the formation of focal adhesions, which recruit proteases to drive local ECM degradation. Finally, cell contraction occurs, pulling the cell body towards the leading edge of the pseudopodium. Since this process critically depends on cell polarization, the formation of pseudopodia and binding of ECM ligands, it occurs poorly in 2D culture where ECM substrates are absent [138]. Conversely, the amoeboid mode of cell migration is integrin-independent, and cells using this mode of migration can migrate very quickly because they rely only on transient weak interaction with the substrate [138].

RET activation is known to activate Rho family GTPases such as Rac and Cdc42, proteins critical for cytoskeletal remodelling, the formation of cell protrusions, and migration [134, 137, 140, 141]. Additionally, RET activation is known to activate PI3K, which is involved in cell polarization, although the exact molecules responsible for cell polarization are not yet known [96]. Here we propose a model to explain the reduction in overall cell migration we observe in WT and EV cells upon GDNF stimulation in 2D culture: RET becomes activated and PI3K activates Cdc42 and Rac, but the cells do not undergo polarization due to the lack of a GDNF concentration gradient to induce differential RET activation across the cell membrane. At the same time, the cells extend pseudopodia to bind ECM, but this process occurs poorly in the absence of matrigel [138], and at some point during this process the cells cease migration. Consistent with this, we observe significant increases in both cell protrusion frequency and length in response to GDNF in all MiaPaCa-2 cell lines except total-RET KD, despite the absence of any significant difference in 2D cell migration (Figure 3.12 & Figure 3.11). These protrusions may represent the second stage of mesenchymal cell migration: the formation of pseudopodia, a Cdc42 dependent process [134]. These protrusions must then bind ECM ligands to allow for the formation of focal adhesions and to continue the process of mesenchymal cell migration [138]. Notably, MiaPaCa-2 RET51 KD cell lines had relatively greater 2D cell migration than EV cells, both in the presence and absence of GDNF (Figure 3.11). This increase in 2D motility was concurrent with a significant reduction in both cell protrusion frequency and length (Figure 3.12), and may represent a relative increase in amoeboid cell migration as the primary form of motility. This same trend was observed in RET9 KD cells, although the changes were not statistically significant when the cells were stimulated using GDNF. This disparity in the behaviours of RET9 KD and RET51 KD cells suggests important differences between the activities of RET9 and RET51 in MiaPaCa-2. It appears that, within the context of mesenchymal cell migration and cell protrusion formation, RET51 plays a greater role relative to RET9.

Total-RET KD cells on the other hand have significantly less 2D migration in response to RET knockdown, as well as significantly fewer and shorter cell protrusions. In combination with a more flattened and scale-like morphology, and relatively increased expression of E-cadherin (Figure 3.6), this phenotype may be a result of a transition of the cells from highly motile state to a relatively more immobile one, through a process such as MET [142]. The migration of total-RET KD cells did not change in response to GDNF treatment, but they did appear to take on a slightly more spindled appearance relative to their unstimulated morphology, perhaps due to the activation of remaining RET to induce causing cytoskeletal remodelling (Figure 3.12C). In addition, these GDNF-treated cells appear to form pseudopodia which are stunted and terminate without extending from the cell body, consistent with the formation of these cell protrusions in MiaPaCa2 cells being RET dependent. The presence of these stunted protrusions suggests that, although total-RET knockdown does not prevent the initiation of cell protrusion formation, RET activation is required for lamellipodia formation to extend the cell protrusions [137].

A similar trend is seen in RET9 and RET51 KD cells: Following 24 hours of incubation with GDNF, both knockdowns result in significantly fewer and significantly shorter cell protrusions relative to the EV cells. In addition, RET51 KD cells form significantly shorter protrusions relative to RET9 KD. These differences between RET9 and RET51 knockdown cells might be the result of their differential abilities to generate cell polarity, or to direct lamellipodia formation [137]. It has previously been shown that the production of PIP3 by activated PI3K is critical for the maintenance of cell polarity and directional migration [143]. Owing to RET51's greater abundance at the cell membrane [28], it is possible that this isoform of RET is able to activate more effectively polarize the cell by activating PI3K and Src [130, 134, 135, 137] (Figure 4.3). The significant increase in cell migration we observed for RET51 KD cells relative to WT and EV cells (Figure 3.11) may support this role for RET51. Keeping in mind that RET51KD cells express mostly RET9, and RET9 KD cells express mostly RET51 (Figure 4.4), we are able to compare the relative effectiveness of each isoform by measuring cell migration after GDNF stimulation. Since only RET51 KD cells migrated significantly more than WT and EV, this suggests that the activation of RET9 affected cell migration relatively less than RET51 activation. Since we believe that the effect of RET activation on cell migration in MiaPaCa-2 is a result of uniform Cdc42 activation throughout the cell [61, 65], this suggests that by knocking down RET51, and leaving RET9 as the more abundant RET isoform, we have depleted the major mediator of cell polarization in MiaPaCa-2 cells.

Another possible mechanism through which RET9 and RET51 might influence cell protrusion and lamellipodia formation is the Rac cell motility pathway. This family of GTPases is involved in lamellipodia formation and cytoskeletal remodelling, and has been shown to be activated downstream of RET by VAV2/3 in the same manner as Cdc42 [134, 140, 141, 144-147]. The Rac1 GTPase can be activated by RET both via PI3K, and through a cAMP-dependent mechanism [137]. The latter is critical to lamellipoda formation, while PI3K mediated activation enhances lamellipodia formation. Owing to the fact that lamellipodia formation is critical for the extension of cell protrusions [137], the difference in cell protrusion length we observe in RET9 and RET51 knockdown cell lines suggests that RET51 KD cells do not form lamellipodia as effectively as RET9 KD cells, and further reinforces our suspicion that PI3K is activated differentially by the RET isoforms.

The dominance of the mesenchymal mode of cell migration in MiaPaCa-2 is supported by data from 3D migration and invasion Boyden chamber assays. In these assays, matrigel simultaneously serves as a barrier to invasion and as ECM to allow cell-substrate interaction. The combination of matrigel and the tissue culture insert leads to slow diffusion of GFLs from the lower chamber to generate a concentration gradient. Our data show that the activation of RET greatly enhances the invasion of MiaPaCa-2 cells along a GFL concentration gradient. In negative control experiments, we find that EV MiaPaCa-2 cells continue to invade through the matrigel despite the lack of GDNF. This baseline is reduced by RET knockdown, suggesting that RET is also contributing to cell migration in the absence of GDNF (Figure 3.14). It is possible that matrigel contains low concentrations of GDNF, or other GFLs such as ARTN, and thus can still activate RET at low levels to induce invasion. Matrigel also contains several other growth factors, such as nerve growth factors (NGFs) and epidermal growth factors (EGFs) [148], and the activation of other RTKs by these growth factors may mediate RET independent cell migration. Additionally, crosstalk of RET with other RTKs has been identified in other studies, and could also contribute to cell invasion in the absence of GDNF [149-153]. Although RET9 KD cells consistently appeared to invade slightly more than RET51 KD cells in response to GDNF, we did not detect significant differences in initial experiments. Subsequent use of ARTN, which activates RET through the much more abundant GFRα3 coreceptor, identified 2-3 fold increases in invasiveness relative to that seen with GDNF, and allowed us to resolve the significantly greater invasiveness of RET9 KD cells relative to RET51 KD cells in response to RET activation

(Figure 3.13). Together, these data suggest that RET51 plays a greater role relative to RET9 in driving cell invasiveness and migration in MiaPaCa-2.

4.4 RET knockdown, downstream protein phosphorylation and isoform specific differences

Throughout the assays conducted during this project, it became obvious that the phenotypes generated by RET51 KD, while not always significantly different from RET9 KD, were typically slightly more severe relative to those generated by RET9 KD. This was particularly evident during the MiaPaCa-2 invasion assays using GDNF and ARTN (Figure 3.13), where RET51 KD cells appeared slightly less invasive relative to RET9 KD cells upon GDNF treatment, and significantly so when ARTN was used to activate RET at higher levels.

Based on our qRT-PCR data for RET isoform expression in MiaPaCa-2, the greater severity of RET51 KD on cell phenotype did not appear to be a result of lesser overall RET expression. WT and EV cells contain approximately 7000 copies of RET9 and 4500 copies of RET51 mRNAs per 400ng of total RNA (Figure 4.4), or approximately 11500 RET mRNAs in total. In the RET9 KD and RET51 KD cells the expression of the targeted RET isoform was reduced by approximately 70%. However, because MiaPaCa-2 cells express about twice as much RET9 as RET51 (Figure 3.1), the RET9 KD cells retain about 6000 RET mRNAs per 400ng total RNA, while the RET51 KD cells retain about 7000 RET mRNAs. Thus, overall expression of RET is actually greater in RET51 KD cells relative to RET9 KD cells. This suggests that the more severe phenotypes we observed in our RET51 KD cell lines (relative to RET9 KD), were not attributable to overall lower total RET abundance. Therefore, each of the effects we observed were more likely the result of differences between the RET9 and RET51 isoforms. Keeping this in mind, we go on to examine some of the differences between RET9 and RET51 identified above.

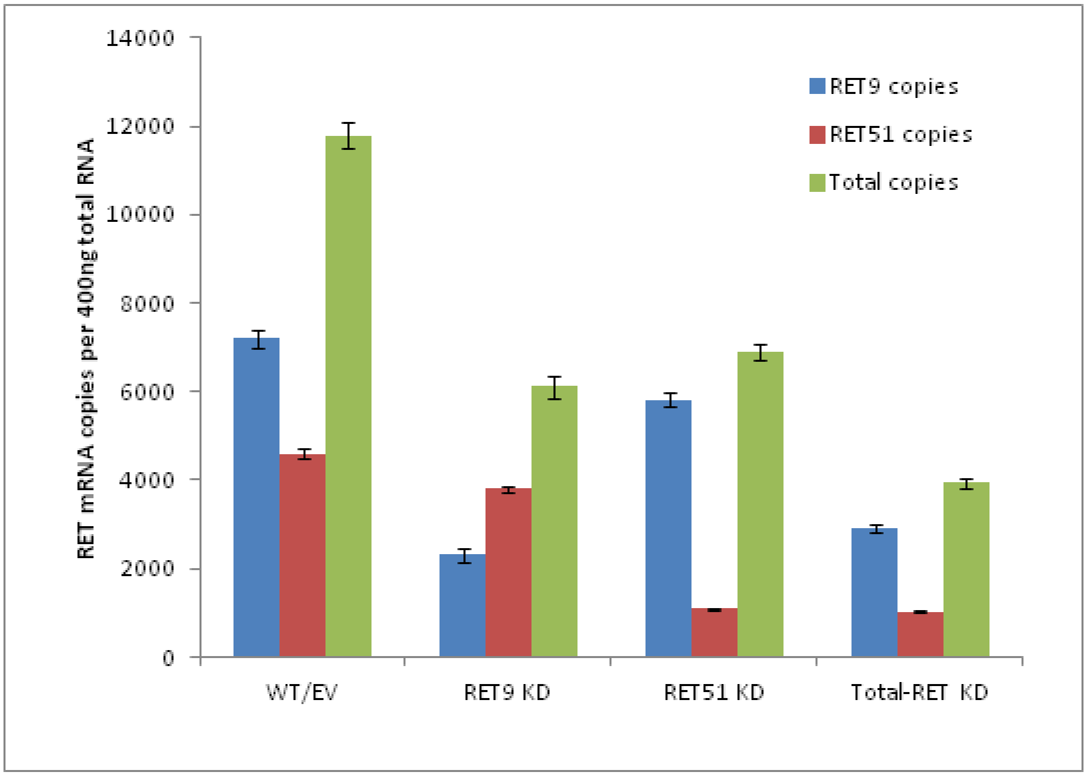

Figure 4.4 MiaPaCa-2 RET mRNA copy numbers. WT and EV transduced cells contain approximately 7000 copies of RET9 and 4500 copies of RET51 mRNAs per 400ng of total RNA (11500 total RET mRNAs). RET9 and RET51 KDs each reduce the expression of their respective targets by approximately 70%, however RET51 KD additionally reduces RET9 expression slightly. Overall, RET9 KD cells retain about 6000 RET mRNAs per 400ng total RNA, while the RET51 KD cells retain about 7000 RET mRNAs.

We begin by examining the phosphorylation status of ERK, STAT3 and AKT in MiaPaCa-2 following activation of RET by GDNF. The ERK pathway was constitutively active due to driving mutations specifically of K-Ras, in MiaPaCa-2 cells [123-125]. Thus, GDNF-mediated RET activation did not increase ERK activity in the EV, RET9 KD, or RET51 KD cells. We did, however, observe a significant decrease in pERK relative to EV in GDNF treated total-RET KD cells (Figure 3.14A). In future studies, repeating these experiments using ARTN to activate RET through GFRα3 might further clarify differences between EV, RET9 KD and RET51KD cells. When ARTN was used to activate RET in invasion assays (Figure 3.13B), the greater levels of RET activation revealed significant differences in the effects of RET9 KD and RET51 KD on cell invasiveness. This relationship between higher RET activation and our ability to resolve significant differences between the RET isoforms means that the coreceptor involved in RET activation should be an important consideration for our future experiments. We will need to use our data from GFRα expression analyses to optimize our assays.

Although the overall decrease in pERK in total-RET KD MiaPaCa-2 cells cannot be confirmed without further investigation, it might be related to changes in cellular programs induced in MiaPaCa-2 by RET knockdown. MiaPaCa-2 cells were noted to take on a scale-like morphology and had increased E-cadherin expression in response to RET knockdown, indicative of mesenchymal-epithelial transition (MET) [111, 142]. This process involves a switch from polarized, migratory, fibroblastoid cell morphology to a more stationary, epithelial phenotype, and involves the upregulation and downregulation of many genes and alterations in signal transduction programs [154]. In particular, several protein kinase phosphatases are upregulated during this process, including dual-specificity phosphatase (DUSP) which acts to dephosphorylate ERK [154] and is known to antagonize the activity of K-Ras [155].

The phosphorylation of STAT3 and AKT more clearly show the effects of RET knockdown in MiaPaCa-2. STAT3, which interacts with RET at tyrosines 752 and 928 [156], had significantly reduced phosphorylation levels relative to EV in response to RET knockdown (Figure 3.14B). In addition, the activation of RET by GDNF significantly increased pSTAT3 levels in EV and RET9 KD cells, but not in RET51 KD cells. Consistent with our previous findings regarding cell protrusion and invasion, this suggests that the RET51 isoform might also play a relatively greater role in activating STAT3. As RET51 is more abundant at the cell membrane [28], and STAT3 is activated by RTKs at the cell membrane [157, 158], it is likely that RET51 KD had a greater effect on STAT3 phosphorylation relative to RET9 KD. What is particularly interesting about the relationship between pSTAT3 and RET in MiaPaCa-2, is that pSTAT3 appears to decrease in abundance in response to GDNF in total-RET KD cells. These cells still retain approximately 20% of their total RET at the protein level (Figure 3.4B), and so, should still respond to GDNF. However, rather than an increase in pSTAT3 following treatment with GDNF as we would expect, we saw a significant decrease in pSTAT3. Although the mechanism for this process is not yet clear, it is possible that the activation of RET in stationary, epitheloid cells that have undergone MET activates different pathways relative to those activated in migratory mesenchymal-type cells. To delve further into this mechanism we will first need to confirm these findings using ARTN to induce greater activation of RET.

We found that, AKT was also constitutively and robustly phosphorylated in MiaPaCa-2, and the activation of RET by GDNF did not affect either total-AKT or pAKT levels (Figure 3.14C). This was consistent with the presence of constitutively active K-Ras [124] expressed by MiaPaCa-2, which constitutively activates AKT in combination with ERK [125]. Notably, each RET KD cell line displayed a significant decrease in both total-AKT and pAKT relative to EV cells. This suggests that RET can not only activate AKT, but can also modulate the total amount of AKT expressed in a cell. Previously, Xu *et al.* [159] demonstrated that AKT expression was regulated by STAT3 activation. Thus, it is possible that the decrease in pSTAT3 we observed in response to RET knockdown might be responsible for this reduction in AKT expression. In combination with constitutively active K-Ras, the regulation of AKT expression by STAT3 explains why we observed decreasing total-AKT in response to RET KD. Overall, the relationship between K-Ras, RET, STAT3, ERK and AKT in MiaPaCa-2, appears as illustrated in Figure 4.5.

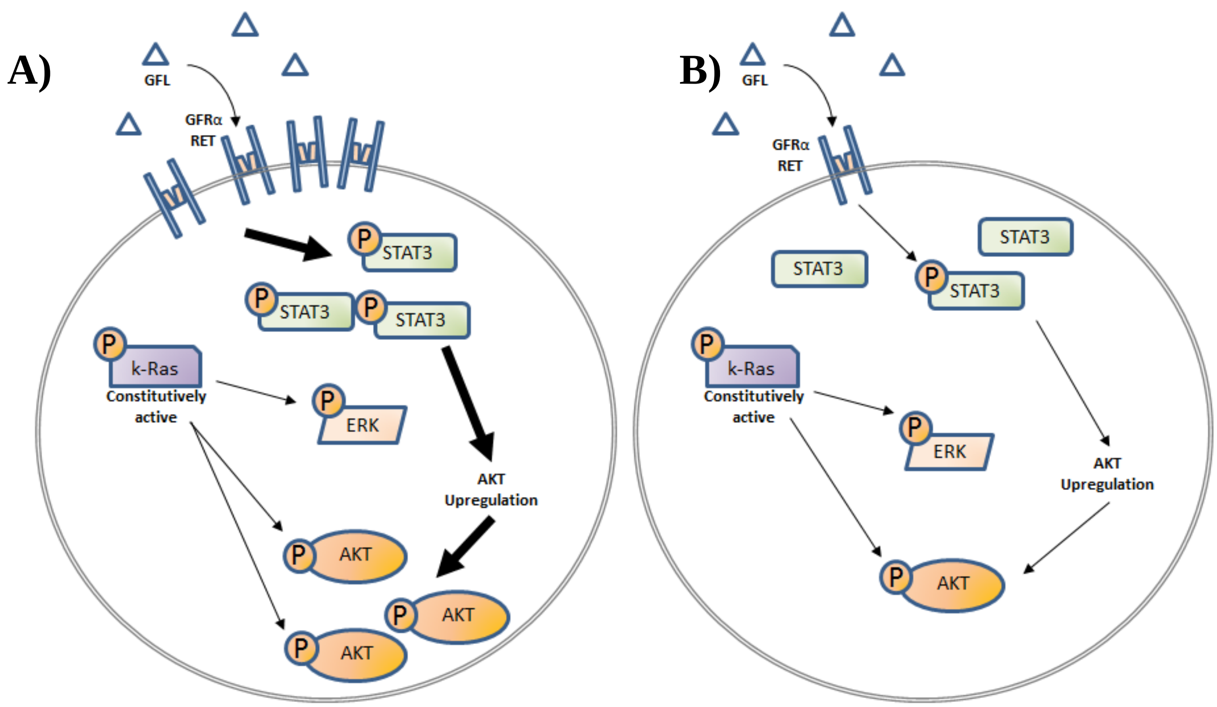

Figure 4.5 STAT3, ERK, and AKT phosphorylation in MiaPaCa2, in the presence and absence of RET knockdown. A) Normal RET expressing cells. When RET is activated at the cell surface, STAT3 is activated downstream and signals to upregulate the expression of AKT. Due to the presence of consitutively active K-Ras in MiaPaCa-2, both ERK and most of the expressed AKT are subsequently phosphorylated. **B)** RET knockdown cells. Although RET has been knocked down, these cells still express small quantities of RET at their cell surfaces. Activation of this small amount of RET does not phosphorylate STAT3 as strongly relative to the cell in A), resulting in less upregulation of AKT expression, and lower total AKT expression. Due to the presence of constitutively active K-Ras, AKT remains strongly phosphorylated, but due to lower STAT3 activation, there is less AKT overall. ERK expression is not affected by RET knockdown, and RET does not significantly affect the amount of pERK present, due to the majority of ERK being phosphorylated by constitutively active K-Ras.

It is unclear why RET knockdown had an effect on the phosphorylation and expression levels of the downstream proteins we examined even in the absence of GDNF. BLAST (http://blast.ncbi.nlm.nih.gov/) was used to validate the shRNA sequences used for RET knockdown, and off target effects were not found during the initial validation, so we should not expect this decrease in pSTAT3 to be caused by knockdown of something other than RET. However, MiaPaCa-2 cells are known to express a polymorphic variant of RET containing a G691S substitution, which is predicted to enhance the kinase activity of RET [126].It is possible, that this mutation renders RET more sensitive to low levels of GFLs, and that small amounts of FBS or GDNF left in the culture medium might result in low level activation of RET. If this is the case, then these results might be amended by additional serum starving and washing steps to ensure complete removal of RET activating ligands prior to cell lysis and immunoblotting. The morphological changes we observed in direct response to RET KD (Figure 3.5) might offer additional insight into the processes at work in our cells. The distinct cell morphologies of our knockdown cells were observed both in the presence of FBS, and in serum starved cells, suggesting that the changes induced in MiaPaCa-2 cells by RET KD can persist through serum starvation. Again, Cdc42 is a potential candidate to explain this behaviour. Previously, Nakaya *et al.* [160] reported that the expression and activation of Cdc42 in combination with the Rac1 GTPase was critical for chick embryo cells to maintain a mesenchymal phenotype, and that low Cdc42 activity induces epithelialization through MET. Thus, the morphological changes we observed in response to RET KD could be due to decreased activation of Cdc42 and Rac1 by RET, and the epithelialization of total-RET KD cells (Figure 4.6). The difference we observed in phenotype between RET9 KD and RET51 KD might be attributed to their differential abilities to activate Cdc42 and Rac1. Since RET51 KD cells were phenotypically more similar to total-RET

KD cells, RET51 may have greater ability to signal through Cdc42 and Rac1, possibly due to its greater abundance on the cell membrane, where Cdc42 and Rac1 are localized [28, 128, 161]. This is consistent throughout our assays, where RET51 KD has been shown to reduce migration, invasion, and cell protrusion in both MiaPaCa2 and TT cells to a greater degree than RET9 KD. Within the context of PNI in cancer, this means that tumour cells that express higher quantities of RET, and in particular RET51, would invade more rapidly, and be more aggressive relative to cells expressing either lower levels of RET, or relatively greater levels of RET9. In addition, if the mesenchymal phenotype of MiaPaCa-2 is maintained through Cdc42 and Rac1 activation by RET, and RET knockdown decreases this activation and results in epithelialization, it is possible that previously epithelioid RET expressing cells might undergo EMT and transition to a more invasive mesenchymal phenotype in response to RET activation. If such a process occurs *in vivo*, the expression of RET in tumours might be an important driver of PNI, by allowing RET expressing cells residing within a growing tumour mass to undergo EMT and invade towards peripheral nerves. These implications might open up opportunities to use RET expression as a clinical marker to identify more aggressive and higher risk tumours, or as a therapeutic target to slow the spread of aggressive, inoperable tumours such as late stage PDACs.

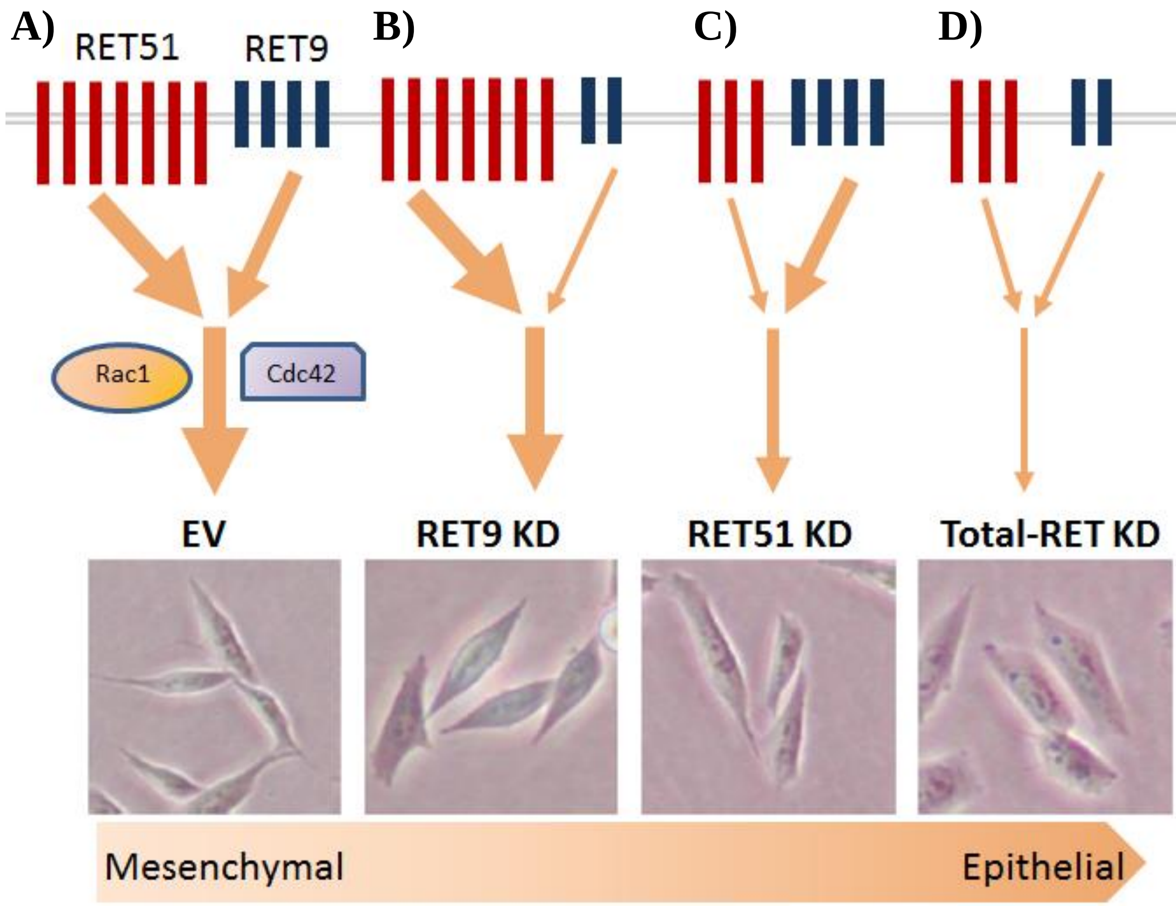

Figure 4.6 Epithelialization of MiaPaCa-2 in response to RET9, RET51 or total-RET knockdown due to differential activation of Rac1 and Cdc42. A) WT or EV cells cultured in FBS strongly activate Rac1 and Cdc42 to maintain a mesenchymal phenotype. **B)** RET9 KD cells have reduced RET9 levels at the cell membrane, but retain the more abundant RET51 isoform, thus maintaining high Rac1 and Cdc42 activation. **C)** RET51 KD cells lose most of their RET51, and the remaining RET9 localized at the cell membrane is not sufficient to maintain a normal mesenchymal phenotype. **D)** Total-RET KD reduces both RET9 and RET51 levels at the cell membrane, thus decreasing Rac1 and Cdc42 activation sufficiently to induce epithelialization.

4.5 Conclusions & Future Directions

We have shown that there are distinct functional differences between RET9 and RET51 in the way they influence cell morphology, migration, invasion and cell protrusion. Further, we have shown that the RET51 isoform appears to play a greater role in these processes relative to

RET9, and that the activation of RET by a GFL greatly enhances cell invasiveness and chemotaxis in both thyroid and pancreatic cancer cell lines. Although we did not establish the exact pathways responsible for the differential activities of RET9 and RET51, as membrane localized proteins capable of directing cell polarization, migration and mesenchymal-epithelial transition, Cdc42 and Rac1 might be worthy of further investigation to examine their roles in response to RET activation.

Further areas that remain to be addressed are the significant decreases in pERK and pSTAT3 we observed in total-RET KD MiaPaCa-2 in response to GDNF. Although it is likely that this can be attributed to the epithelialization of the cells in response to RET KD (Figure 4.6), we will need to examine the pathways proposed in this project to confirm that RET activation is responsible for maintenance of a mesenchymal phenotype in these cancer cells. Additionally, we might explore whether relatively greater RET activation by ARTN in MiaPaCa-2, or PSPN in TT cells [162] might reveal statistically significant differences between single RET isoform KD cell lines where consistent differences between RET9 and RET51were seen. The greater levels of RET activation resulting from greater GFL-GFRα binding might allow us to resolve these differences between RET9 and RET51, as we demonstrated during the MiaPaCa-2 invasion assay.

Further in the future, we will want to examine the effects of RET KD on PNI *in vivo*, as well as in a variety of additional cancers where PNI is known to be a marker of poor prognosis, such as head & neck, prostate, breast, and gastrointestinal cancers [89, 90]. A sciatic nerve injection model of PNI [163] could be employed to validate our findings in the current study, as well as expand our model of RET-directed PNI to several different cancer types. This project has brought to light several potential roles for RET in directing PNI, and suggests that RET is an important molecule in a variety of cancers, which can influence tumour behavior and may have significant clinical implications. The ability for RET to drive chemotaxis, cell polarization, invasion and possibly EMT, could position RET as an important marker of aggressive cancers, and suggests that it might be a useful target, not only in cancers where RET drives tumourigenesis, but also in the progression of many other tumours where it is expressed.

Bibliography of References

1. Takahashi, M., J. Ritz, and G.M. Cooper, *Activation of a novel human transforming gene, ret, by DNA rearrangement.* Cell, 1985. **42**: p. 581-588.
2. Traugott, A.L. and J.F. Moley, *The RET Protooncogene.* Cancer Treat Res, 2010. **153**(5): p. 303-19.
3. Tahira, T., et al., *Characterization of ret proto-oncogene mRNAs encoding two isoforms of the protein product in a human neuroblastoma cell line.* Oncogene, 1990. **5**(1): p. 97-102.
4. Myers, S.M., et al., *Characterization of RET proto-oncogene 3' splicing variants and polyadenylation sites: a novel C-terminus for RET.* Oncogene, 1995. **11**(10): p. 2039-45.
5. Pachnis, V., B. Mankoo, and F. Costantini, *Expression of the c-ret proto-oncogene during mouse embryogenesis.* Development, 1993. **119**(4): p. 1005-17.
6. Avantaggiato, V., et al., *Developmental expression of the RET protooncogene.* Cell Growth Differ, 1994. **5**(3): p. 305-11.
7. Marcos-Gutierrez, C.V., et al., *The zebrafish homologue of the ret receptor and its pattern of expression during embryogenesis.* Oncogene, 1997. **14**(8): p. 879-89.
8. Attie-Bitach, T., et al., *Expression of the RET proto-oncogene in human embryos.* Am J Med Genet, 1998. **80**(5): p. 481-6.
9. Schuchardt, A., et al., *Defects in the kidney and enteric nervous system of mice lacking the tyrosine kinase receptor Ret.* Nature, 1994. **367**(6461): p. 380-3.
10. Srinivas, S., et al., *Dominant effects of RET receptor misexpression and ligand-independent RET signaling on ureteric bud development.* Development, 1999. **126**(7): p. 1375-86.
11. Schuchardt, A., et al., *Renal agenesis and hypodysplasia in ret-k- mutant mice result from defects in ureteric bud development.* Development, 1996. **122**(6): p. 1919-29.
12. Tang, M.J., et al., *Ureteric bud outgrowth in response to RET activation is mediated by phosphatidylinositol 3-kinase.* Dev Biol., 2002. **243**(1): p. 128-136.
13. de Graaff, E., et al., *Differential activities of the RET tyrosine kinase receptor isoforms during mammalian embryogenesis.* Genes Dev, 2001. **15**(18): p. 2433-44.
14. Jain, S., et al., *Critical and distinct roles for key RET tyrosine docking sites in renal development.* Genes Dev, 2006. **20**(3): p. 321-33.
15. Edery, P., et al., *Mutations of the RET proto-oncogene in Hirschsprung's disease.* Nature, 1994. **367**(6461): p. 378-80.
16. Jing, S., et al., *GDNF-induced activation of the Ret protein tyrosine kinase is mediated by GDNFR-a, a novel receptor for GDNF.* Cell, 1996. **85**: p. 1113-1124.
17. Airaksinen, M.S. and M. Saarma, *The GDNF family: signalling, biological functions and therapeutic value.* Nat Rev Neurosci, 2002. **3**(5): p. 383-94.
18. Airaksinen, M.S., A. Titievsky, and M. Saarma, *GDNF family neurotrophic factor signaling: four masters, one servant?* Mol Cell Neurosci, 1999. **13**(5): p. 313-25.
19. Scott, R.F. and C.F. Ibáñez, *Determinants of ligand binding specificity in the GDNF family receptor alphas (GFRas).* J Biol Chem, 2001. **276**: p. 1450-1458.
20. Arighi, E., et al., *Identification of Shc docking site on Ret tyrosine kinase.* Oncogene, 1997. **14**(7): p. 773-82.

21. Lorenzo, M.J., et al., *RET alternative splicing influences the interaction of activated RET with the SH2 and PTB domains of Shc, and the SH2 domain of Grb2.* Oncogene, 1997. **14**: p. 763-771.
22. Wong, A., et al., *Phosphotyrosine 1062 Is Critical for the In Vivo Activity of the Ret9 Receptor Tyrosine Kinase Isoform.* Mol Cell Biol., 2005. **25**(21): p. 9661-9673.
23. Besset, V., R.P. Scott, and C.F. Ibanez, *Signaling complexes and protein-protein interactions involved in the activation of the Ras and phosphatidylinositol 3-kinase pathways by the c-Ret receptor tyrosine kinase.* J Biol Chem, 2000. **275**(50): p. 39159-66.
24. Califano, D., et al., *Signaling through Ras is essential for ret oncogene-induced cell differentiation in PC12 cells.* J Biol Chem, 2000. **275**(25): p. 19297-305.
25. Scott, R.P., et al., *Distinct turnover of alternatively spliced isoforms of the RET kinase receptor mediated by differential recruitment of the Cbl ubiquitin ligase.* J Biol Chem, 2005. **280**(14): p. 13442-9.
26. Ishiguro, Y., et al., *The role of amino acids surrounding tyrosine 1062 in ret in specific binding of the shc phosphotyrosine-binding domain.* Endocrinology, 1999. **140**(9): p. 3992-8.
27. Schuetz, G., et al., *The neuronal scaffold protein Shank3 mediates signaling and biological function of the receptor tyrosine kinase Ret in epithelial cells.* J Cell Biol, 2004. **167**(5): p. 945-52.
28. Richardson, D.S., et al., *Differential subcellular localization and trafficking of RET isoforms.* In Preparation for submission to Neuron, 2009.
29. Tsui-Pierchala, B.A., et al., *The long and short isoforms of Ret function as independent signaling complexes.* J Biol Chem, 2002. **277**(37): p. 34618-25.
30. Hickey, J.G., et al., *RET-mediated gene expression pattern is affected by isoform but not oncogenic mutation.* Genes, Chromosomes and Cancer, 2009. **48**(5): p. 429-440.
31. Rossel, M., et al., *Distinct biological properties of two RET isoforms activated by MEN 2A/FMTC and MEN 2B mutations.* Oncogene, 1997. **14**: p. 265-275.
32. Iwashita, T., et al., *Biological and biochemical properties of Ret with kinase domain mutations identified in multiple endocrine neoplasia type 2B and familial medullary thyroid carcinoma.* Oncogene, 1999. **18**(26): p. 3919-22.
33. Le Hir, H., et al., *Relative expression of the RET9 and RET51 isoforms in human pheochromocytomas.* Oncology, 2000. **58**(4): p. 311-8.
34. Pasini, A., et al., *Oncogenic activation of RET by two distinct FMTC mutations affecting the tyrosine kinase domain.* Oncogene, 1997. **15**(4): p. 393-402.
35. Veit, C., et al., *Activation of phosphatidylinositol 3-kinase and extracellular signal-regulated kinase is required for glial cell line-derived neurotrophic factor-induced migration and invasion of pancreatic carcinoma cells.* Cancer Res, 2004. **64**(15): p. 5291-300.
36. Ivanchuk, S.M., S.M. Myers, and L.M. Mulligan, *Expression of RET 3' splicing variants during human kidney development.* Oncogene, 1998. **16**(8): p. 991-6.
37. Kaplinovsky, T. and A.M. Cunningham, *Differential expression of RET receptor isoforms in the olfactory system.* Neuroscience, 2011. **175**: p. 49-65.
38. Enomoto, H., et al., *RET signaling is essential for migration, axonal growth and axon guidance of developing sympathetic neurons.* Development, 2001. **128**(20): p. 3963-3974.
39. Burzynski, G.M., et al., *Identifying candidate Hirschsprung disease-associated RET variants.* Am J Hum Genet, 2005. **76**(5): p. 850-8.

40. Gabriel, S.B., et al., *Segregation at three loci explains familial and population risk in Hirschsprung disease.* Nat Genet, 2002. **31**(1): p. 89-93.
41. Bolk, S., et al., *A human model for multigenic inheritance: phenotypic expression in Hirschsprung disease requires both the RET gene and a new 9q31 locus.* Proc Natl Acad Sci U S A, 2000. **97**(1): p. 268-73.
42. Carrasquillo, M.M., et al., *Genome-wide association study and mouse model identify interaction between RET and EDNRB pathways in Hirschsprung disease.* Nat. Genet., 2002. **32**(2): p. 237-244.
43. Griseri, P., et al., *A rare haplotype of the RET proto-oncogene is a risk-modifying allele in hirschsprung disease. .* Am J Hum Genet., 2002. **71**(4): p. 969-974.
44. Griseri, P., et al., *An intronic nucleotide variant of the RET proto-oncogene causes Hirschsprung disease by interfering with RNA splicing. .* Gene Function & Disease. , 2000. **1**(5): p. 184–188.
45. Seri, M., et al., *Frequency of RET mutations in long- and short-segment Hirschsprung disease.* Hum Mutat, 1997. **9**(3): p. 243-9.
46. Garcia-Barcelo, M., et al., *TTF-1 and RET promoter SNPs: regulation of RET transcription in Hirschsprung's disease.* Hum Mol Genet, 2005. **14**(2): p. 191-204.
47. Jeanpierre, C., et al., *RET and GDNF mutations are rare in fetuses with renal agenesis or other severe kidney development defects.* J Med Genet, 2011. **48**(7): p. 497-504.
48. Lee, K.Y., et al., *3' Splicing variants of ret receptor tyrosine kinase are differentially expressed in mouse embryos and in adult mice.* Biochim Biophys Acta, 2003. **1627**(1): p. 26-38.
49. Lin, S.L., J.D. Miller, and S.Y. Ying, *Intronic microRNA (miRNA).* J Biomed Biotechnol, 2006. **2006**(4): p. 26818.
50. Lin, S.L., H. Kim, and S.Y. Ying, *Intron-mediated RNA interference and microRNA (miRNA).* Front Biosci, 2008. **13**: p. 2216-30.
51. Richardson, D.S., A.Z. Lai, and L.M. Mulligan, *RET ligand-induced internalization and its consequences for downstream signaling.* Oncogene, 2006. **25**(22): p. 3206-11.
52. Richardson, D.S., et al., *Transcript level modulates the inherent oncogenicity of RET/PTC oncoproteins.* Cancer Res, 2009. **69**(11): p. 4861-9.
53. Tansey, M.G., et al., *GFRalpha-mediated localization of RET to lipid rafts is required for effective downstream signaling, differentiation, and neuronal survival.* Neuron, 2000. **25**(3): p. 611-623.
54. McBride, K., S.G. Rhee, and S. Jaken, *Immunocytochemical localization of phospholipase C-gamma in rat embryo fibroblasts.* Proc Natl Acad Sci U S A, 1991. **88**(16): p. 7111-5.
55. Lasserre, R., et al., *Raft nanodomains contribute to Akt/PKB plasma membrane recruitment and activation.* Nat Chem Biol, 2008. **4**(9): p. 538-47.
56. Livak, K. and T. Schmittgen, *Analysis of relative gene expression data using real-time quantitative PCR and the 2(-Delta Delta C(T)) Method.* Methods, 2001. **25**(4): p. 402-408.
57. Takahashi, M., *The GDNF/RET signaling pathway and human diseases.* Cytokine Growth Factor Rev, 2001. **12**(4): p. 361-73.
58. Runeberg-Roos, P. and M. Saarma, *Neurotrophic factor receptor RET: structure, cell biology, and inherited diseases.* Ann Med, 2007. **39**(8): p. 572-80.

59. Koper, J.W. and S.W. Lamberts, *Sporadic endocrine tumours and their relationship to the hereditary endocrine neoplasia syndromes.* Eur J Clin Invest, 2000. **30**(6): p. 493-500.
60. Lai, A.Z., T.S. Gujral, and L.M. Mulligan, *RET Signaling in Endocrine Tumors: Delving Deeper into Molecular Mechanisms.* Endocrine Pathology, 2007. **18**(2): p. 57-67.
61. Srinivasan, S., et al., *Rac and Cdc42 play distinct roles in regulating PI(3,4,5)P3 and polarity during neutrophil chemotaxis.* J Cell Biol, 2003. **160**(3): p. 375-85.
62. Wood, L.D., et al., *The genomic landscapes of human breast and colorectal cancers.* Science, 2007. **318**(5853): p. 1108-13.
63. Futami, H., et al., *A novel somatic point mutation of the RET Proto-oncogene in tumor tissues of small cell lung cancer patients.* Jpn J Cancer Res, 1995. **86**(12): p. 1127-30.
64. Cerrato, A., V. De Falco, and M. Santoro, *Molecular genetics of medullary thyroid carcinoma: the quest for novel therapeutic targets*. J Mol Endocrinol, 2009. **43**(4): p. 143-55.
65. Irazoqui, J.E., A.S. Gladfelter, and D.J. Lew, *Scaffold-mediated symmetry breaking by Cdc42p.* Nat Cell Biol, 2003. **5**(12): p. 1062-70.
66. Mulligan, L.M., et al., *Specific mutations of the RET proto-oncogene are related to disease phenotype in MEN 2A and FMTC.* Nat Genet, 1994. **6**(1): p. 70-4.
67. Mulligan, L.M., et al., *Germ-line mutations of the RET proto-oncogene in multiple endocrine neoplasia type 2A.* Nature, 1993. **363**(6428): p. 458-60.
68. Hofstra, R.M., et al., *A mutation in the RET proto-oncogene associated with multiple endocrine neoplasia type 2B and sporadic medullary thyroid carcinoma.* Nature, 1994. **367**(6461): p. 375-6.
69. Marx, S.J., *Molecular genetics of multiple endocrine neoplasia types 1 and 2.* Nat Rev Cancer, 2005. **5**(5): p. 367-75.
70. Santoro, M., et al., *Activation of RET as a dominant transforming gene by germline mutations of MEN2A and MEN2B.* Science, 1995. **267**: p. 381-383.
71. Gujral, T.S., et al., *Molecular mechanisms of RET receptor-mediated oncogenesis in multiple endocrine neoplasia 2B.* Cancer Res, 2006. **66**(22): p. 10741-9.
72. Songyang, Z., et al., *Catalytic specificity of protein-tyrosine kinases is critical for selective signalling.* Nature, 1995. **373**: p. 536-539.
73. Runeberg-Roos, P., H. Virtanen, and M. Saarma, *RET(MEN 2B) is active in the endoplasmic reticulum before reaching the cell surface.* Oncogene, 2007.
74. Grieco, M., et al., *PTC is a novel rearranged form of the ret proto-oncogene and is frequently detected in vivo in human thyroid papillary carcinomas.* Cell, 1990. **60**: p. 557-563.
75. Santoro, M., R.M. Melillo, and A. Fusco, *RET/PTC activation in papillary thyroid carcinoma: European Journal of Endocrinology Prize Lecture.* Eur J Endocrinol, 2006. **155**(5): p. 645-53.
76. Bunone, G., et al., *Induction of RET proto-oncogene expression in neuroblastoma cells preceded neuronal differentiation and is not mediated by protein synthesis.* Exp Cell Res, 1995. **217**: p. 92-99.
77. Santoro, M., et al., *Molecular characterization of RET/PTC3; a novel rearranged version of the RETproto-oncogene in a human thyroid papillary carcinoma.* Oncogene, 1994. **9**(2): p. 509-16.

78. Kohno, T., et al., *KIF5B-RET fusions in lung adenocarcinoma.* Nat Med, 2012. **18**(3): p. 375-7.
79. Stephens, P.J., et al., *The landscape of cancer genes and mutational processes in breast cancer.* Nature, 2012. **486**(7403): p. 400-4.
80. Gutierrez, C. and R. Schiff, *HER2: biology, detection, and clinical implications.* Arch Pathol Lab Med, 2011. **135**(1): p. 55-62.
81. Zeng, Q., et al., *The Relationship between Overexpression of Glial Cell-derived Neurotrophic Factor and Its RET Receptor with Progression and Prognosis of Human Pancreatic Cancer.* The Journal of International Medical Research, 2008. **36**: p. 656.
82. Hezel, A.F., et al., *Genetics and biology of pancreatic ductal adenocarcinoma.* Genes Dev, 2006. **20**(10): p. 1218-49.
83. Hidalgo, M., *Pancreatic cancer.* N Engl J Med., 2010. **362**(17): p. 1605-1617.
84. Bartsch, D.K., T.M. Gress, and P. Langer, *Familial pancreatic cancer--current knowledge.* Nat Rev Gastroenterol Hepatol, 2012. **9**(8): p. 445-53.
85. Lohr, M., et al., *Frequency of K-ras mutations in pancreatic intraductal neoplasias associated with pancreatic ductal adenocarcinoma and chronic pancreatitis: a meta-analysis.* Neoplasia, 2005. **7**(1): p. 17-23.
86. Pellegata, N.S., et al., *K-ras and p53 gene mutations in pancreatic cancer: ductal and nonductal tumors progress through different genetic lesions.* Cancer Res, 1994. **54**(6): p. 1556-1560.
87. Schneider, G. and R.M. Schmid, *Genetic alterations in pancreatic carcinoma.* Mol Cancer, 2003. **2**(15): p. 15.
88. Donahue, T.R. and O.J. Hines, *CXCR2 and RET single nucleotide polymorphisms in pancreatic cancer.* World J Surg, 2009. **33**(4): p. 710-5.
89. Nakao, A., et al., *Clinical significance of carcinoma invasion of the extrapancreatic nerve plexus in pancreatic cancer.* Pancreas, 1996. **12**(4): p. 357-61.
90. Liebig, C., et al., *Perineural invasion in cancer: a review of the literature.* Cancer, 2009. **115**(15): p. 3379-91.
91. Wagner, M., et al., *Curative resection is the single most important factor determining outcome in patients with pancreatic adenocarcinoma.* Br J Surg, 2004. **91**(5): p. 586-594.
92. Okada, Y., et al., *Experimental implication of celiac ganglionotropic invasion of pancreatic-cancer cells bearing c-ret proto-oncogene with reference to glial-cell-line-derived neurotrophic factor (GDNF).* Int J Cancer, 1999. **81**(1): p. 67-73.
93. Okada, Y., et al., *Glial cell-derived neurotrophic factor upregulates the expression and activation of matrix metalloproteinase-9 in human pancreatic cancer.* Surgery, 2003. **134**(2): p. 293-9.
94. Baloh, R.H., et al., *Artemin, a novel member of the GDNF ligand family, supports peripheral and central neurons and signals through the GFRalpha3-RET receptor complex.* Neuron, 1998. **21**(6): p. 1291-1302.
95. Andres, R., et al., *Multiple effects of artemin on sympathetic neurone generation, survival and growth.* Development, 2001. **128**(19): p. 3685-95.
96. Kim, D. and G.R. Dressler, *PTEN modulates GDNF/RET mediated chemotaxis and branching morphogenesis in the developing kidney.* Dev Biol, 2007. **307**(2): p. 290-9.
97. Gardell, L.R., et al., *Multiple actions of systemic artemin in experimental neuropathy.* Nat Med, 2003. **9**(11): p. 1383-9.

98. Bockman, D.E., M. Buchler, and H.G. Beger, *Interaction of pancreatic ductal carcinoma with nerves leads to nerve damage.* Gastroenterology, 1994. **107**(1): p. 219-30.
99. Mologni, L., *Development of RET kinase inhibitors for targeted cancer therapy.* Curr Med Chem, 2011. **18**(2): p. 162-75.
100. Antonelli, A., et al., *New targeted therapies for thyroid cancer.* Curr Genomics, 2011. **12**(8): p. 626-31.
101. Thornton, K., et al., *Vandetanib for the treatment of symptomatic or progressive medullary thyroid cancer in patients with unresectable locally advanced or metastatic disease: U.S. Food and Drug Administration drug approval summary.* Clin Cancer Res, 2012. **18**(14): p. 3722-30.
102. Lu, D.Y., et al., *Glial cell line-derived neurotrophic factor induces cell migration and matrix metalloproteinase-13 expression in glioma cells.* Biochem Pharmacol, 2010. **80**(8): p. 1201-9.
103. Funahashi, H., et al., *The role of glial cell line-derived neurotrophic factor (GDNF) and integrins for invasion and metastasis in human pancreatic cancer cells.* J Surg Oncol, 2005. **91**(1): p. 77-83.
104. Gujral, T.S., et al., *A novel RET kinase-beta-catenin signaling pathway contributes to tumorigenesis in thyroid carcinoma.* Cancer Res, 2008. **68**(5): p. 1338-46.
105. Holmes, K., et al., *Detection of siRNA induced mRNA silencing by RT-qPCR: considerations for experimental design.* BMC Res Notes, 2010. **3**(53): p. 53.
106. Cockburn, J.G., et al., *RET-mediated cell adhesion and migration require multiple integrin subunits.* J Clin Endocrinol Metab, 2010. **95**(11): p. E342-6.
107. Kim, L.T., et al., *Focal adhesions and associated proteins in medullary thyroid carcinoma cells.* J Surg Res, 2003. **111**(2): p. 177-84.
108. Pool, M., et al., *NeuriteTracer: a novel ImageJ plugin for automated quantification of neurite outgrowth.* J Neurosci Methods, 2008. **168**(1): p. 134-9.
109. D'Alessio, A., et al., *Expression of the RET oncogene induces differentiation of SK-N-BE neuroblastoma cells.* Cell Growth Differ, 1995. **6**(11): p. 1387-94.
110. Uesaka, T., et al., *Diminished Ret expression compromises neuronal survival in the colon and causes intestinal aganglionosis in mice.* J Clin Invest, 2008. **118**(5): p. 1890-8.
111. Wells, A., C. Yates, and C.R. Shepard, *E-cadherin as an indicator of mesenchymal to epithelial reverting transitions during the metastatic seeding of disseminated carcinomas.* Clin Exp Metastasis. , 2008. **25**(6): p. 621-628.
112. Gainor, J.F. and A.T. Shaw, *The new kid on the block: RET in lung cancer.* Cancer Discov, 2013. **3**(6): p. 604-6.
113. Taatjes, D.J., B.E. Sobel, and R.C. Budd, *Morphological and cytochemical determination of cell death by apoptosis.* Histochem Cell Biol, 2008. **129**(1): p. 33-43.
114. Carlomagno, F., et al., *Point mutation of the RET proto-oncogene in the TT human medullary thyroid carcinoma cell line.* Biochem Biophys Res Commun, 1995. **207**(3): p. 1022-8.
115. Saarma, M., *GDNF recruits the signaling crew into lipid rafts.* Trends Neurosci, 2001. **24**(8): p. 427-9.
116. Bongarzone, I., et al., *The Glu632-Leu633 deletion in cysteine rich domain of Ret induces constitutive dimerization and alters the processing of the receptor protein.* Oncogene, 1999. **18**(34): p. 4833-8.

117. Lodyga, M., et al., *XB130, a tissue-specific adaptor protein that couples the RET/PTC oncogenic kinase to PI 3-kinase pathway.* Oncogene, 2009. **28**(7): p. 937-949.
118. Freche, B., et al., *Inducible dimerization of RET reveals a specific AKT deregulation in oncogenic signaling.* J Biol Chem, 2005. **280**(44): p. 36584-91.
119. Golub, T., S. Wacha, and P. Caroni, *Spatial and temporal control of signaling through lipid rafts.* Curr Opin Neurobiol, 2004. **14**(5): p. 542-550.
120. Andreozzi, F., et al., *Protein kinase Calpha activation by RET: evidence for a negative feedback mechanism controlling RET tyrosine kinase.* Oncogene, 2003. **22**(19): p. 2942-9.
121. Wen, H.C., et al., *Negative regulation of phosphatidylinositol 3-kinase and Akt signalling pathway by PKC.* Cell Signal, 2003. **15**(1): p. 37-45.
122. Li, L., et al., *Protein kinase C negatively regulates Akt activity and modifies UVC-induced apoptosis in mouse keratinocytes.* J Biol Chem, 2006. **281**(6): p. 3237-43.
123. Castellano, E. and J. Downward, *RAS Interaction with PI3K: More Than Just Another Effector Pathway.* Genes Cancer, 2011. **2**(3): p. 261-274.
124. Berrozpe, G., et al., *Comparative analysis of mutations in the p53 and K-ras genes in pancreatic cancer.* Int J Cancer, 1994. **58**(2): p. 185-91.
125. Sheng, H., J. Shao, and R.N. Dubois, *K-Ras-mediated increase in cyclooxygenase 2 mRNA stability involves activation of the protein kinase B1.* Cancer Res, 2001. **61**(6): p. 2670-5.
126. Sawai, H., et al., *The G691S RET polymorphism increases glial cell line-derived neurotrophic factor-induced pancreatic cancer cell invasion by amplifying mitogen-activated protein kinase signaling.* Cancer Res, 2005. **65**(24): p. 11536-44.
127. Xue, G. and B.A. Hemmings, *PKB/Akt-dependent regulation of cell motility.* J Natl Cancer Inst, 2013. **105**(6): p. 393-404.
128. Etienne-Manneville, S., *Cdc42--the centre of polarity.* J Cell Sci, 2004. **15**(117): p. 1291-1300.
129. Simons, K. and D. Toomre, *Lipid rafts and signal transduction.* Nat Rev Mol Cell Biol, 2000. **1**(1): p. 31-9.
130. Tatin, F., et al., *A signalling cascade involving PKC, Src and Cdc42 regulates podosome assembly in cultured endothelial cells in response to phorbol ester.* J Cell Sci, 2006. **119**(Pt 4): p. 769-81.
131. Natarajan, D., et al., *Requirement of signalling by receptor tyrosine kinase RET for the directed migration of enteric nervous system progenitor cells during mammalian embryogenesis.* Development, 2002. **129**(22): p. 5151-60.
132. Dormann, D. and C.J. Weijer, *Chemotactic cell movement during development.* Curr Opin Genet Dev, 2003. **13**(4): p. 358-64.
133. Melillo, R.M., et al., *The insulin receptor substrate (IRS)-1 recruits phosphatidylinositol 3-kinase to Ret: evidence for a competition between Shc and IRS-1 for the binding to Ret.* Oncogene, 2001. **20**(2): p. 209-218.
134. Aoki, K., et al., *Local phosphatidylinositol 3,4,5-trisphosphate accumulation recruits Vav2 and Vav3 to activate Rac1/Cdc42 and initiate neurite outgrowth in nerve growth factor-stimulated PC12 cells.* Mol Biol Cell, 2005. **16**(5): p. 2207-17.
135. Bustelo, X.R., *Regulatory and signaling properties of the Vav family.* Mol Cell Biol, 2000. **20**(5): p. 1461-77.

136. Timpson, P., et al., *Coordination of cell polarization and migration by the Rho family GTPases requires Src tyrosine kinase activity.* Curr Biol, 2001. **11**(23): p. 1836-46.
137. Fukuda, T., K. Kiuchi, and M. Takahashi, *Novel mechanism of regulation of Rac activity and lamellipodia formation by RET tyrosine kinase.* J Biol Chem, 2002. **277**(21): p. 19114-21.
138. Friedl, P., *Prespecification and plasticity: shifting mechanisms of cell migration.* Curr Opin Cell Biol, 2004. **16**(1): p. 14-23.
139. Roussos, E.T., J.S. Condeelis, and A. Patsialou, *Chemotaxis in cancer.* Nat Rev Cancer., 2007. **11**(8): p. 573-587.
140. van Weering, D.H. and J.L. Bos, *Glial cell line-derived neurotrophic factor induces Ret-mediated lamellipodia formation.* J Biol Chem, 1997. **272**(1): p. 249-54.
141. Chiariello, M., et al., *Signalling of the Ret receptor tyrosine kinase through the c-Jun NH2-terminal protein kinases (JNKS): evidence for a divergence of the ERKs and JNKs pathways induced by Ret.* Oncogene, 1998. **16**(19): p. 2435-2445.
142. Bose, B. and P.S. Shenoy, *Non insulin producing cell line, MIA PaCa-2 is rendered insulin producing in vitro via mesenchymal epithelial transition.* J Cell Biochem, 2013. **114**(7): p. 1642-1652.
143. Wang, F., et al., *Lipid products of PI(3)Ks maintain persistent cell polarity and directed motility in neutrophils.* Nat Cell Biol, 2002. **4**(7): p. 513-8.
144. Murakami, H., et al., *Rho-dependent and -independent tyrosine phosphorylation of focal adhesion kinase, paxillin and p130Cas mediated by Ret kinase.* Oncogene, 1999. **18**(11): p. 1975-82.
145. Mueller, B.K., *Growth cone guidance: first steps towards a deeper understanding.* Annu Rev Neurosci, 1999. **22**: p. 351-88.
146. Luo, L., *Rho GTPases in neuronal morphogenesis.* Nat Rev Neurosci, 2000. **1**(3): p. 173-80.
147. Dickson, B.J., *Rho GTPases in growth cone guidance.* Curr Opin Neurobiol, 2001. **11**(1): p. 103-10.
148. BD. *BD Matrigel Basement Membrane Matrix Growth Factor Reduced*. [cited 2013; Available from: http://www.bdbiosciences.com/external_files/dl/doc/manuals/live/web_enabled/356230_Guidelines.pdf.
149. Tsui-Pierchala, B.A., J. Milbrandt, and E.M. Johnson, Jr., *NGF utilizes c-Ret via a novel GFL-independent, inter-RTK signaling mechanism to maintain the trophic status of mature sympathetic neurons.* Neuron, 2002. **33**(2): p. 261-73.
150. Esposito, C.L., et al., *A cross-talk between TrkB and Ret tyrosine kinases receptors mediates neuroblastoma cells differentiation.* PLoS One, 2008. **3**(2): p. e1643.
151. Plo, I., et al., *Nerve growth factor-induced protein kinase C stimulation contributes to TrkA-dependent inhibition of p75 neurotrophin receptor sphingolipid signaling.* J Neurosci Res, 2004. **77**(4): p. 465-74.
152. Jo, M., et al., *Cross-talk between Epidermal Growth Factor Receptor and c-Met Signal Pathways in Transformed Cells*.* J Biol Chem, 2000. **275**(12): p. 8806-8811.
153. Negri, T., et al., *Functional mapping of receptor tyrosine kinases in myxoid liposarcoma.* Clin Cancer Res, 2010. **16**(14): p. 3581-93.
154. Jechlinger, M., et al., *Expression profiling of epithelial plasticity in tumor progression.* Oncogene, 2003. **22**(46): p. 7155-69.

155. Wong, V.C., et al., *Tumor suppressor dual-specificity phosphatase 6 (DUSP6) impairs cell invasion and epithelial-mesenchymal transition (EMT)-associated phenotype.* Int J Cancer, 2012. **130**(1): p. 83-95.
156. Schuringa, J.J., et al., *MEN2A-RET-induced cellular transformation by activation of STAT3.* Oncogene, 2001. **20**(38): p. 5350-8.
157. Bild, A.H., J. Turkson, and R. Jove, *Cytoplasmic transport of Stat3 by receptor-mediated endocytosis.* EMBO J, 2002. **21**(13): p. 3255-63.
158. Kermorgant, S. and P.J. Parker, *Receptor trafficking controls weak signal delivery: a strategy used by c-Met for STAT3 nuclear accumulation.* J Cell Biol, 2008. **182**(5): p. 855-863.
159. Xu, Q., et al., *Targeting Stat3 blocks both HIF-1 and VEGF expression induced by multiple oncogenic growth signaling pathways.* Oncogene, 2005. **24**(36): p. 5552-5560.
160. Nakaya, Y., et al., *Mesenchymal-epithelial transition during somitic segmentation is regulated by differential roles of Cdc42 and Rac1.* Dev Cell., 2004. **7**(3): p. 425-438.
161. Bustelo, X.R., et al., *Rac-ing to the plasma membrane: the long and complex work commute of Rac1 during cell signaling.* Small GTPases, 2012. **3**(1): p. 60-6.
162. Lindahl, M., et al., *Human glial cell line-derived neurotrophic factor receptor alpha 4 is the receptor for persephin and is predominantly expressed in normal and malignant thyroid medullary cells.* J Biol Chem, 2001. **276**(12): p. 9344-51.
163. Gil, Z., et al., *Paracrine regulation of pancreatic cancer cell invasion by peripheral nerves.* J Natl Cancer Inst, 2010. **102**(2): p. 107-18.